Neuronal Profilins – from cellular functions to learning behavior

Von der Fakultät für Lebenswissenschaften

der Technischen Universität Carolo-Wilhelmina zu Braunschweig

zur Erlangung des Grades

eines Doktors der Naturwissenschaften

(Dr. rer. nat.)

genehmigte

D i s s e r t a t i o n

von Maximilian Klasmeier
aus Dachau

1. Referentin oder Referent: Professor Dr. Martin Korte
2. Referentin oder Referent: Professor. Dr. Reinhard Köster
eingereicht am: 07.06.2012
mündliche Prüfung (Disputation) am: 16.07.2021

Druckjahr 2021

Vorveröffentlichungen der Dissertation

Teilergebnisse aus dieser Arbeit wurden mit Genehmigung der Fakultät für Lebenswissenschaften, vertreten durch den Mentor der Arbeit, in folgenden Beiträgen vorab veröffentlicht:

Posterbeiträge

Klasmeier, M., Meßerschmidt, T., Hinz, D., Rothkegel, M.und Korte, M. mit ”Functions of profilins in the tripartite synapse from structural plasticity to functional modulation 11th FENS Frum of Neuroscience Society, online conference (2020)

Klasmeier, M., Meßerschmidt, T., Hinz, D., Rothkegel, M.und Korte, M. mit ”Profilins as modulators of neuronal morphology and transmission 11th Actin Assembly for Intracellular Functions, Freiburg (2020)

Klasmeier, M., Meßerschmidt, T., Ohlrogge, C., Rothkegel, M.und Korte, M.

“Neuronal profilins as modulators of dendritic complexity and structural plasticity”, 13th Meeting of the German Neuroscience Society, Göttingen (2019)

‘I solemnly swear

that I am up to no good’

George Weasley (by J.K.Rowling)

Inhalt

Abstract

Profilins are actin-binding proteins and influence actin dynamics via their binding. In the central nervous system, neuronal transmission depends on cell morphology. Therefore, profilins are of high importance in neurons. The two isoforms of profilin are relevant for cellular functions and are therefore closely related to synaptic plasticity and processes such as learning and memory formation. However, the exact influence of the two isoforms of profilin on various cellular functions has not yet been conclusively investigated. It is known that profilins can have isoform-specific and also overlapping functions.

In the mouse hippocampus, profilins modulate the actin network, resulting in changes in the morphology of dendrite and spine processes. Although the function and regulation of profilins is critical for neuronal morphology, the resulting physiological consequences have not been studied in detail. To be able to study the role of both isoforms in neuronal systems, the CRISPR Cas9 genome editing system was used. Thus, cell type- and isoform specific knockout of profilins can be achieved. In this context, simultaneous knockout of both profilin isoforms precluded mutual compensation.

Analyses of neuronal morphology in primary hippocampal cultures indicate an essential role for profilin2a in dendritic complexity, confirming previous studies from this laboratory. Combining the Cas9 genome editing system with the adeno-associated viruses allowed the study of mouse behavior in learning and memory. This work shows for the first time cognitive impairments related to memory retrieval. Moreover, this study reports physiological deficits in amplitude and frequency of excitatory postsynaptic currents (EPSCs) as a consequence of the loss of the profilin. Intriguingly, this phenomenon did not occur in the case of a double knockout.

In summary, this work demonstrated the relevance of profilins for cellular morphology in hippocampal neurons, the necessity of both profilins in the hippocampus for learning and memory behavior, and finally an essential role of profilins in neuronal transmission.

Zusammenfassung

Profiline sind Aktin-bindende Proteine und beeinflussen über ihre Bindung die Aktindynamik. Im zentralen Nervensystem hängt die neuronale Transmission von der Morphologie der Zellen ab. Daher sind Profilin in Nervenzellen von einer hohen Bedeutung. Die beiden Isoformen des Profilins sind für zellulären Funktionen relevant und hängen daher eng mit der synaptischen Plastizität und Prozessen wie Lernen und Gedächtnisbildung zusammen. Der genaue Einfluss der zwei Isoformen von Profilin auf die verschiedenen zellulären Funktionen ist allerding noch nicht abschließend erforscht. Es ist bekannt, dass Profiline isoformspezifische und auch überlappende Funktionen haben können. Im Hippocampus der Maus modulieren die Profiline das Aktinnetzwerk, was zu einer Veränderung der Morphologie von Dendriten- und Dornenfortsätzen führt. Obwohl die Funktion und Regulation der Profiline für die neuronale Morphologie von entscheidender Bedeutung ist, sind die daraus resultierenden physiologischen Konsequenzen noch nicht genauer untersucht worden. Um die Rolle beider Isoformen in neuronalen Systemen untersuchen zu können, wurde das CRISPR Cas9 Genome Editing System eingesetzt. So kann ein Neuronen- und isoformspezifischer Knockout von Profilinen erzielt werden. Dabei konnte durch den simultanen Knockout beider Profilin-Isoformen eine gegenseitige Kompensation ausgeschlossen werden.

Analysen der neuronalen Morphologie in primären hippokampalen Kulturen weisen auf eine essentielle Rolle von Profilin2a für die dendritische Komplexität hin, was frühere Studien aus diesem Labor bestätigen. Durch die Kombination des Cas9-Genome-Editing-Systems zur mit den Adeno-assoziierten Viren war die Untersuchung des Verhaltens von Mäusen in Bezug auf Lernen und Gedächtnis möglich. Diese Arbeit zeigt zum ersten Mal kognitive Beeinträchtigungen in Bezug auf Gedächtnisabrufens. Darüber hinaus berichtet diese Studie über physiologische Defizite in Amplitude und Frequenz exzitatorischer postsynaptischer Ströme (EPSCs) in Folge des Verlusts von Profilin. Erstaunlicherweise ist dieses Phänomen im Falle eines Doppel-Knockout nicht aufgetreten.

Zusammenfassend konnte in dieser Arbeit die Relevanz der Profiline- für die zellulären Morphologie in pyramidalen Neuronen des Hippocampus‘, die Notwendigkeit beider Profiline im Hippocampus für das Lern- und Gedächtnisverhalten und schließlich eine essentielle Rolle der Profiline in der neuronalen Transmission gezeigt werden.

Introduction

The human brain is an organ capable of the most wonderful capabilities, competences or skills. Basic instincts, decision making, cognitive functions and memory are a just a few of them. Regarded from outside the brain does not seem to be place for physiological and psychological processes which accompany our whole life. Therefore, trying to understand the underlying mechanisms in our brain has been the core focus of various scientific branches worldwide.

In 1881 the professor of pathology Heinrich Gottfried Wilhelm von Waldeyer-Hartz made an 'educated guess' and coined the term 'neuron' (Greek for 'nerve') as the cellular subunit of the brain. This was one of the first steps into the basic research of neuroscience as we know it today. Nowadays, the term 'neuron' still describes the smallest cellular subunit of the brain but also includes a variety of subtypes with different morphology and function of approx. 100 billion cells in different brain regions. However, an end of complexity is far from being reached here.

In 1858 the scientist, author, politician and "pope of medicine" Rudolf Virchow reported from glia cells (Greek for glue) in the brain in his publication "Cellular Pathology". For the majority of the 20th century, these cells were considered as a matrix, merely a scaffold for neurons and thus of much less importance. Santiago Ramón y Cajal who worked with golgi stainings did further classification of neurons and glia cells.

Today, the interaction and connectivity between neurons and the three glia cell types known: astrocytes, microglia and oligodendrocytes. The relationship between these cell types in heath and disease is studied only to limited extend. Aspects of development, maintenance and plasticity of the neuronal network, surveillance, inflammation and aging are just some processes which involve a variety of cell types, their interaction and regulation in and beyond the central nervous system.

The concept of the chemical synapse as a connection of two neurons where electrical stimuli were transmitted is outdated. Synapses are seen as plastic units of tight regulation and are more illustrated as a tripartite or even quadripartite synapse consisting of 2 neurons, astrocytes and partly of microglia. Furthermore, the communication of neural cells is plastic. This plasticity the main reason for our brain's capability to react, learn and adapt and forget to an ever changing environment.

The hippocampus and learning and memory

Most interesting was an observation after brain surgery of a schizophrenic patient in 1957. After the removal of larger parts the hippocampus, Henry Molaison lost the ability to memorize recent events. The research on patients treated similarly indicated that certain experiences were processed in the hippocampus but also suggested the existence of different types of memory (Scoville and Milner, 1957). Due to these revolutionary findings several studies aimed at enlightening the hippocampal functions. Impairment of memory function due to hippocampal damage suggested that the hippocampus is involved in the encoding and retrieval of spatial information as well as the terms long and short term memory (Morris et al., 1982, Morris et al., 1986).

The hippocampus named after the typical curved form (Greek for 'seahorse') is localized in the medial temporal lobe of both hemispheres. The three cellular layers *stratum oriens, stratum pyramidale* and *stratum radiatum* of neurons form the *cornu ammonis* (CA) and build with the dentate gyrus (DG) the hippocampus. The formation of the three major regions, the DG, the CA1 and CA3 sub regions, build the 'trisynaptic loop' (Figure 1) which is described to inhabit the neurons necessary for spatiotemporal processing of information (Andersen, 1975).

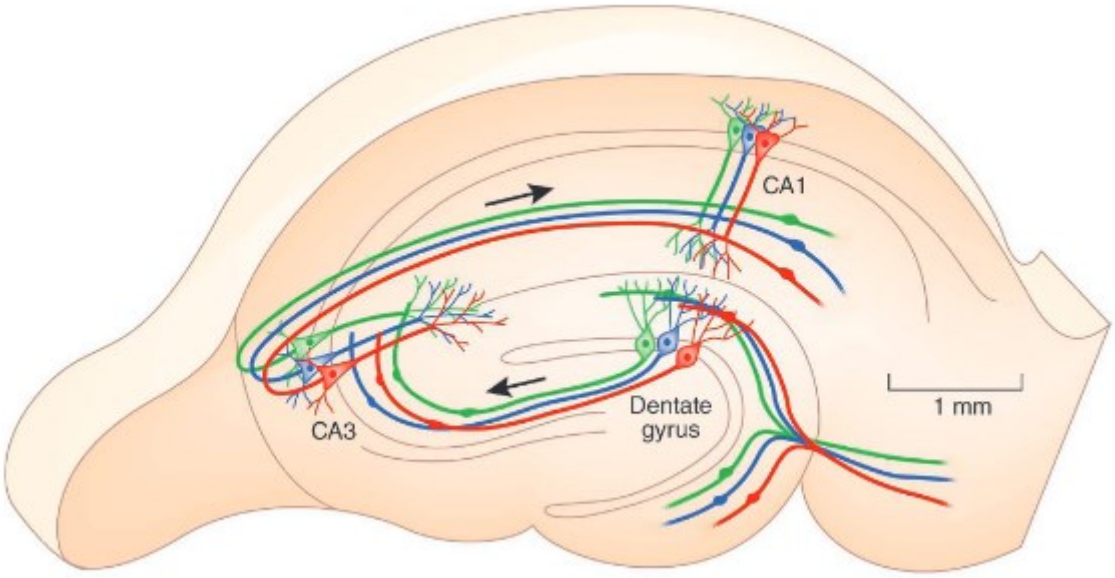

Figure 1: A Scheme of the dorsal hippocampus with the 'trisynaptic loop' connecting the dentate gyrus and the CA3 and CA1 subregion (Moser, 2011). The transmission originating from the entorhinal cortex excite cells in the DG. The signals succeed to the pyramidal cells of the CA3 via the mossy fibers and in turn the projection of input

from CA3 to CA1 neurons via the Schaffer collateral pathway. The cells of the CA1 area project their axons to the subiculum and also to the entorhinal cortex.

Therefore, transmission to the hippocampus and from the entorhinal cortex and the cortical regions activates these areas simultaneously. During the processing of input, the neuronal synapses are strengthened over time. The experience is then coded in cells and synapses which were activate during the experience from the different brain regions, forming an engram (Tanaka and McHugh, 2018). Over time the engram and the according synaptic characteristics may be transferred to cortical brain regions. A hypothesis nowadays is that the hippocampal originated engram serves as a framework for cortical representation, a storable pattern of cellular activity during experience. However, the mechanistic and cellular processes which underlie memory formation, transfer and recall remain elusive.

Hippocampal neurons

The hippocampus is mostly inhabited by excitatory pyramidal neurons which can be distinguished according to their morphology. These neurons are known to be involved in learning and memory processes (Morris et al., 1986, Magee and Johnston, 1997, Dupret et al., 2007) and connected via synapses. The pyramidal neurons in the CA1 and CA3 hippocampal area consist of cell soma shaped in a triangle like form and dendritic tree which can be divided into apical (

Figure 2, a) and basal dendrites (

Figure 2, b). The dendrites of all three cell types form small membrane protrusions which are called spines. These dendritic spines are part of synaptic connections and form the postsynaptic compartment.

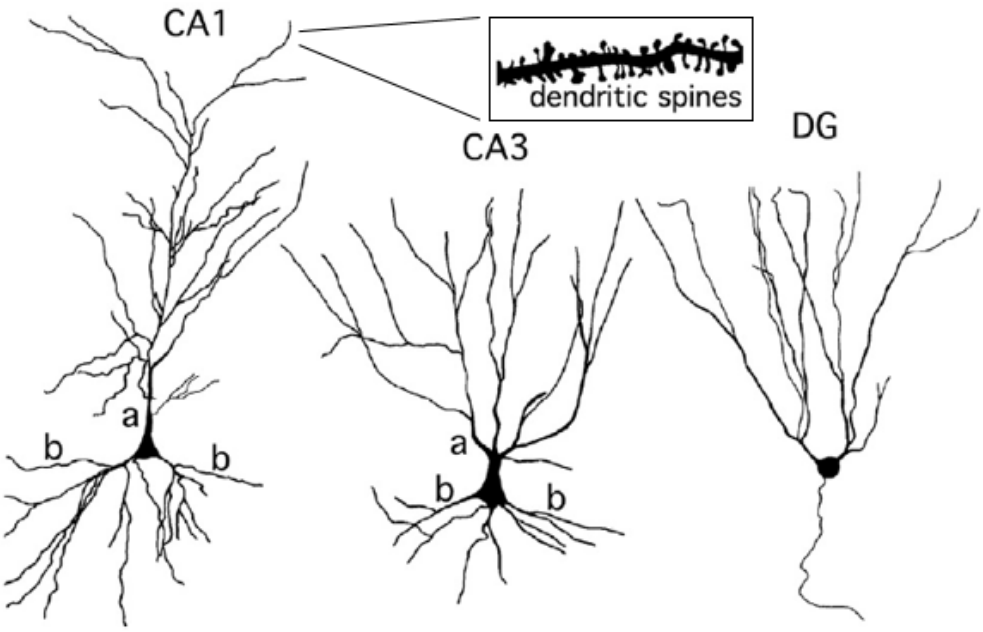

Figure 2: Hippocampal neurons and their differences in morphology. CA1 and CA3 pyramidal neurons with multi-branching apical **(a)** and basal **(b)** dendritic tree. Dendritic spines are present on all cell types' dendrites (box). DG granular cell differs from pyramidal cells in morphology adapted from (Spencer and Bland, 2019).

Cells from the dentate gyrus belong to the granular cells. In the schematic representation, the DG cell is orientated with a dendritic tree facing upwards and an axon emerging at the bottom, whereas only the dendritic tree is displayed of the pyramidal cells. Furthermore, the hippocampus inhabits interneurons as well as glia cells like astrocytes, microglia and oligodendrocytes. Thereby neurons are closely connected via synapses formed by the dendritic spines and axonal buttons.

Synaptic transmission and plasticity

Synaptic connections consist of a presynaptic button and a postsynaptic spine which protrudes from dendrites. The arriving action potential causes a depolarization of the synaptic button via Ca^{2+} influx and initiates presynaptic vesicles fusion with the membrane. The neurotransmitter causing either excitation of inhibition diffuses into the synaptic cleft and finally binds to postsynaptic receptors. The binding on the postsynaptic site initiates an opening of Ion permeable channels. Due to the resulting influx of sodium and following calcium ions the postsynaptic membrane also depolarizes. If the amplitude of the electrical

stimulus is strong enough, mostly by input of multiple synapses the signals accumulate in the cell soma and when overcome the threshold limit another action potential will built up and stimulate subsequent cells.

Cellular mechanisms underneath these processes are complex are supposed to be tightly regulated in space and time (Figure 3). It includes the maintenance of the membrane potential and ion homeostasis, the preparation and recycling of presynaptic vesicles. Furthermore, it involves the clearance and involvement of intercellular connection to glia cells like astrocytes and microglia. Finally, postsynaptic receptor presentation and retraction, ion homeostasis, local protein synthesis and membrane potential as well as regulation of cytoskeletal dynamics are elements contributing to synaptic plasticity.

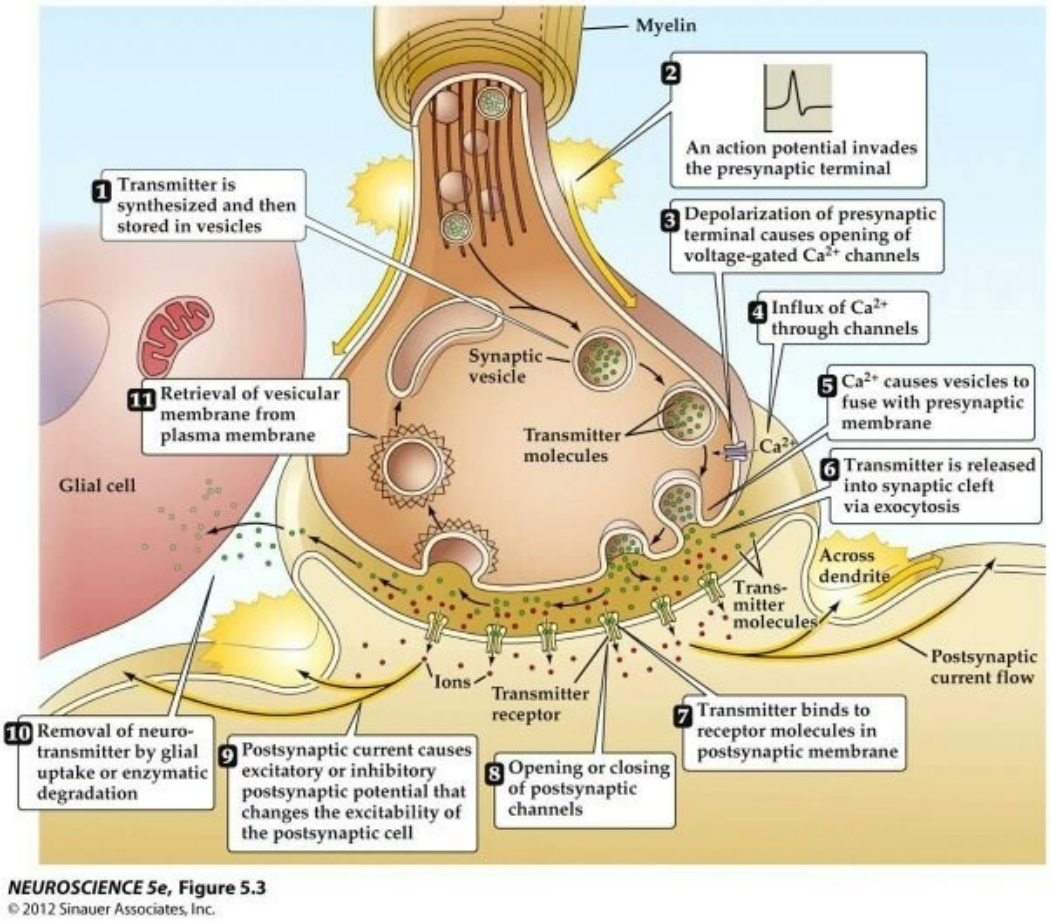

Figure 3: Schematic view of a chemical synapse: Incoming action potential is driving depolarization of presynaptic button and vesicle fusion with the membrane. Neuronal transmitter travelling through synaptic cleft and bind to postsynaptic receptors. Receptor binding causes postsynaptic ion channels to open and postsynaptic signals evoked. Recycling of neurotransmitters and ion homeostasis rebuild after this event (from textbook "Neuroscience", 5th Edition, 2012, Sinauer Associates, Inc.).

For the longest time the synapse itself has been considered as the locus of memory storage. Back in 1894 Ramòn y Cajal postulated that the morphological changes in synaptic connections could be key to the storage of information. Although his work was mainly anatomical in nature, the hypothesis laid the foundation for today's view of cellular processes during electrical stimulation, paving the way for current branches of research.

To provide a holistic picture of the mechanisms underlying synaptic plasticity, the mentioning of correlation of structural and functional plasticity is inevitable. Donald Hebb was the first who could provide evidence that synaptic connections strengthen due to the simultaneous stimulation:

“When an axon of Cell A is near enough to excite a Cell B and repeatedly or persistently takes part in firing it, some growth process or metabolic change takes place in one or both cells such that A’s efficiency, as one of the cells firing B, is increased.” ((Hebb, 1949), p. 62) (Morris, 1999). This fundamental idea still coins the phrase “what fires together wires together” and is the base of today’s picture of synaptic plasticity.

Following studies could indeed prove the correlation of synaptic strengthening in an activity-dependent manner, called long term plasticity, and on the other hand weakening over time, called long term depression. Thereby, the structural plasticity is based on the actin cytoskeleton. Therefore, the regulation and dynamics of the actin filament are closely connected to the physiological property like synaptic currents due to receptor presentation on the post synaptic density (PSD).

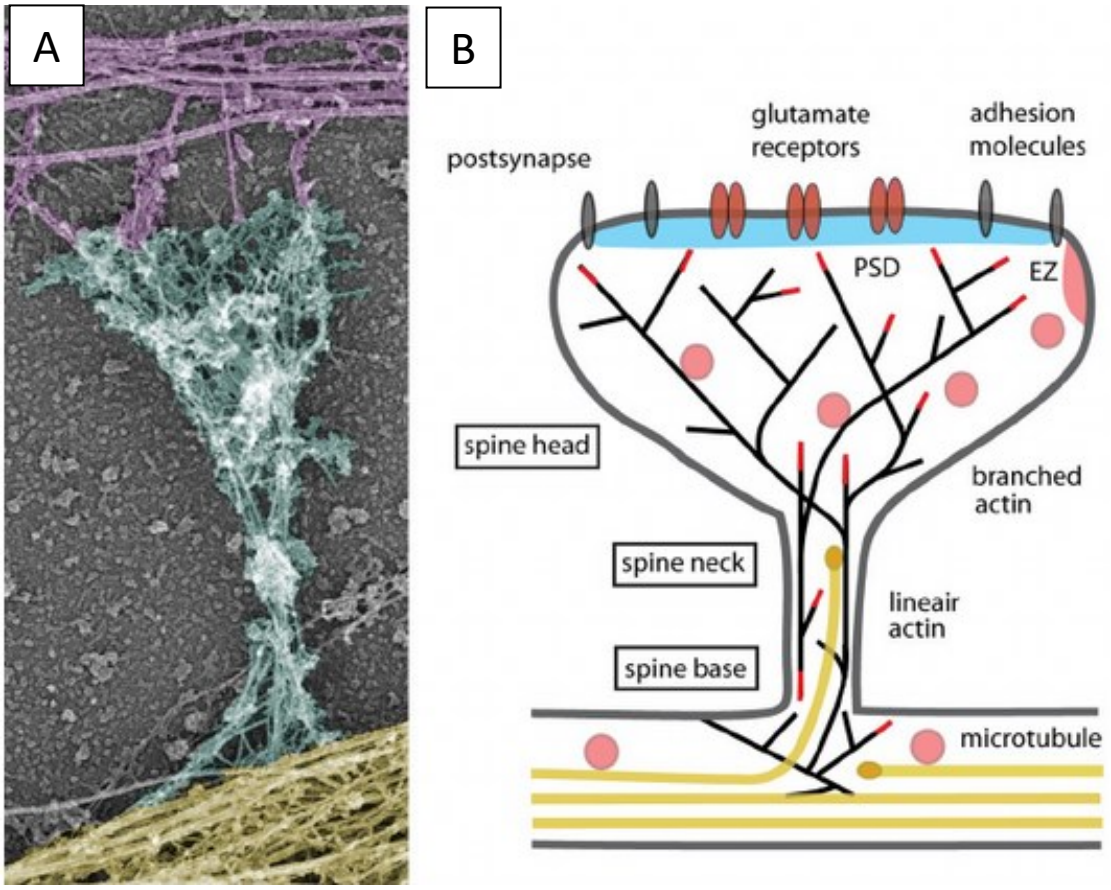

Figure 4: Dendritic spines and the actin cytoskeleton. **(A)** Actin and microtubule cytoskeleton organization in a mature dendritic spine from cultured hippocampal neurons visualized by platinum replica electron microscopy. Axonal cytoskeleton (purple), dendritic shaft (yellow) and dendritic spine (cyan). The spine head typically contains a dense network of short cross-linked branched actin filaments, whereas the spine neck contains loosely arranged longitudinal actin filaments, both branched and linear. **(B)** Schematic diagram of a mature mushroom-shaped spine showing the postsynaptic membrane containing the postsynaptic density (PSD; blue), adhesion molecules (gray) and glutamate receptors (reddish brown), the actin (black lines) and microtubule (yellow) cytoskeleton, and organelles. The endocytic zone (EZ) is located lateral of the PSD in extrasynaptic regions of the spine and recycling endosomes (pink) are found in the shaft and spines. Figure and text adapted from (Hotulainen and Hoogenraad, 2010).

Actin dynamics in dendritic spines

Interestingly, the dynamic regulation of the postsynaptic cytoskeleton is the key to structural plasticity. The actin cytoskeleton is the main structural compartment in dendritic spines and is essential for spine development and plasticity. The initiation of spine formation is believed to be random based as well as signal-induced. Thereby free, globular actin monomers (G-actin) serve as the pool for actin filaments (F-actin) with then can occur as linear structure or a branched network. For the elongation of F-actin the protein profilin is necessary. Moreover, there are a variety of actin regulation proteins involved in the nucleation, branching and

capping as well as the depolymerization via actin depolymerization factors (ADFs) like cofilin and recycling of network components. This process must be regarded highly dynamic in the spine tips (turn over times of approx. 40 seconds) (Honkura et al., 2008) and is described as a 'treadmilling' process that takes place during reorganization of actin filaments (Wegner, 1976).

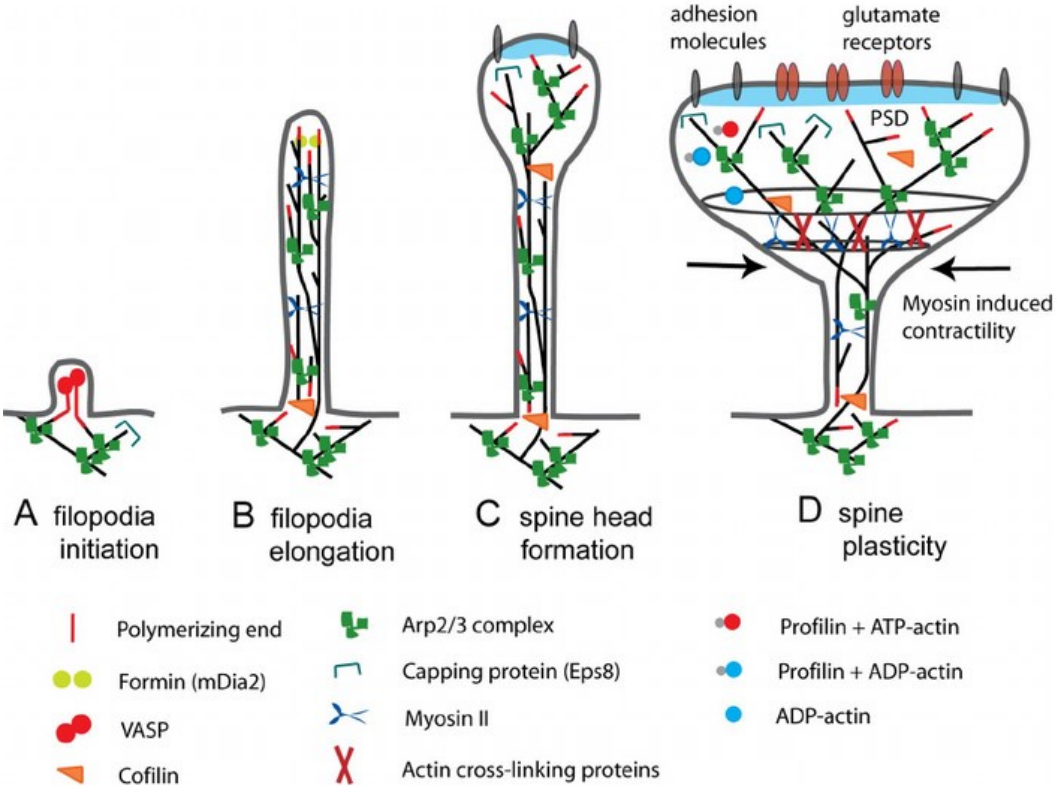

Figure 5: Actin regulatory mechanisms during spine development and plasticity. **(A)** Spine development starts with the initiation of the dendritic filopodium and its elongation. Ena/VASP proteins could induce filopodia elongation from Arp2/3 complex–generated branched filaments by anti-capping the actin barbed ends. **(B)** mDia2 promotes actin filament polymerization in the filopodium tip. Ena/VASP and myosin X might take part in filopodia elongation. At this stage, the elongation of dendritic filopodia protrusions is mechanistically more similar to the promotion of lamellipodia protrusions. The factors driving actin filament polymerization in the base of filopodia remain to be identified. **(C)** Extensive actin branching occurs at the filopodium tip and the spine head begins to form. The mechanism of actin assembly is now increased and the large Arp2/3-nucleated branched actin filament network leads to enlargement of the spine head. The function of ADF/cofilins, in addition to replenishing the cytoplasmic actin monomer pool in neurons, is to control the proper length of actin filaments and thus to prevent formation of abnormal protrusions from spine heads. **(D**) Mature spines are still dynamic but maintain their overall morphology. Dynamics occur as small Arp2/3 complex–induced protrusions on the surface of the spine head (morphing). Myosin II–dependent contractility and cross-linking of actin filaments further modulate the shape of the spine head. During LTP, the activities of Arp2/3, profilin, actin cross-linking proteins, myosin II, and actin filament capping proteins might be increased whereas activity of cofilin is reduced. The actin-ring structure is oversimplified to highlight the possible dynamic changes in the spine head morphology. Figure and text adapted from (Hotulainen and Hoogenraad, 2010).

Neuronal profilin involved in actin regulation and formation

Profilin (Pfn) is one of the actin binding protein and is involved in its regulation. Profilin is a 15 kDa small protein which is conserved in all eukaryotes. From its discovery in 1976 by Carlsson and coworkers via co-immunoprecipitation with monomeric actin (Carlsson et al., 1977), profilins were found and studied in various organisms. The diversity of organisms profilin was found in differes from lower eukaryotes to fungi, plants invertebrates and vertebrates. There has been evidence of a viral analogue of this small protein (Blasco et al., 1991). Although the sequence varies over the different species, the tertiary structure is conserved (Schluter et al., 1997, Jockusch et al., 2007). In mammalians there are four isoforms of profilins (Birbach, 2008). The conserved structure but not sequence indicates an evolvement prior to the according taxonomic classes. Pfn1 is expressed ubiquitously whereas profilin 2 and both of its splicing variants Pfn2a and Pfn2b are neural tissue restricted (Di Nardo et al., 2000), which rose the question of isoform specific and overlapping functions. The isoforms profilin 3 is kidney and profilin 4 testis specific expressed.

Interestingly, in neuronal tissue the isoform Pfn2 is most abundantly expressed in contrast to the rest of the body in which profilin 1 is dominant (Witke et al., 2001).

The profilins have a binding site for actin (Carlsson et al., 1977) which is also capable of the interaction with actin related proteins like Arp2 and Arp3 (Machesky et al., 1994, Rotty et al., 2015). The different isoforms of the protein have the capability of protein binding due to a poly-L-proline binding site (PLP). This PLP site allows interaction with several actin related proteins like Ena/VASP, formins, WAVE/WASP (Reinhard et al., 1995, Chang et al., 1996, Miki et al., 1998).

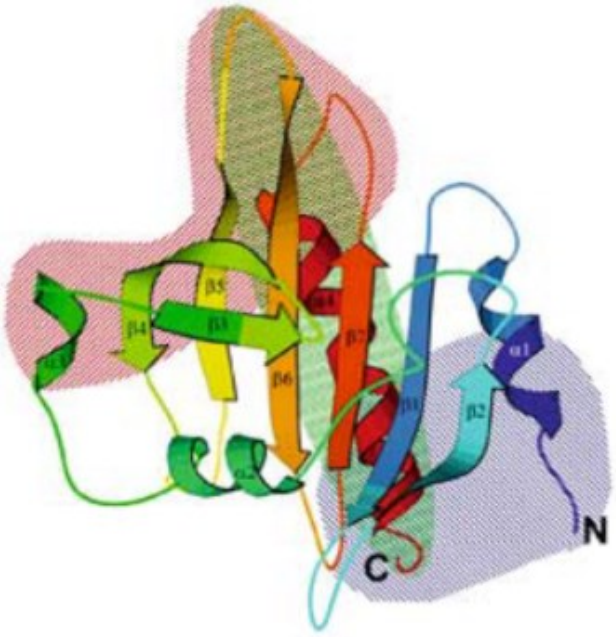

Figure 6: The three major ligand-binding sites on profilin. Schematic representation of the binding sites for actin (red), poly-L-proline (PLP, blue) and phosphatidylinositol-4,5-bisphosphate (PIP2, green) on the surface of a profilin molecule. Note that the PIP2-binding area forms an extensive patch which overlaps with the binding areas for actin and PLP (Jockusch et al., 2007).

Moreover, profilins are able to bind phosphatidylinositol-4,5-bisphosphate (PIP_2) (Lassing and Lindberg, 1985, Goldschmidt-Clermont et al., 1990b). The binding of profilins of PIP_2 at the membrane prevents the lipid of hydrolyzing by the phospholipase C (PLC)γ1 to inositol trisphosphate (IP_3) (Sohn et al., 1995). Profilin1 contains even two binding sites for these lipids (Skare and Karlsson, 2002) (Figure 6, green).

The resulting physiological functions of the different profilin isoforms in mammalian cells differ. The main function of profilin is the binding of ADP-actin and the catalyzing of ADP to ATP-actin monomers. The change of the ADP bound status to the ATP-bound state of actin monomers leads to a recycling of the pool of ready-state molecules of G-actin which can bind to the (+) end of actin filament and thus contribute to elongation and polymerization (Goldschmidt-Clermont et al., 1991). Although it was described as an actin filament sequestering protein in the past, the providing of G-actin ATP monomers and thus the contribution to actin filament polymerization is regarded as its main function. Moreover, the varying cellular localization of profilins indicate even more functions. The PIP_2 binding relocates cytoplasmic profilins to the membrane, whereas Pfn2a has been shown to be localized in an activity dependent manner in dendritic spines (Ackermann and Matus, 2003).

Due to the interaction with membrane associated proteins, profilins has been shown to be involved in endocytosis (Witke et al., 1998, Gareus et al., 2006) and the neuronal machinery of exocytosis which is an essential mechanism for synaptic vesicle release (Pilo Boyl et al., 2007).

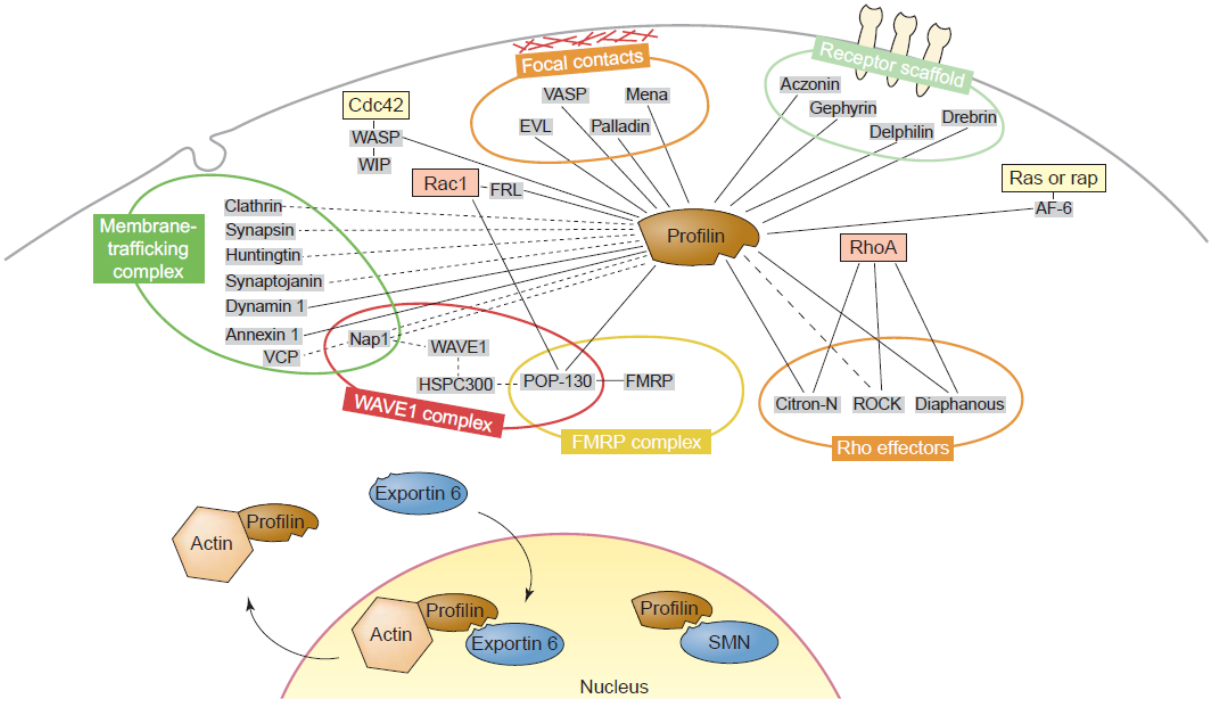

Figure 7: Network of molecular interactions of profilin. Abbreviations: AF-6, All-1 fusion partner from chromosome 6; EVL, Ena VASP like; FMRP, fragile X mental retardation protein; FRL, formin-related gene in leukocytes; HSP, heat-shock protein; Mena, mouse homolog of Drosophila enabled; POP, partner of profilin; SMN, survival of motor neuron; VASP, vasodilator-stimulated phosphoprotein; VCP, valosine-containing protein; WASP, Wiskott–Aldrich syndrome protein; WAVE, WASP family verprolin-homologous protein; WIP, WASP-interacting protein (Witke, 2004).

Proteins that are known to interact with profilin are grouped according to their cellular location or the complexes in which they are found. Some of the profilin ligands are shared among different complexes (indicated by the intersecting fields), which suggests a crosstalk among signaling platforms, with profilin as the common denominator. Several links exist to small GTPases such as Rac1, RhoA, cdc42, Ras and Rap that are part of pathways that signal to the actin cytoskeleton (Figure 7). For simplicity, the term profilin is commonly used for profilin 1 and profilin 2. Direct interactions between profilin and the ligands are indicated by unbroken lines, whereas potentially direct interactions are indicated by broken lines.

Due to the numerous and various functions of profilin, the regulation of profilin itself is tightly controlled. Profilin2a provides due to the amino acid sequence 14 residues which can be phosphorylated (Walter et al., 2020). The position 137 is well studied. Ser-137

phosphorylation of profilin1 has been reported to inhibit cytoplasmic functions. Moreover, the amino acid residue phosphorylation and cellular localization has been reported to interfere in tumor inhibition (Diamond et al., 2015). Despite these studies of the phosphorylation sites the physiological relevance and cellular consequences are poorly understood.

Furthermore it was reported that profilin2a but not 1 is essential for dendritic complexity (Michaelsen et al., 2010). Highly interesting results indicated an isoform specific function for Pfn2a in the dendritic complexity as the reduction could not be restored by simultaneous overexpression of pfn1 in pfn2a knockdown cells. Moreover, the induction of pfn1 overexpression could rescue the deficits in spine density after the shRNA mediated knockdown of profilin2a. These results highlighted the complex and thigh regulation of neuronal actin dynamics and also emphasized the possibility of isoform specific as well as overlapping functions of this protein. But not only in neurons profilins fulfill interesting functions. In astrocytes, the most abundant glia cell type in the mammalian brain, both profilin1 and 2a are expressed and are involved in morphology as well as the motility of astrocytic protrusions (PAPs) (Molotkov et al., 2013, Schweinhuber et al., 2015).

Neuronal profilin isoforms have also been reported to be addressed by different signaling pathways which both react to KCl-based activated synapses in terms of protein concentration but only Pfn2a respond to postsynaptic NMDA receptor activity (Murk et al., 2012). In the course of studying the relevance of profilins, the Pfn1 knockout mouse revealed no alteration in physiological neuronal functions (Gorlich et al., 2012). This was striking as the structural and functional plasticity as believed to be closely related.

Interestingly, the behavior study of fear conditioning in rats could show an increase in profilin level in dendritic spines (Lamprecht et al., 2006). Pilo-Boyl and colleagues could show that the genetic deletion of profilin2a leads to an increased novelty seeking behavior which could result of a higher vesicle release probability and more presynaptic vesicles in the presynapse of the knockout animals (Pilo Boyl et al., 2007).

Aim of study

The modulation and regulation of the actin cytoskeleton is not only important for basic cellular functions such as motility and cell shape, but also for neuronal morphology, which is closely linked to functional plasticity. Furthermore, the importance of functional brain regions such as the hippocampus, which is associated with learning and memory, has been shown to depend on proper neuronal signaling. Neuronal morphology, specifically dendritic complexity and spine density and morphology, are crucial for cognitive functions. In this context, the regulation of actin dynamics plays an essential role for the expression of structural and thus also synaptic plasticity. Among the many actin-regulating proteins, the profilins are part of this complex machinery, whereby even two different isoforms are expressed in the central nervous system.

The aim of this study is to elucidate the cellular functions of profilins 1 and 2a in the brain, identifying the specific and the overlapping functions of the isoforms in neurons. In particular, the targeted knockout of the profilins will be used to analyze their influence on neuronal morphology and physiology as well as on the processes of learning and memory formation. By using the CRISPR Cas9 editing system in combination with recombinant adeno-associated virus particles, it will be possible to investigate the link between cellular functions and the level of learning behavior.

In summary, this study will provide evidence to support the following hypotheses:

- Profilin acts as a key regulator of dendritic and spine morphology.
- Profilin modulates learning and memory behavior.
- Profilin is critical for neuronal transmission.

Material and Methods

AbbreviationsaCSF Artificial cerebrospinal fluid

ADP	Adenosine di-phosphate
ATP	Adenosine tri-phosphate
CA	cornu ammonis
CTRL	Control
DIV	Days *in vitro*
dpt	Days post transduction
F-actin	Filamentous actin
G-actin	Globular actin
GFP	Green fluorescent protein
HBSS	Hanks balanced salt solution
IP_3	Inositol triphosphate
KI	Knockin
KD	Knockdown
KO	Knockout
mEPSC	Miniature excitatory postsynaptic currents
ms	Millisecond
MT	Mutant
NB(-)/NB(+)	Neurobasal (-) medium / Neurobasal (+) medium
NMDAR	N-methyl-D-aspartate receptor
PCR	Polymerase chain reaction
PFA	Paraformaldehyde
Pfn	Profilin

Pfn1	Profilin 1
Pfn2a	Profilin 2a
PIP_2	Phosphatidylinositol-4,5-biphosphate
PLC	Phospholipase C
PSD	Postsynaptic density
PVDF	Polyvinylidene fluoride membrane
RNA	Ribonucleic acid
ROCK	Rho-associated protein kinase
sEPSC	Spontaneous excitatory postsynaptic currents
SDS-PAGE	Sodium dodecyl sulfate polyacrylamide gel electrophoresis
shRNA	Short hairpin RNA
WAVE	WASP-family verprolin-homologous protein
WT	Wildtype

Materials

Devices

Table 1 Devices

DEVICE	NAME
APOTOME SOFTWARE	LEICA System
CFX CONNECT REAL-TIME PCR	Detection Systems BIORAD
CRYOTOME 'CM3050 S'	Leica Biosystems
ELISA READER EPOCH	BioTek Instruments, Inc.
FLUORESCENT MICROSCOPE	Zeiss Axioplan 2 and M2
MRX MICROPLATE READER	Dynatech Medical Products
O2/ISOFLURAN VAPORISER	Norvap International

„LUNA VAPORISER TEC 3 STYLE, KEY FILL LUNA“	
RODENT HEAD FIXING APPARATUS	STOELTING Co.
SINGLE CELL ELECTROPORATOR ‘AXOPORATOR 800A’	Axon CNS, Molecular Devices
STED/CONFOCAL MICROSCOPE	LEICA DMi8 M
STED/CONFOCAL SOFTWARE	LEICA App Suite X 3.5.5.199976
VERTICAL MICROPIPETTE PULLER ‘PC-10’	Narishige
VIBRATOME “VT 1000S”	LEICA
WARMING PADS „RODENT WARMER X2”	STOELTING

Reagents

Reagents and enzymes were ordered from Sigma-Aldrich Chemie GmbH, Sigma-Aldrich Chemie GmbH, Carl Roth GmbH & Co. KG, Applichem and NEB if not stated otherwise.

Media, buffers and solutions

LYSOGENY BROTH MEDIUM (LB)		
	Trypton	10 g/L
	NaCl	10 g/L
	Yeast extract	5 g/L
IF NECESSARY MIXED WITH AMICILLIN (FINAL CONC. 100 µG/L)		

Table 2 Media for cell culture use

NAME	**DISTRUBUTOR**
NEUROBASAL MEDIUM (NB-),#21103049	Thermo Fisher
FCS	PAA Laboratories
DULBECCO'S MODIFIED EAGLE MEDIUM (DMEM)	Gibco (ThermoFisher)

CULTURE MEDIUM, NB+ PRIMARY CULTURES		
	Neurobasal medium (NB-)	45 mL
	B27	1 mL
	L-Glutamin	125 µL
	N2 (10x)	5 mL

GEY'S BALANCED SALT SOLUTION		
	CaCl2*2H2O	1.5 mM
	D-Glucose	5.5 mM
	KCl	5 mM
	KH2PO4	0.22 mM
	MgCl*6H2O	1 mM
	MgSO4*7H2O	0.28 mM
	NaCl	137 mM
	NaHCO3	2.7 mM
	NaH2PO4	0.86 mM
DILUTE IN DH_2O; STERILE FILTRATE (STORE AT 4°C)		

KYNURENIC ACID		
	Kynurenic acid	946 mg
	NaOH 1 M	5 mL
ADD 45 ML DH2O; STERILE FILTRATE (STORE IN 1 ML FRACTIONS AT -20°C)		

ANTIMOTICS		
	Uridine	1 mM
	Cytosin-β-D-Arabinofuranosid Hydrochlorid	1 mM
	5-Fluoro-2´-Deoxyuridin	1 mM

STOCK SOLUTIONS 1:1; STERILE FILTERED (STORED AT -20°C)

SERUM MEDIUM		
	DMEM	10 mL
	FCS	200 µL

PREPARATION SOLUTION ORGANOTYPIC CULTURES		
	GBSS	98 mL
	Glucose (50%)	1 mL
	Kynurenic acid	1 mL

ADJUST PH TO 7.2 (1 M HCL), STERILE FILTRATED (STORE AT 4°C)

CULTURE MEDIUM ORGANOTYPIC CULTURES		
	BME-Medium	100 mL
	HBSS	50 mL
	Equine donor serum	50 mL
	L-Glutamin (200mM)	1 mL
	Glucose (50%)	2 mL

Table 3 Components used for cell culture transfection

ACSF (PH 7.3-7.4)		
	NaCl	125 mM
	KCl	2.5 mM
	NaH2PO4 *6H2O	1.25 mM
	MgCl2 *6H2O	2.0 mM
	NaHPO3	26.0 mM
	D+-Glucose (waterfree)	25.0 mM
	CaCl *2H2O	2.0 mM

Table 4 Components used for cell culture transfection

COMPONENT	DISTRUBUTOR
B27	Gibco
L-GLUTAMIN	Gibco
LIPOFECTAMINE® 2000	Invitrogen

Table 5 Components for electrophysiological experiments

COMPONENT	DISTRUBUTOR
TETRODOTOXIN CITRATE	Torcris

Table 6 Components used for stereotactic injections

NAME	DISTRUBUTOR
“AUGEN UND NASENSALBE BEPANTHEN®”	Bayer
DESINFECTION SOLUTION “BETAISODONA”	Mundipharma GmbH
ISOFLURANE CP (1ML/ML)	CP pharma
THREAD 7-0 BV175-8	Prolene™
VETERINARY FLUOSORBER	Havard apparatus

Table 7 Components used for cryotome cutting

NAME	DISTRUBUTOR
O.C.T. TISSUE-TEK	Sakura Finetek
BLADES FOR CRYOTOME	Leica
BRUSH	Farber castell

Buffers sorted by matter of experiments

Table 8 Buffers used for Genotyping

10X TAE		
	Tris-HCL pH 7.5	48.46 g
	Eisessig	12.01 g
	EDTA *Na2*2 H2O	3.72 g
	in MQ-H2O	1 L

1X TAE		
	10x TAE Buffer	200 mL
	MQ-H_2O	1800 mL

TRIS HCL		
	TRIS diluted (in H2O)	10 mM or 100 mM
ADJUST PH WITH HCL TO 7.5 OR 8.0		

CELL LYSIS BUFFER		
	Tris HCL, pH 7.5	10 mM
	EDTA	10 mM
	NaCl	100 mM

Table 9 Buffers for biochemical experiments

10X MEOH BLOT BUFFER		
	TRIS	0.25 M
	Glycine	1.5 M
	MQ-H_2O	Ad 2 L
	adjust pH to 8.6	

1X MEOH BLOT BUFFER		
	Methanol	100 mL
	10x MeOH blot buffer	100 mL
	in MQ-H2O	800 mL

10X TBS-T		
	TRIS	0.2 M
	NaCl	1.37 M
	Tween 20	0.1%
IN MQ-H_2O ADJUST PH TO 7.6		

1X TBS-X		
	10x TBS-X	200 mL
	MQ-H_2O	Ad. to 2 L

1X TBS-T		
	10x TBS-T	200 mL
	in MQ-H2O	1.8 L

10X TBS-X PH TO 7.6		
	TRIS	0.2 M
	NaCl	1.37 M

	Triton-X 100	0.1%
	in MQ-H2O	

BRADFORD REAGENT 5X		
	Phosphoric acid	100 mL
	Ethanol	50 mL
	Coomassie Brilliant Blue G250	100 mg
	in MQ-H2O	100 mL

LYSIS BUFFER FOR WESTERN BLOT		
	Tris-HCl pH 7.5	30 mM
	NaCl	150 mM
	Chaps	1%
	MQ-H_2O	

MILK 5% IN TBS-T		
	Milk powder	5% (W/V)
	in 1x TBS-T	

SDS BUFFER 4X		
	Tris-HCL pH 7.5	0.375 M
	SDS	2%
	Glycerol 87%	12%
	Bromphenol blue	0.05% (V/V)
	ß-Mercaptoethanol	10% (V/V)

STKM BUFFER (+)		
	Saccharose	250 mM
	Tris-HCL pH 7.5	50 mM
	KCl	25 mM
	$MgCl_2$	5 mM
	PIMM	1/1000
ADJUST PH TO 7.5 AT 4°C		

BRADFORD REAGENT 5X		
	Phosphoric acid	100 mL
	Ethanol	50 mL
	Coomassie Brilliant Blue G250	100 mg
	In MQ-H_2O	100 mL

LYSIS BUFFER FOR WB		
	Tris-HCl pH 7.5	30 mM
	NaCl	150 mM
	Chaps	1%
	In MQ-H2O	

Table 10 Buffers used AAV production

LYSIS BUFFER FOR AAV HARVEST		
	Tris-HCl pH 7.5	50 mM
	NaCl	150 mM
IN MQ-H2O, PH 8.5		

REAGENTS FOR QPCR	DISTRIBUTOR	QC REPORT/ MODIFICATIONS	SEQUENCE
AAV2-ITR-FWD	eurofins	-	GGAACCCCTAGTGATGG AGTT
AAV2-ITR-FWD	eurofins	-	CGGCCTCAGTGAGCGA
AAV2-ITR-PROBE	eurofins	MALDI, 5'-FAM, 3'-BHQ1	CACTCCCTCTCTGCGCG CTCG
UNIVERSAL SYBR MASTER MIX 2X	Biozym		

Table 11 Buffers for electrophysiological experiments

INTERNAL SOLUTION		
	K-Gluconate	126 mM
	KCl	4 mM
	HEPES	10 mM
	MgATP	4 mM
	Na_2 Phosphocreatin	10 mM
	Na GTP	0.3 mM
	pH 7.3, 290 ± 10 mOsm	

Table 12 Solutions used for cryotome cutting

CRYOPROTECTION SOLUTION		
	1x PBS Buffer	50 % (V/V)
	Ethylene Glycol	20 % (V/V)
	Glycerol	30 % (V/V)

Usesd plasmids

Table 13 List of used plasmids

PLASMID NUMBER	NAME	PRODUCER
L81	pmApple-N1	M. W. Davidson
E411	pAAV U6-tGFAP-Cre	H. Demuth/M. Rothkegel
E418	pAAV-sgPFN1B-hSyn-Cre	D. Hinz/M. Rothkegel
E420	pAAV-sgPFN2A-hSyn-Cre	D. Hinz/M. Rothkegel
E452	pAAV-U6sgP1A+2B-hSyn-Cre	D. Hinz
E454	pAAV-U6sgP1B+2A-hSyn-Cre	D. Hinz
E455	pAAV-U6sgP1B+2B-hSyn-Cre	D. Hinz
E457	pAAV-U6sgP1C+2A-hSyn-Cre	D. Hinz
E463	pAAV-U6sgP1B+2A-tGFAP-Cre	M. Klasmeier
E472	pAAV-U6-sgLacZ-tGFAP-Cre	S. Henning/M. Rothkegel
E473	pAAV-U6-sgLacZ-hSyn-Cre	S. Henning/M. Rothkegel
E494	pAAV-2.13-delta-Apple-mPFN2a_mod	L. Schulz/ M. Rothkegel
E495	pAAV-2.13-delta-mApple-PFN2a_S138Amod	L. Schulz/ M. Rothkegel
E496	pAAV-2.13-delta-mApple-PFN2a_S138Dmod	L. Schulz/ M. Rothkegel
E509	pAAV-sgPFN2A-hSyn-Cre-T2A-Apple-F	T. Meßerschmidt

Table 14 List of used antibodies

ANTIBODY	ANTIBODY CLASS	DILUTION	HOST	USED FOR	DISTRIBUTOR	CATALOG NUMBER
À GAPDH	primary	1/9000	rabbit	WB	Sigma	G9545
À TUBULIN	primary	1/30 000	mouse	WB	Sigma Aldrich	T9026
À GFP	Primary	1/1000	mouse	IC	Millipore	MAB3580
À GFP	Primary	1/500	chicken	IHC	Sigma Aldrich	A2554
À PROFILIN 1 (P1C)	primary	1/5000	rabbit	WB	Sigma Aldrich	P7624
À PROFILIN 2A (AS361)	primary	1/20 000	rabbit	WB	Bioscience	-
À CRE RECOMBINASE	primary	1/1000	mouse	IHC	millipore	Mab3120
À RABBIT HRP	secondary	1/20 000	goat	WB	Sigma Aldrich	A0545
À CHICKEN IGG	secondary	1/500		IHC	Aves	F-1005
À RABBIT IGG	secondary	1/500		WB	Dianova	111-165-144
DAPI				IC/IHC	applichem	

SOFTWARE	DISTRIBUTOR
ADOBE ILLUSTRATOR	Adobe Systems Software
ANYMAZE	Stoelting Europe
EASYWIN32	Herolab GmbH
IMAGEJ	Wayne Rasband, NIH, USA
MICROSOFT EXCEL	Microsoft Corporation

MICROSOFT WORD	Microsoft Corporation
PRISM GRAPHPAD	Graph Pad Software Incorporation

Statistical analysis was performed via Prism Graphpad 8 and lower versions. A list of means, SEMs, statistic values and tests used can be found in the supplements.

Methods

Construction of plasmids

For construction of plasmids, here at the example of pAAV-U6sgP1B+2A-tGFAP-Cre plasmid, the insert of interest (sgPFN1B+2A) was amplified by PCR from vector B157-pCR-U6sgP1B+2A-KM. The vector backbone E411 pAAV-U6-tGFAP-Cre and the insert were cut with the same restriction enzymes to gain a linearized plasmid and insert that could be fit in reading direction of the respective promoter. In order to do so, a master mix for restriction was generated in which the enzyme was kept cool as long as possible and added last:

DIGESTION MIX	
DNA	2µg
10X CUT SMART BUFFER	2 µL
KPNI-HF	0.5µL
MLUI-HF	0.5µL
MQ H_2O	Ad. to 20 µL
TOTAL VOLUME	20 µL

The restriction mix was incubated for 2 h at 37°C. To investigate the result, DNA was loaded onto a agarose gel (0.8% - 1.2% agarose concentration) and separated by gel electrophoresis. Therefore, samples were mixed with 6x DNA sample buffer and a DNA ladder standard were loaded onto a 0.8% agarose gel (agarose concentration differed according to fragment size). Electrophoresis was performed with 80 V, 150 mA and 150 W for 30 min to 45 min. Next, the DNA fragments were identified using UV light and cut from the gel using blades.

After the photo documentation, the corresponding DNA fragments are cut out of the agarose gel and eluated using the DNA extraction kit QIAEx (QIAGEN, Hilden). The DNA fragments were mixed with 500 µL QX buffer in a 1.5 mL reaction tube and 10 µL glass milk were added. This

mix was shaken for 10 to 15 min at 50°C and then the samples are centrifuged for 1 min at 13000 rpm, RT. The supernatant was discarded and fresh 500µL QX buffer was added, vortexed and centrifuged and the supernatant discarded as in the step before. The pellet was then resuspended in 500 µL PE buffer and again centrifuged (1 min, 13000 rpm, RT).

The reaction tube was then placed in the thermomixer at 50 °C without shaking until the pellet was dry. Next, the pellet was resuspended in 20mM Tris-HCL buffer (pH 7.4) and shaken in the thermocycler for several hours. Finally, the samples were centrifuged with 13.000 rpm at RT for 3 min and the supernatant was transferred into a new reaction tube. The DNA concentration and purity was measured using a microliter photometer (Denovix).

The insert DNA was then used for ligation which was performed at 16°C overnight. Therefore, a ligation mix was prepared as seen below (Table 15):

Table 15 ligation mix

LIGATION MIX	
VECTOR DNA	0.5µg
INSERT DNA	5 µL
10X LIGATION BUFFER	1µL
T4 DNA LIGASE	0.5µL
MQ H_2O	Ad. to 10 µL
TOTAL VOLUME	10 µL

The ligation was proven by gel electrophoreses of the linearized plasmid and an additional restriction step with known fragment sizes and restriction sites which were only available after successful ligation. DNA gel electrophoreses was performed in a 0.8 -2% agarose gel in TAE buffer. The probe was mixed with DNA sample buffer 5 + 1 Volume equivalents and loaded onto the gel. Each gel also was loaded with a DNA standard to compare fragment sizes and amount of DNA. The gel was run for 45 min, 80 V, 150 mA and 150 W.

Transformation of competent bacteria

After ligation, DH5α or XL1 blue competent bacteria cells were transformed with the plasmid DNA from ligation. In order to do so, 200 µL of competent cells were gently defrosted at 4°C and 10 µL of the ligation mix were added on ice and incubated for 30 min. Next, a heat shock of 42°C for 90 s was performed to allow the plasmid DNA to enter the cell. Afterwards, 500 µL of lysogeny broth medium (LB medium) was added and the transformation mix was incubated 30 min at 37°C in a thermomixer. The samples then were plated onto LB agar plated containing an appropriate antibiotic that only allowed successfully transformed bacterial cells to grow due to the antibiotic resistance. The plated were incubated at 37°C overnight.

The next day, bacterial colonies were counted and 3 mL LB medium each were inoculated with individual colonies. These cultures were incubated for 4 h at 37°C shaking and upon opaque LB indicating medium bacterial grow the 3 mL were transferred sterile into 200 mL of LB medium and a MIDI preparation was performed.

Medium scale plasmid DNA preparation

Medium scale plasmid DNA preparation was performed using the QIAGEN MIDI Kit, which contained all mentioned buffers and reagents if not claimed otherwise and was modified as following.

24 h previous transformed *E. coli* colonies were picked and transferred in 3 mL LB medium with appropriate antibiotic and incubated several hours at 37°C until cloudiness was notable. The 3 mL cell suspension were transferred into 200 -250 mL LB medium with antibiotic and the culture was shaken at 37°C overnight.

After 14-16h the *E. coli* cells were harvested by centrifugation for 20 min at 6000 rpm and 4°C. The supernatant was discarded and the pellet was resuspended in 4 mL P1 buffer. The P1 was added freshly with 1/1000 RNAse and Lyse Blue before usage. Next 4 mL of P2 buffer were added to the sample and inverted 5 times carefully until the lysate got blue and incubated for 5 min at RT. Next 4 mL ice cold P3 was added and the sample was inverted 5 times until the lysate got white. The samples were incubated 20 min on ice and several times inverted. Afterwards, the lysates were centrifuged for 30 min and 20000 xg at 4°C. The supernatant was poured through a damped filter and loaded onto a with 4 mL QBT buffer preincubated column.

After the solution run through, the column was washed 2 times with 10 mL QC buffer. Next the DNA was eluated from the column by adding 5 mL QF buffer. 3.5 mL isopropanol was carefully to the eluate and then shaken thoroughly. The sample was centrifuged for 30 min at 4°C at 15 000rpm the supernatant was discarded. The DNA pellet was washed with 1 mL 70% non-denatured ethanol in MQ H_2O and transferred into a 1.5 mL reaction tube. The pellet was centrifuged for 10 min at 13 000 rpm and RT. The supernatant was discarded and washed in 1 mL 70% ethanol in MQ H_2O again. After this second washing step the DNA pellet was dried at 70°C and resolved afterwards in 200 µL 20 mM steril Tris-HCL buffer (pH 7.4). For resolving the sample was incubated overnight and shaken for 1 h at 37°C the next day. Finally, the DNA concentration was measured using a microliter photometer (Denovix).

Bl6/Cas9 mouse strain

Experiments done in this thesis were authorized by the animal welfare representative of the TU Braunschweig and the LAVES (Oldenburg, Germany, Az. §4 (02.05) TSchB TU BS). Mice were hold in standardized cages and lived in a 12h light/dark cycle. Food and water were given *ad libitum.* Mice were if not claimed otherwise in B6J.129 (B6N)-Gt(ROSA)26Sor $^{tm1(CAG-cas9*,-EGFP)Fezh}$/J (Rosa26-LSL-Cas9 knocking on B6J, Rosa26-floxed STOP-Cas9 knocking on B6J) (Platt *et al*. 2015). These mice had Cre recombinase-dependent expression of CRISPR associated protein 9 (Cas9) endonuclease and enhanced green fluorescent protein (eGFP) driven by a CAG promotor. By expression of a Cre recombinase in combination with a single guide RNA (sgRNA) the expression of Cas9 and eGFP was enabled and the knock out of a gene of interest targeted by the sgRNA was possible *in vivo* and *ex vivo*. For this study homozygote mice, which were viable and fertile were used.

DNA extraction of Bl6/Cas9 mice for genotyping

For Genotyping mouse tail biopsy was performed and DNA was extracted. Therefore, 410 µL DNA lysis buffer, 80 µL of 10% SDS and 10 µL proteinase K (10 mg/mL) was added to the tissue and incubated 2 h at 65 °C in a thermomixer. The sample was shaken until the tissue resolved and centrifuged 5 min for 13.000 rpm. The supernatant was transferred into a new 1.5 mL reaction tube and mixed with 225 µL 4M sodium chloride for 1 min until coagulation was

visible. The supernatant was transferred into a new 1.5 mL reaction tube and 450µL isopropanol was added and vortexed thoroughly. The sample was centrifuged 10 min for 13.000 rpm and the supernatant again transferred into a fresh 1.5 mL reaction tube.500 µL 70% Ethanol was added to the supernatant and vortexed for 30 sec. Next the sample was centrifuged at 13k rpm for 10 min at RT. This washing step was repeated. Finally, the supernatant was discarded and the pellet dried at 70 °C for 5 to 10 min and resuspended with 50 to 100 µL 10 mM Tris-HCl buffer (pH 7.5) and the concentration was measured via the nanodrop photometer.

PCR for genotyping

The genomic DNA from mouse tail biopsy was used to identify the genotype of mice via polymerase chain reaction (PCR) using specific primers for the gene of interest: the *hSpCas9* in the Rosa26 locus (Table 16).

Table 16 Primer used for genotyping

DATABASE SIGNATURE	TARGET	CONCENTRATION	SEQUENCE (BP)
G117, FORWARD	wildtype/mutant	5 pmol/µL	AAG GGA GCT GCA GTG GAG TA (20)
G118, REVERSE	wildtype	5 pmol/µL	CCG AAA ATC TGT GGG AAG TC (20)
G119, REVERSE	mutant	5 pmol/µL	CGG GCC ATT TAC CGT AAG TTA T (22)

The PCR was performed in a thermocycler as below (Table 17) with DNA extracted from mouse tail biopsy:

Table 17 PCR for genotyping

PCR SAMPLE		POLYMERASE CHAIN REACTION		
REAGENT	volume [µL]	step	Time [sec]	Temperature [°C]
SAMPLE DNA	1	1	30	94
5X QUICKLOAD BUFFER NEB	5	2	20	94
DNTPS [2MM EACH]	2	3	30	54
FWD PRIMER	2	4	30	68
REVERSE PRIMER	2	Steps 2 to 4 were repeated 40 times total		

ONE TAQ POLYMERASE [5U/µL] NEB	0.125	5	300	68
MILLIQ WATER	Ad to 25	6	∞	4

After the PCR was finished 5 µL of the sample was mixed with 5 µL of 6x DNA loading buffer and loaded onto a 2% agarose gel in TAE buffer. Additionally, a 50 bp Marker Fastload was loaded and the gel was run at 80 V, 150 mA, 10 W for 10 min. The result of the DNA gel electrophoreses was analysed on an UV table and documented.

AAV production

HEK 293T cell culturing

HEK 293T cells were cultured in DMEM with 4.5 g/L Glucose in 10 cm cell culture plate and passaged every 2 to 3 days according to cell density by using 0.2x Trypsin EDTA in PBS. For passaging, cells were washed with 1x PBS carefully before adding 1 mL Trypsin EDTA onto the cells. A confluent 10 cm petri dish was split and passaged onto 2 new 10 cm petri dish. One day previous to the transfection, a confluent grown culture with 8 to $9 \cdot 10^6$ cells were seeded onto a 15 cm plate and cultured overnight at 37°C, 10% CO_2 and 90% humidity. Next day cells were transfected with plasmid DNA for AAV production.

Transfection of HEK 293T cells

8 to $10 \cdot 10^6$ HEK 293T cells on a petri dish of 15 cm diameter covered with 20-25 mL DMEM (high Glucose) were used. The helper plasmid pDP8 (22004 bp, 1µg/µL, PlasmidFactory) was mixed with the plasmid DNA (here 6579 bp) in a equimolar ratio. The ratio between DNA and polyethylenimine (PEI) is 1 to 3.

$$\frac{6579}{22004} bp = \frac{1}{3.3} bp$$

$$\frac{28 \mu g}{4.3} = 6.51\ \mu g$$

$$28 \mu g - 6.51\ \mu g = 21.49 \mu g$$

In this example 5.5µL plasmid DNA of the virus and 22.5µL of the helper plasmid were mixed in 2mL of FCS without medium. Next 84 µL PEI was added to the DNA solution dropwise under

constant vortexing. The solution was incubated for 30 min at RT without stirring. Afterwards, the DNA-PEI solution was added dropwise to the medium and the cells were incubated for 4 h at 37°C with 10% CO_2 and 90% humidity. Subsequently, the complete medium was exchanged without washing and after 72h the transfection cells were harvested.

AAV harvesting and purification

At this step only plastic utilities were used. 20 mL of the medium of the transfected cells was collected and so that cells were scraped in a rest of 5 mL medium. The cell suspension was homogenized by gentle pipetting and added to the previous collected medium. Subsequently, the cells were centrifuged for 10 min at 400 xg. The supernatant was discarded and the cells of one 15 cm cell culture plate were resuspended in 1 mL cell lysis buffer. Afterwards, the suspension was processed in a 3-times "freeze and thaw"- cycle in liquid nitrogen and at 37°C in a water bath. In liquid state, the suspension was regularly vortexed. Next 2 µL Benzonase (25U/µL) was added and the suspension was incubated at 37°C for 30 min and vortexing every 5 min. The suspension was the centrifuged at 4°C and 5000 xg for 30 min. The supernatant was collected and sterilized through a filter with 0.45 µm pores. The AAVs solution was stored at -70 °C in 50 µL aliquots. Finally, the virus titer was measured via quantative PCR (qPCR).

Quantitative PCR

The concentration of the purified recombinant AAVs was determined by qPCR. Therefore, several dilutions steps of plasmid DNA, which served as a standard, was used. All dilutions (Table 18) as well as the negative control were prepared in aqua ad iniectabilia (Aai).

Table 18 Schema for dilution of dilution for standard plasmid DNA

	DILUTION	DNA [µL]	AAI µL	COPIES OF PLASMID /µL	COPIES OF PLASMID IN QPCR-DILUTION (5µL SL)	EQUAL TO AAV-GENOMES
	SL			2.99×10^{11}		
S0	1:149	5 (SL)	740	2×10^{9}		
S1	1:10	10 (S0)	90	2×10^{8}	1×10^{9}	2×10^{9}
S2	1:10	10 (S1)	90	2×10^{7}	1×10^{8}	2×10^{8}

S3	1:10	**10** (S2)	**90**	2×10^6	1×10^7	2×10^7
S4	1:10	**10** (S3)	**90**	2×10^5	1×10^6	2×10^6
S5	1:10	**10** (S4)	**90**	2×10^4	1×10^5	2×10^5
S6	1:10	**10** (S5)	**90**	2×10^3	1×10^4	2×10^4

Before the determination of the rAAV solution titer, the solution needed purification. Therefore, 5 µL of the AAV solution were digested using 1µL RQ DNase in 12 µL Aai and 2µL RQ DNase Buffer to remove the remaining non-viral DNA at 37°C for 30 min without shaking. This solution was also diluted and 4 different concentrations were measured.

Table 19 Steps of dilution for quantative PCR

	DILUTION.	µL RAAV	µL AAI	DILUTION FACTOR
V1	1:20	**5**	**95**	**80**
V2	1:100	**20** (V1)	**80**	**400**
V3	1:500	**20** (V2)	**80**	**2.000**
V4	1:2.500	**20** (V3)	**80**	**10.000**
V5	1:12.500	**20** (V4)	**80**	**50.000**

For the qPCR, a master mix was prepared as following (Table 20):

Table 20 Reaction mix of qPCR

Component	Volume Per Reaction (µl)	Total Volume for 75 Reactions + (15)%
Supermix (2 x)	10,000	862,5
100 µM Forward Primer (AAV Quantifizierung ...	0,080	6,9
100 µM Reverse Primer (AAV Quantifizierung...	0,080	6,9
100 µM Probe (AAV Quantifizierung 75)	0,040	3,5
Template	(5,00)	(431,3)
Water	4,800	414,0
Total Volume (Excluding Template)	15,000	1293,8

5µL of the virus solution was added to 15µL of the master mix. The PCR mix was centrifuged for 5 min at 2415 xg in a swing out rotor. The program of the qPCR cycler CFX Connect was:

Table 21 Protocol for qPCR

STEP	TEMPERATURE [°C]	TIME [MIN]
1	95	5
2	95	0:10
3	61	0:30
4		
	STEPS 2 TO 4, 40 TIMES TOTAL	
5	20	0:30

Analysis of the qPCR

The analysis of the quantative PCR was done via Microsoft excel. The values of Cq and SQ of the plasmid DNA standard were plotted and the resulting linear equation was taken to calculate resulting SQ values of samples (values from example preparation, Figure 7):

$$x = \frac{y - 41.967}{-2.838}$$

$$y = Cq - value$$

$$10x = SQ - value$$

$$\frac{AAVgc}{5\mu L} = SQ * diultionfactor$$

$$\frac{AAVgc}{mL} = SQ * diultionfactor * 200$$

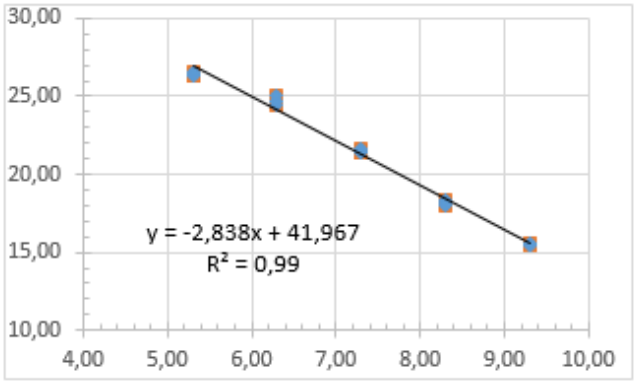

	VF	AAV463-8	
		Cq-Wert	GC/mL
V2	400	21,08	1,86E+12
V3	2.000	22,28	4,02E+12
V4	10.000	24,72	2,42E+12
V5	50.000	25,99	4,13E+12
Mittelwert AAV-GC/mL			**3,11*10^{12}**

Figure 7: Standard curve (left) of plasmid DNA and resulting titers form a sample preparation

Subsequently the dilution factors were considered and the virus titer estimated. Values only were taken into account and considered as reliable if the Aai control resulted into values out of reach of the highest dilution step and sample SQ values reflected the dilution step. Titers were claimed in GC/mL (genome copies per milliliter). From a confluent 10 cm cell culture dish, 2 mL of virus particle solution with titers of 5x10^{11} to 1*10^{13} GC/mL were achieved.

Characterization of Knock out efficiency

Preparation of coverslips for dissociated hippocampal cultures

Coverslips (15mm diameter) were incubated in 10 M NaOH for 4h at 100°C. The coverslips were then washed 5 times with MQ-H_2O for 20 min each time. Next, they were dried at 225°C for 6h and incubated with 0.5 $^{mg}/_{mL}$ in borate buffer at 4°C overnight. The next day, the coverslips were washed in MQ-H_2O 5 times and afterwards dried at RT. Before using the coverslips were placed in the 24-well plates and stored at 4°C until used.

Preparation of dissociated hippocampal neurons

The preparation of primary hippocampal cell cultures, mice embryos were killed at embryonic day E18.5. In order to do so, time mated female mice were quickly killed by cervical dislocation and the embryos were exposed from the peritoneum and the uterus using scissors and forceps. Next, embryos were decapitated and the head was hold at 4°C in GBSS. The skull was removed and the brain was taken out as quickly as possible and separated into the both hemispheres by a blade. The *pia mater* was removed and the hippocampus was extracted and

stored in 4°C cold GBSS. The collected hippocampi were transferred into 1 mL Trypsin EDTA and incubated for 27 min at 37°C. After removal of the Trypsin EDTA the hippocampi were washed 6 times with 1 mL of serum medium. Next, the hippocampi were homogenized via shear force by pressing them through the narrow tip of a Pasteur pipette. Cells were centrifuged for 5 min at 1500 rpm. The supernatant was discarded and the pellet resolved into 1 mL of complete medium. The cell number was estimated in a 1:10 dilution in a Neubauer counting chamber and adjusted to a concentration of 70.000 cells per 150 µL complete medium. The suspension with adjusted cell concentration was plated in a 24 well plate with a poly-L-lysine coated coverslip (Ø 1.5 cm) for 3 h at 37°C and 5% CO_2. After 3h the wells were filled up to a total volume of 350 µL complete medium. Cells were kept in 37°C and 5% CO_2 and the 10 % of the cell medium was changed weekly and cells were cultured 21 days *in vitro* (DIV21).

Transduction of primary dissociated hippocampal neurons

For characterization of the PFN KO system, primary hippocampal cell cultures were transduced with a multiplicity of infection of $5 * 10^4 \frac{GC}{cells}$. After establishing a time course DIV 10 was identified as the transfection point of time to be most effective and the relative amount of protein was analyzed 11 days later at DIV21 as neurons were considered to be mature at that time. For the aim of transduction, the virus particle solution was diluted with NB(+) medium and vortexed. The mixture was added to the cell culture medium and cells were cultured as described before.

Preparation of total protein extracts

To prepare total protein extracts, cells were harvested and collected in previous weighted and labeled 1.5 mL reaction tubes. Pellets were resuspended in STKM buffer (with freshly added proteinase inhibitor mix, $1\,{\mathrm{mL}}/{\mathrm{gram}}$ cell pellet), but at least 40µL were used. Next, cells were treated in 2 – 4 “freeze and thaw” cycles in liquid nitrogen and a water bath at 37°C. Samples were shortly vortexed in between and centrifuged for 20 min at 4°C at 13.000 xg in a table centrifuge. The supernatant was transferred into a new 1.5 mL reaction tube and prediluted if necessary. The protein concentration was then determined via the Bradford protein assay.

Therefore, one sample was diluted 5 times and each dilution was measured in a 96-well plate containing 100 µL Bradford reagent. As a reference, BSA dilutions of 5 steps with known concentrations between 20 $^{\mu g}/_{mL}$ and 200 $^{\mu g}/_{mL}$ were measured in the same 96-well plate. The absorption at 595 nm was measured with an ELISA reader (BioTek) and concentration could be calculated. Samples were then set to a protein concentration of 1 µg/µL in 4x SDS sample buffer and boiled at 90°C for 3 min. Afterwards samples were either loaded onto a SDS PAA gel or stored at –20°C.

SDS PAA gel electrophoresis (SDS-PAGE)

For separation of protein, 5-12.5 µg protein was loaded onto a SDS PAA gel. This 15% polyacrylamide gels were prepared as described below:

REAGENTS	VOLUME	REAGENTS	VOLUME
MQ H_2O	62 mL	MQ H_2O	30 mL
COLLECTION GEL BUFFER	25 mL	separation gel buffer	30 mL
ACRYLAMIDE	13 mL	acrylamide	60 mL
TEMED	50 µL	TEMED	40 µL
10% APS	1000 µL	10% APS	800 µL

Additionally, each paa gel was loaded with a protein standard 5 µL of PageRuler Plus Prestained Protein Ladder. The gels were covered with SDS running buffer and run at 225V, ~ 10 mA and 100W until the samples reached the separation gel. The settings were then changed to 20 mA. The run was ended after about an hour or when the band of the bromophenol blue ran out of the gel.

Next, the gels were washed in buffer for 30 min, exchanging the buffer every 10 min. Working with gloves, a polyvinylidene fluoride membrane (PVDF membrane) was equilibrated in blotting buffer (containing 10% MeOH) for 20 minutes. Also 4 pieces of Whatman paper per gel were equilibrated in blotting buffer. In order of semidry blotting, 2 pieces of Whatman paper in the size of the gel were placed on the blotter, the blotting buffer soaked PVDF membrane was placed on top. Next the gel was placed on top and finally 2 pieces of Whatman paper as top layer. Overlaying pieces were removed using scissors. Lastly, air bubbles in

between the layers were removed by rolling a glass pipette gently on the stack. The blotting device was set to 100 V, 200 mA (for two gels) and 10 W for 1 h.

The PVDF membrane then was blocked in a 1x TBS-T buffer containing 5% milk powder at RT in a see-saw, 1 h. The membrane was then washed in 1x TBS-T 5 times and incubated in TBS-T containing the primary antibody at 4 °C overnight afterwards.

The next day, the PVDF membrane was washed in 1x TBS-T 5 times and then incubated the secondary antibody coupled to a HRP diluted in 1x TBS-T for 90 min at RT shaking on a see-saw. Subsequently, the membrane was washed in 1x TBS-T 5 times, in TBS-X 5 times and in H_2O 7 times. Finally, the membrane was dried and incubated with Luminata™ Crescendo Western HRP (~2 mL) for 2 to 3 minutes (depending on the strength of the signal on the film). The membrane was then placed in a CURIX cassette and X-ray films could be developed in a dark room. Depending on the intensity of the HRP signal, films were developed respectively between 30 sec and 8 minutes. The film was then developed and fixing solution and lastly washed and dried. For analysis the film was photographed with a Herolab E.A.S.Y. RH system and the relative protein values compared to a reference protein level (GAPDH) were then determined by single spot analysis in Herolab software.

Methods of morphological analysis

Transfection of primary dissociated hippocampal cultures

In order to analyze Profilin deficient neurons, Bl6/Cas9 mice of either sex were used for preparation of primary hippocampal cultures which was performed as described before. The cells which were grown on coverslips were transfected twice with plasmid DNA to achieve a knock out of the gene of interest at the one hand and also to mark cells via a strong fluorescent signal to enable morphological analysis on the other hand. The first transfection aimed to knock out profilin and was carried out at DIV 10 according to the previously developed time schedule to achieve highest loss of profilin in the transfected cells. The table lists all used plasmid DNA (see Table 22).

Table 22 List of used plasmid DNA for morphological analysis

DATA BASE SIGNATURE	NAME
E455	pAAV-U6sgP1B+2B-hSyn-Cre

E464	pAAV-U6sgP1B+2B-tGFAP-Cre
E473	pAAV-U6sgLacZ-tGFAP-Cre
E472	pAAV-U6sgLacZ-hSyn-Cre

The plasmid DNA were mixed 50 µL of NB^- medium (without glucose) per approach by vortexed and incubated for 5 min at RT. Next a master mix containing 2 µL Lipofectamin 2000 and 50 µL NB^- medium per approach was prepared. Subsequently, the DNA mix and master mix were combined to equal volumes, vortexed and incubated for 20 min at RT. For transfection the medium of the cells were removed and collected in an empty well of the 24-well plate and 1mL of fresh NB (+) medium (with glucose) per well was added. Cells were quickly covered with 300 µL of NB (-) medium which was previously stored in the 5% CO_2 incubator at 37°C to adapt. Next, 100 µL of the transfection mix was added dropwise on top of the 300 µL of NB^- medium and approach was incubated for 40 min at 5% CO_2 and 37°C. Finally, the transfection mix was removed completely and 500µL of the previously removed NB^+ medium was added to the cells.

For the purpose of Sholl analysis primary dissociated hippocampal cultures were transfected a second time at DIV 20 with a DNA expressing a strong fluorescent dye. In order transfect 70.000 cells in one 24-well plate well, 0.8 µg of the plasmid was mixed with 50 µL of NB medium (-). The transfection mix was incubated 5 min with several vortexing steps in between at RT. Separately, 2µL of Lipofectamine™ 2000 was incubated with 50µL NB- medium and mixed thoroughly multiple times. Finally, 250 µL of each solution were combined in separate tube and incubated for 20 min at RT. Next the medium of the cells was placed in an empty well and cells were placed in pre-warmed 300µL NB without glucose and 100 µL of the combined transfection mix was added dropwise to the well. Cells were incubated for 40 min at 37°C in 5%CO2. Last the transfection medium was discarded and a 1:1 mix of old NB medium with fresh NB medium was resupplied to the cells.

Fixation and staining of primary dissociated hippocampal neurons

For incubation of dissociated hippocampal neurons with antibodies, cells were fixed and permeabilized previously. Therefore, the medium was discarded and cells were placed in 37°

warm PBS with 4% PFA for 10 min at RT. The PBS with PFA was removed and cells were washed in 1x PBS and placed in PBS with 0.2 % Triton for 15 min at RT. Afterwards cells were washed again in 1x PBS 3 times. Next first antibody dilution in PBS was added and cells were placed in 37°C for hours in a humidity chamber. Again cells were washed in 1x PBS. In case of low antibody dilution volume, 1x PBS with 1% BSA was used. Second antibody dilution was placed onto the cells for 2 h in 37°C for hours in a humidity chamber. Within the last 10 min 1/1000 DAPI solution in PBS was added to the secondary antibody dilution and cells were placed at RT in the dark. Lastly cells were washed with 1x PBS 3 times and once with VE water before dripping the water into a towel and flip the coverslip into a drop of Fluorogel and let it dry overnight at RT.

Sholl analyse of primary dissociated hippocampal neurons

To investigate the dendritic complexity, primary dissociated hippocampal neurons from Bl6/Cas9 mice of either sex were transfected at DIV10 with sgRNA constructs and analyzed at DIV21 according to the knock out efficiency of the protein of interest. At DIV 21 wells were fixed and image with 10x or 20x objective at an Axioplan 2 imaging (Carl Zeiss, Jena) were processed in Neurolucida by reconstruction of the morphological shape of the fluorescent cells. This scheme was then analyzed using the program Neuroexplorer (

Figure 8). The number of intersection, the soma size, total dendritic length was measured. For statistic comparisons data was transferred to Graph pad prism and two way anaova was performed.

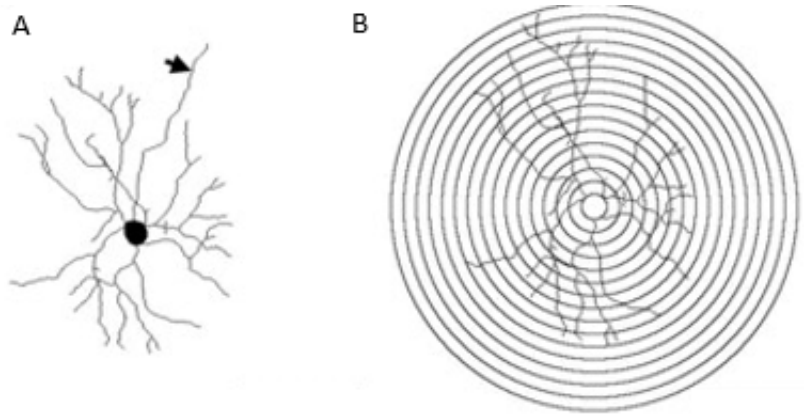

Figure 8: Schematic view of a neuron which was converted to a digital drawing **(A)** and **(B)** application of concentric circles around cell soma for Sholl analysis.

Preparation of organotypic hippocampal slice cultures

Organotypic hippocampal slice cultures were prepared at postnatal day 5 (P5) from both juvenile male and female Cas9 mice. The mice were quickly decapitated and the hippocampus was isolated in ice-cold sterile GBSS. 400 µm, transversal sections were cut with a tissue chopper (McIlwain) and quickly transferred onto Millicells CM membrane inserts (Millipore, 0.4 µm pore size). The slice cultures were cultivated) at 37°C and 5% CO2. After DIV3 an antimitotic drug was supplied to the medium to minimize glia cell proliferation. After another 24h cells were placed in fresh medium and 50% Medium change was applied every 7 days.

Transduction of organotypic hippocampal slice cultures

Transduction of primary organotypic hippocampal slice cultures from P5 B6/Cas9 mice of either sex was performed at DIV4 with 5µL of $1 * 10^9 \, {}^{GC}/_{\mu L}$ of the respective virus particle solution. Cells were transduced with the following constructs (Table 23):

Table 23 List of constructs used for transduction

DATABASE SIGNATURE	NAME	TARGETED GEN
E418	pAAV-U6sgP1B-hSyn-Cre	*Pfn1*
E420	pAAV-U6sgP2A-hSyn-Cre	*Pfn2*
E454	pAAV-U6sgP1B+2A-hSyn-Cre	*Pfn1 and pfn2*
E473	pAAV-U6sgL-hSyn-Cre	*LacZ*
E494	pAAV-2.13-delta-mApple-mPFN2a_mod	*Pfn2*

E495	pAAV-2.13-delta-mApple-mPFN2a_S138Amod	*Pfn2*
E496	pAAV-2.13-delta-mApple-mPFN2a_S138Dmod	*Pfn2*

The virus particle solution was diluted with organotypic culture medium and added dropwise on top of the slices so that the slice was covered with solution. Organotypic hippocampal slice cultures were cultured as described before.

Single cell electroporation of CA3 pyramidal neurons from organotypic hippocampal slice cultures

At DIV20, pyramidal neurons of the CA3 region of from organotypic hippocampal slice cultures organotypic of Bl6/Cas9 mice were used to perform single cell electroporation in order to express mApple fluorescent dye from plasmid DNA. Cell cultures were placed in sterile HBSS containing 1/1000 penicillin and streptavidin. The plasmid DNA was diluted in HBSS to 150 ng. The plasmid DNA was centrifuged at 13.000 rpm for 10 min at RT. Glass capillaries were pulled at 2 steps mode: first step at 73.6°C and second at 47.2°C leading to a resilience of 4-8 MΩ. 10 µL of plasmid DNA was loaded in the capillaries and pressure was put at 10 MPa. The Axoporator was set to -5.0V, the DC offset to 0.0, the pulse mode to Train 100 ms, the Frequency to 200 Hz and the width to 1.0 ms. CA3 pyramidal neurons were identified visually. Up to 3 cells were electroporated and 24 to 48 h later fixed. The point of time upon when the cultures were fixed was due to the intensity of fluorescence although 48h of expression was the latest.

Fixation of organotypic hippocampal slice cultures

Primary organotypic hippocampal slice cultures in which CA3 neurons underwent single cell electroporation were fixed 24 to 48h later depending on the fluorescent intensity. Therefore, the 6-well plate with the organotypic hippocampal slice cultures in the wells were filled 2 mL of PBS with 4% PFA and incubated at 4°C in the dark. Subsequent, the slice cultures were washed with PBS 3 times for 10 min at a see-saw at the dark at RT. Finally the membranes

with 4 slices were cut out from the insert and placed on microscope slides and Fluorogel was added on top as well as a coverslip. The samples were dried at 4°C in the dark for 24 h minimum.

Imaging and analysis of neurons from organotypic hippocampal slice cultures

Primary organotypic hippocampal slice cultures were imaged using a confocal microscope (Leica). Pictures were taken for analysis of spine density in a 1024x1024 formats, image size of 109.6 x 109.6 µm and pixel size of 107.18 nm with a zoom factor 1.14. The laser intensity was kept between 3-11% according to the strength of the fluorescent signal. The analysis of the spine density was done in imagej 1.51j8 with the

Whole cell patch clamp experiments

For whole cell patch clamp experiments excitatory neurons in the CA3 region of organotypic hippocampal slices from Cas9 mice were analyzed. Preparation and transduction was performed as described previously. The slice cultures were transduced with the respective rAAV particles at 72 h after preparation. Analysis was performed from DIV 21-28 (days in vitro). During the recording the cultures were kept in an open chamber and carbogeneted artificial cortical spine fluid (aCSF, Konnerth) was supplied in an open loop (1 mL/min) at 32°C. For recording of miniature excitatory post synaptic currents (mEPSCs) was supplemented with 1 µM tetrodoxin.

Before recording, slices were transferred into the chamber and adapt for 20 min. Glass pipettes from borosilicate capillaries (1.5 mm) were generated by a vertical micropipette puller (Narishige PC-10) and filled with internal solution (290 ±10 mOsm). The diameter of the capillary tip leads to a physical resistance of 4-7 MΩ. After positioning of the filled pipette under a 40x water-immersion objective, transduced cells were identified by fluorescent microscopy (Axioskop 2 FS Plus, Zeiss, Jena). Neurons were hold in voltage-clamped mode at -70mV and a 2 min record of spontaneous synaptic currents was performed. Afterwards the same cell was hold in current clamp mode and a step wise injection of 100 pA (10 steps) for 400 ms was applied to measure the number of evoked action potential.

Next a sweep-wise application of currents were injected until the release of an action potential scaling with 400 pA/V for 100 ms. The signals were amplified with a MultiClamp 700B amplifier and digitized with a Digidata 1322A digitizer (both Molecular Devices). For current detection analysis Mini Analysis software (Justin Lee, Synaptosoft) and ClampFit 11.0.3 was used. Statistical analysis was performed in Prism 5 (GraphPad) using a two-tailed t test for comparison.

Stereotactic injection

For delivering the virus into the hippocampus, two months male Cas9 mice were taken and anesthetized in a box with 5 L/min oxygen/isoflurane mix (Norvap international, Key fil – tec 3 vaporizer). The status of anesthesia was tested via foot paw reflex test and breathing rhythm was monitored through the whole surgery. Next the head of the mice was shaved and the skin was disinfected with Betaisadona (Mundipharma GmbH) and eyes were covered with Bepanthen® Augen- und Nasensalbe (Bayer). Mice weight was taken and the head of the mice was fixed (STOELTING DIGITAL LAB STANDARD STEREOTAXIC INSTRUMENT, MODEL 51900) and the oxygen rate was adjusted to 2 L/min. The skin was cut rostral ca. 3-4 cm starting between the ears (Figure 9, A). Next the point of injection was marked using the bregma as xIy 0I0 coordinates and move 2 mm dorsal and then 1.5 mm lateral to each side of the hemispheres.

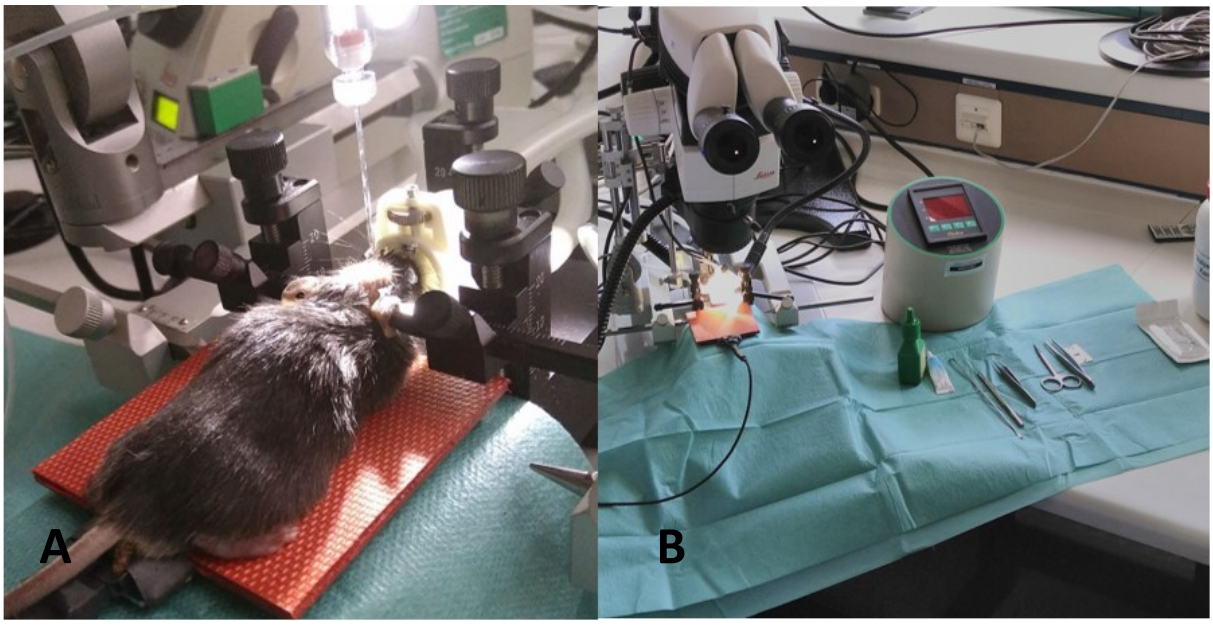

Figure 9: Intracranial surgery of mouse under anesthesia (A) at the workspace (B) with binocular, warming pads and surgical instruments.

Next a hand drill (F S T Dumont) was used to create a whole. Injection capillaries (Havard Apparatus #30-0057) were generated by a vertical micropipette puller (Narishige PC-10) in one step at 67.5°C and 0.5 µL of the respective virus ($5 \cdot 10^{12} - 3 \cdot 10^{13}$ GC/mL, Table 24) mixed 1:1 with 0.02% fast green (- a total volume of 1µL per hemisphere) equally distributed in the depth of 1, 1.3, 1.5; 1.8 and 2 mm with a pressure of 40 psi for 10 msec. The capillary was left in position of the last injection for 10 min to prevent backflow and afterwards slowly retracted. The skin was stitched using a needle and thread (Prolene ™, BV175-8). The mouse was placed back in its cage and watched until full consciousness. The next 5 days the mice were scored using score sheet. Mice were allowed to recover four weeks before morris water maze was performed.

Recombinant adeno associated virus particles were produces at the VCF (viral core facility) from Charité (Universitätsmedizin Berlin) and belonged to the serotype 2/9 in concentrations from: 4.68 *10^{12} to 3.27 *10^{13} GC/mL .

Table 24 RAAVs used for stereotactic injections

DATABASE SIGNATURE	NAME	CONCENTRATION	TARGETED GEN

418	pAAV-U6-sgPFN1B-hSyn-Cre	$4.68 * 10^{12}\ GC/_{mL}$	Pfn 1
420	pAAV-U6-sgPFN2A-hSyn-Cre	$3.27 * 10^{13}\ GC/_{mL}$	Pfn 2
454	pAAV-U6-sgPFN1B+2A-hSyn-Cre	$5.84 * 10^{12}\ GC/_{mL}$	Pfn1, 2
473	pAAV-U6-sgRNALacZ-hSyn-Cre	$5.98 * 10^{12}\ GC/_{mL}$	Lac Z (CTRL)

Morris water maze (MWM)

For behavior analysis, 3 months old male Cas9 mice were used to perform the Morris Water Maze experiment (MWM). These mice underwent stereotactic injection of rAAV particles at an age of 2 months to induce knock out the profilin gens 1 and 2. Mice could recover one month and were closely monitored for 5 days after surgery and were held separately after injection. In the MWM, animals (one at a time) had to find a platform to escape the maze which was hidden under the surface of opaque water in a swimming pool. The pool was 160 cm in diameter and the platform is 10 cm. Mice were put into the pool (maze) at different positions each trial except the south east (SE). Mice were put in at this position for the probe trial only. After reaching the platform the mouse was put back into the cage. Animals were pre trained for 3 days previous to the 8 days of consecutive trainings. In the 3 days pre training phase, the platform was marked and animals could adapt to the experimental set up and find and enter the platform. On day 1 and 3 of the pretraining the mice were weight to document and estimate the animal stress level. During all sessions the water was opaque and held at a temperature between 19 and 24 °C. Three different visual cues were set around the pool for the animals to orientate. During the training phase the entering position varies (N, NE, E, S, SW and W) whereas a 10 cm platform was placed in the NW quadrant.

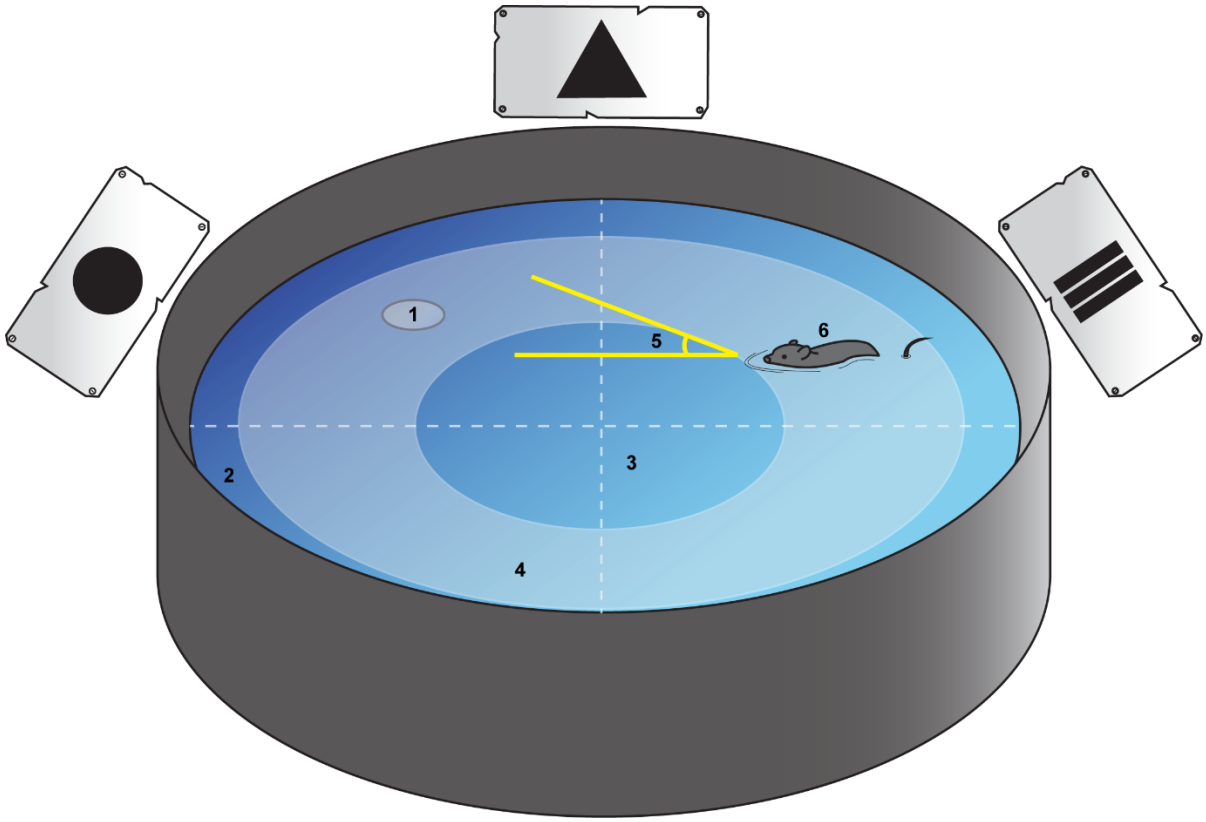

Figure 10: Schematic view of the Morris water maze with visual cues outside the maze. For analysis the pool was divided into 4 quadrants the submerged platform **(1)**, the outer region of the maze **(2)**, the inner region **(3**) and the annulus **(4)**. The mouse **(6)** were put into various starting positions from which an angle **(5)** towards the platform position was set (adapted form(Feuge, 2020)).

In each test run the mouse attempted to find the platform for 60 seconds and could regenerate for 5 min. Every mouse was tested 4 times per day. In case the mouse did not find the platform within the 60 s it was placed onto the platform and let sit for about 10 s and retrieved afterwards. This procedure was repeated in the pretraining as well as in the actual training phase. The swimming pattern was recorded by a camera on the ceiling and tracked via VideoMot2 tracking software (TSE Systems). Thus, the escape latency could be measured from the animal release into the pool upon climbing the platform. Data from mice which remained immobile or stayed at the boarder due to thigmotaxis were excluded from analysis.

Searching strategies

The searching strategies were analysis by categorizing the swim pattern into 1) Thigmotaxis- mouse swam in close proximity to the boarder, 2)'Random Search' – non targeted swimming pattern, 3) 'Chaining' - Circular swimming pattern in the annulus, 4) 'Scanning' – Searching of platform only in the center region and 5) 'Direct Search' – Swimming pattern towards the platform but with explorative loops. 6) 'Direct Swimming' - Swimming directly towards the

platform without detours. The searching strategies 'Direct Swimming' and 'Direct Search' represent hippocampus-dependent search strategies while Thigmotaxis, Random Search, Chaining and Scanning represent hippocampus-independent search strategies (Figure 11).

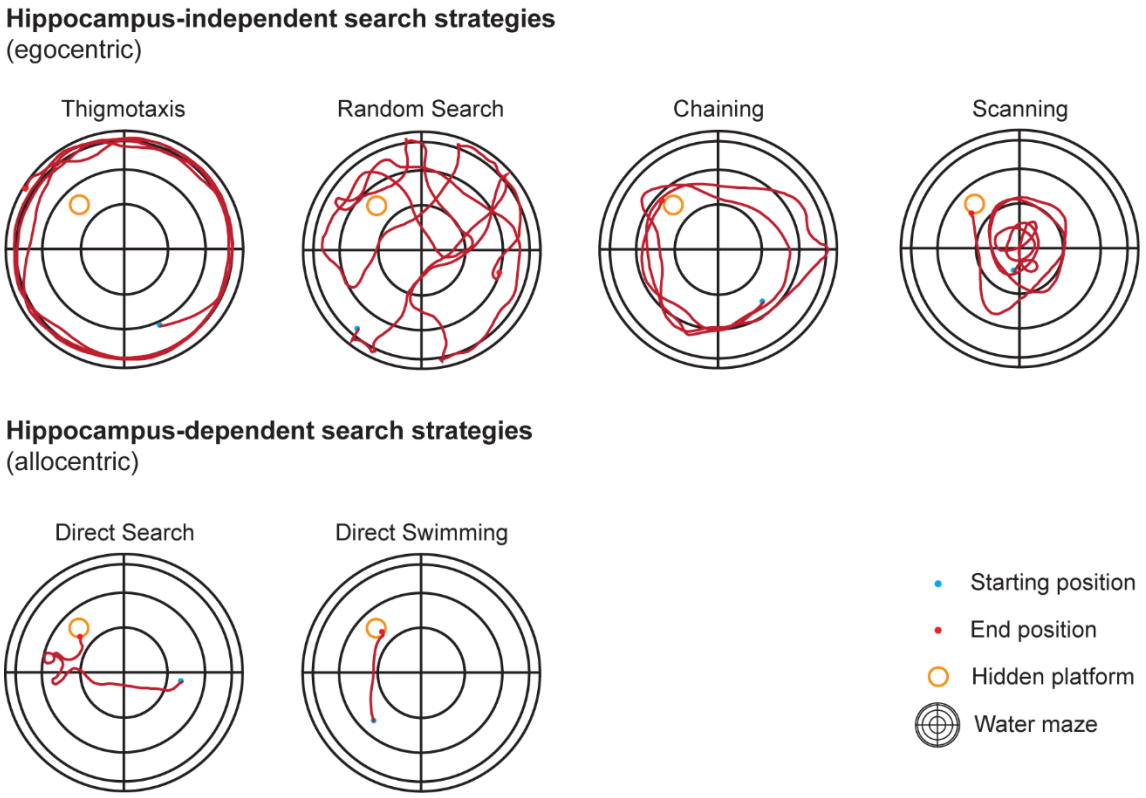

Figure 11: Different searching strategies defined by swimming pattern and categorized into hippocampus dependent and independent. Adapted from (Feuge, 2020).

Reference Memory Test (Probe Trial)

On day 3, 6 and 9 within the training, probe trials were performed previous to the swim training. In this test the platform was removed and animals swam for 45 seconds. By analysis of tracking data quadrant preferences could be examined in which the mouse spent most time finding the platform. Also the number of each platform position crossing was counted. Differences in the escape latency over the training days or quadrant preferences in the probe trial were analyzed using a Two-Way repeated measures ANOVA a two tailed t test.

Cutting of organotypic hippocampal slices via cryotome

For the purpose of visualizing the area of effect of the virus particle infection in the hippocampus via immunohistochemistry, 3 months old B6/Cas9 male mice which underwent stereotactic injection 1 month previous were killed and the brain taken to cut in 40 µm thin slices. Therefore, mice were killed by cervical dislocation after CO2 anesthesia and decapitated. The skin and skull was quickly cut using scissors and the whole brain was removed from the skull using a spatula. The brain was fixed in 4% PFA in PBS for 24 h and then dehydrated 30% Succorse in PBS for another 24 h. The whole brain or one hemisphere was taken and covered in O.C.T. Tissue-Tek and frozen at -70°C. Next the samples were cut with a razor blade to remove unnecessary O.C.T. and the brain glued to the platform of the cryotome with another drop of O.C.T.. The tissue then was cut into 40 µm thin slices and stored in PBS. Finally, the slices were stained and fixed or stored in cryoprotection solution at -20°C.

Staining and imaging of primary organotypic hippocampal slice cultures

For staining of cryotome cut tissue, the slices were placed in a 12-well plate in a net and incubated in PBS with 1% BSA, 0.2% Triton X100 and 10% goat serum for 1 h at RT on a see-saw. Subsequent, the slices were transferred into a fresh 12-well plate and incubated with antibody solution overnight at 4°C. The antibody solution contained 0.2% Triton X100 and 10% goat serum in PBS. Next day, the slices were transferred to a fresh 12-well plate well and washed with PBS 3 times for 30 min each at RT on a see-saw. Afterwards, 2nd antibody solution was prepared in PBS and samples were incubated for 2h at RT. Used antibodies listed above (Table 14):

After the incubation with secondary antibodies, samples were incubated with DAPI in PBS for 10 min at RT. The samples were washed with PBS for 30 min twice at RT on a see-saw and mounted on microscope slides in Fluorogel and sealed with a coverslip.

Coating of microscope slides with gelatin

300 mL of MQ-H2O were prepared in a beaker and 5 g gelatin (1%) at 70°C were solved stirringly. At RT, 0.5 g chrome alum (CrK(SO4)2, 0.1%) and 200 mL MQ-H2O were added. The cooled solution then was filtered. Microscope slides were dipped into the coating solution 3

times for 1 min each. Slides were dried at 70°C dust free for 1 h and stored subsequently dust free at RT.

Vibratome cutting and Golgi staining

For morphological analysis, brains were prepared directly after the end of behavior tasks. Therefore, mice were anesthetized in CO2 and killing was achieved be luxation of the atlas bone (cervical dislocation). Successful killing was determined by testing the reflex check at tail and limbs as well as breathing motion. Next the mice were rapidly decapitated and the skin and the skull were opened by scissors. The whole brain was taken and immediately stored in the 2 mL per hemisphere of equal parts of solution A and B from the "FD Rapid GolgiStainTM Kit" (FD Neurotechnologies, INC.). Brains were stored like this for 14 days at RT in the dark. The solution was exchanged after the first day. Afterwards, brains were transferred into solution C for another 7 days and the solution was changed after the first day.

Subsequently, the brains were cut with a vibratome while kept in 3 % Sucrose in PBS constantly. Slices of 150 µm were cut with a velocity of 6-7 and transferred shortly in solution C and then onto a gelatin coated coverslip. The coverslips were dried in the dark overnight at RT.

Analysis of spine density

After the protocol of "FD Rapid GolgiStainTM Kit", cells were imaged to analyze the spine density. Therefore, dendrites of secondary or third order of CA3 hippocampal neurons were chosen and pictures were taken in bright field mode with a 63 x oil objective with the Axioplan2 microscope. Pictures were also taken as a "z stack" with a distance of 0.5 µm in depth. Pixel size of 0.1 $^{nm}/_{px}$ in x and y direction was used to calculate length of the dendrite of interest so that a ratio of spines per µm dendrite could be achieved. Spines were counted using the program imgej 1.51j8 (free ware) and values were transferred into Microsoft excel for calculations. One dendrite per cell, 5 dendrites of a condition and 3 independent rounds were performed to gain unbiased values.

Data presentation

All graphs and analysis were finally run via GraphPad Prism 5/6. Error bars represent the standard mean error (SEM). Asterisks are representing significant differences: * equals a p value below 0.05, ** equals a p value below 0.01 and *** equals a p value below 0.001.

Results

This thesis aimed for deeper understanding of profilin regarding cellular functions of neurons and astrocytes. Therefore, the CRISPR Cas9 genome editing system seemed suitable to induce profilin single knockouts to examine isoform-specific functions and also to generate a simultaneous knockout of both neuronal profilin isoforms (Pfn1 and Pfn2a) to rule out the possibility of compensatory mechanisms in neurons which had been reported before (Michaelsen et al., 2010). Another advantage of the CRIPSR Cas9 genome editing system was the simple construction and therefore the possibility to insert a cell type specific promoter. In this thesis, the human Synapsin promoter was used to achieve neuron-specific gene editing and for astrocytes a truncated version of the glial fibrillary acidic protein (tGFAP) promoter (Perea et al., 2014) was inserted. It was published that astrocytes express profilin 1 and 2a isoforms (Schweinhuber et al., 2015).

Last, via combination of the CRISPR Cas9 genome editing system with the recombinant adeno associated virus particles (rAAVs), we had the advantages of a conditional knockout system. Thus, we were able to determine a schedule for the highest efficiency of the PFN KO in a specific cell type for profilin 1 or profilin 2a or the simulations KO, respectively. In addition, we could gather information about the cell type specific role of profilins as well as an idea of the relevance of profilins in cellular processes of learning and memory formation.

Generation of recombinant AAV constructs

The construction of recombinant adeno associated virus vectors was the first step to enable the transfection or transduction of the different cell culture systems like primary embryonic hippocampal cultures and primary organotypic hippocampal slice cultures. Due to the simple application and handling of the rAAV particles, the introduction of the CRISPR Cas9 genome

editing system in different cell culture systems was easy to achieve. Previous studies showed that the transfection of NSC19 cells with CRISPR Cas9 all-in-one vectors reached an efficiency of over 90% transgenic cells (Hase, 2016). In addition, these cells which were transfected with plasmid DNA coding for the CRISPR Cas9 genome editing system targeting the profilin genes were vital and even proliferated (Hennig, 2017). The isoform specificity of the sgRNA sequences was also characterized by western blot analysis and revealed a close to 100% specificity to the respective isoform. For the construction of the rAAVs, the homologue sequences of the mouse *pfn1* and *pfn2* genes were essential. The sequences were identified and used as the single guide RNA (sgRNAs, sgRs) of the CRISPR Cas9 genome editing system. For the construction of different plasmids and recombinant adeno-associated virus vectors, three target sequences each for profilin genes 1 and 2a (Figure 12) were used, which were derived from specific "all-in-one" CRISPR/Cas9 vectors (GeneCopoeia, Rockville, USA).

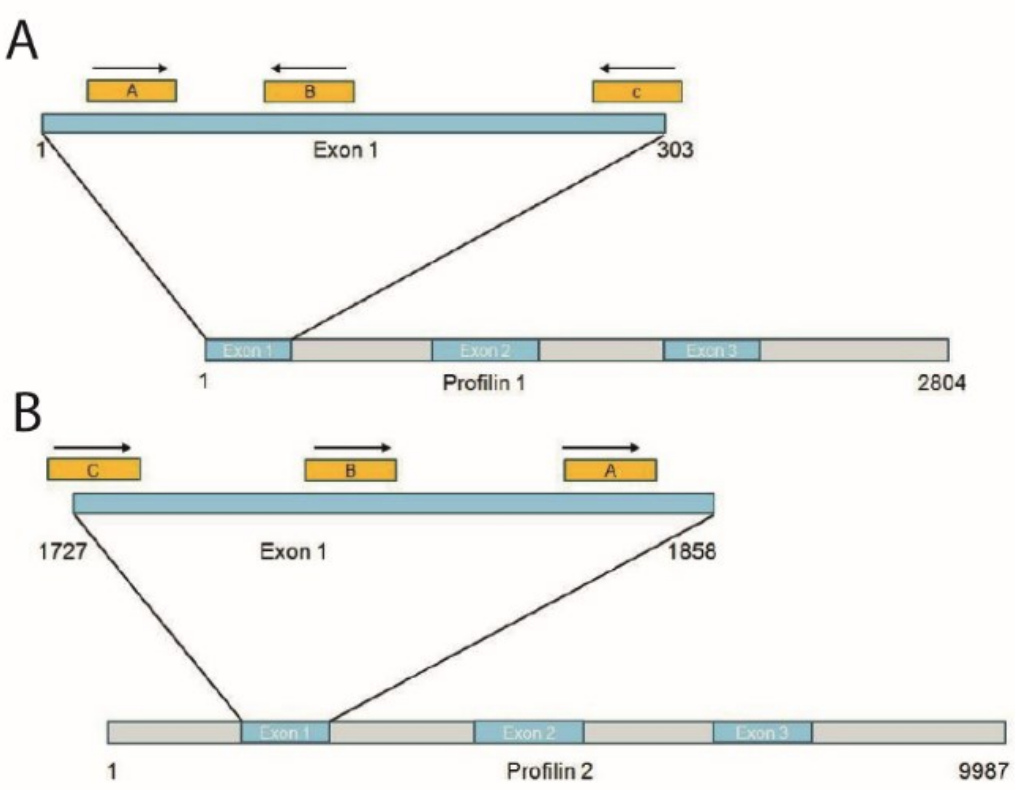

Figure 12: Scheme of sgRNAs (yellow) variants A, B and C with their relative reading direction and homologous region of the **(A)** exon 1 (blue) of the *pfn1* gene (grey and blue). **(B)** Scheme of sgRNAs (yellow) variants A, B and C with their relative reading direction and their locos of the exon 1 (blue) of the *pfn2* gene (grey and blue).

The six different variants of sgRNAs for the two *pfn* genes lead to a variety of possible combinations. To identify the most efficient combination of the specific sgRNAs in reduction of endogenous protein, all possible constructs were generated and tested beforehand. These previous experiments on NSC12 cells revealed which sgRNA sequences lead to a reduction of endogenous protein. In the course of these experiments, cell viability and proliferation in profilin double knockout situation was demonstrated (Hennig, 2017). During this thesis, the four most promising combinations of sgRNA variants were further characterized.

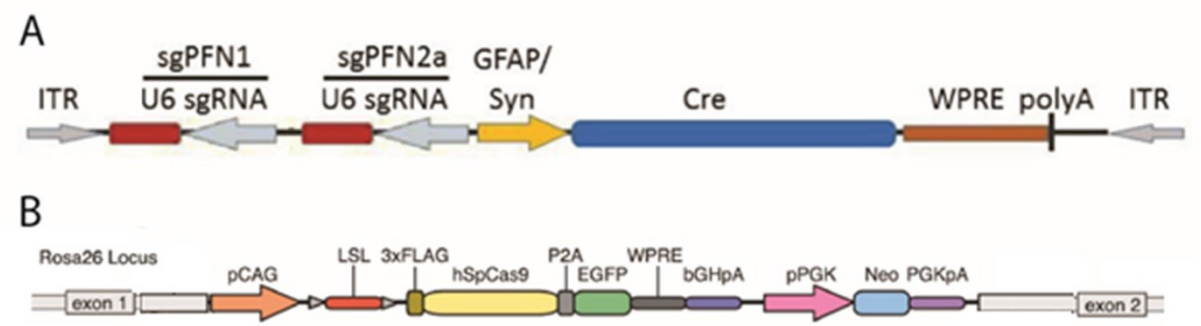

Figure 13: (A) Scheme of a linearized recombinant adeno associated virus construct containing AAV serotype 2 inverted terminal repeats (ITR), sgRNAs for both profilin isoforms (red bar) driven by U6 promoter (grey arrow), a cell type specific promoter (yellow arrow) for the expression of Cre recombinase (blue bar), the Woodchuck Hepatitis Virus Posttranscriptional Regulatory Element (WPRE; orange bar) and a poly adenylation signal (polyA). **(B)** Schematic of the Rosa26 locus of the Cre-dependent Cas9 mouse. The Cas9 transgene expression cassette consists of a 3x FLAG-tagged Streptococcus pyogenes Cas9 linked via a self-cleaving P2A peptide to an enhanced green fluorescent protein (EGFP) to facilitate visualization of Cas9-expressing cells. The transgene is driven by the ubiquitous CAG promoter and is interrupted by a loxP-stop (3x polyA signal)-loxP (LSL) cassette to render Cas9 expression inducible by the Cre recombinase (Platt et al., 2014).

In addition to the appropriate U6 promoter sgRNA cassettes, the constructs contained a Cre recombinase (Cre). The Cre expression was driven by either the human synapsin promoter (hSyn) or a truncated glial fibrillary acidic protein promoter (Perea et al., 2014), which eliminated the floxed stop signaling cassette in the genome of Cas9 mice to induce cell type-specific Cas9 and GFP expression (Platt et al, 2014) (Figure 13).

Production of rAAV particles targeting neuronal and astrocytic profilin isoforms

For the purpose of transduction of organotypic hippocampal slice cultures, recombinant adeno associated virus particles (rAAVs) should be produced. The combination of rAAVs with CRISPR Cas9 genome editing system enabled us to study the role of profilins in neuronal and astrocytic morphology and physiology in an *in vivo* as well as *in situ* situation. Most excitingly these studies also allowed us to decipher the impact of both isoforms individually. In addition, we could gain insight into the consequences of a simultaneous loss of both proteins in neurons

and in astrocytes. The rAAVs were also obtained in a commercially available highly purified manner to allow stereotactic injection followed by behavioral analysis. This has not been done before. In order to produce rAAVs in our laboratory targeting PFN1 and PFN2a in neurons and astrocytes, we used cells from the HEK 293T cell line which were transfected with both the rAAV plasmid and the helper virus plasmid. The transfection efficiency of the HEK 293T and thus the rAAV production cells were examined via fluorescent imaging. The fluorescent signal of the expression of the transgenic enhanced green fluorescent protein (eGFP) indicated a successful transfection and viral genome expression. Upon a sufficient fluorescent signal, the HEK 239T cells were harvested and lysed and the rAAV particles were isolated. The titer of the recombinant adeno associated virus particles was determined by quantitative PCR (qPCR) via double determination of five dilutions using a standard curve prepared with the appropriate plasmid DNA. A list of generated rAAV particles in this thesis can be seen in chapter 'Material and Methods'. Starting from one confluent grown 10cm-culture dish of HEK293T cells (equals approx. 8-10x10^6 cells), yields of 2x10^{12} to 2.5x10^{12} rAAV particles per mL were obtained in a total approx. volume of 2.3 mL of suspension. After cleaning steps of filtering and digestion of non-viral DNA, the purity was sufficient for cell culture application.

Characterization of sgRNA functionality for profilin knockout introduction

Next, we wanted to characterize the efficiency of the CRISPR Cas9 genome editing system for induction of the profilin knockout on primary neuronal cultures. Previous analysis on NSC19 cell line showed that the combination of sgRNAs was crucial for the resulting knockout efficiency related to the endogenous profilins. Depending on the combination, different amounts of the remaining protein were measured after induction of the genome editing system (S. Haak, 2017; S. Hennig, 2017; T. Meßerschmidt, *personal communication*). The most promising combinations of sgRNA were applied on primary embryonic hippocampal cultures. Furthermore, by transductions at different time points, the time point leading to the highest possible loss of endogenous profilin could be determined. However, by application of neuron-specific sgRNAs, only a knockout efficiency of approx. 50% could be achieved. This result was less then described in the literature.

After using constructs targeting neuronal profilins only, a combination of both astrocytic and neuronal targeting vectors was applied. This led to the depletion of both profilin isoforms in

neurons and astrocytes which resulted in a nearly 100% loss of endogenous profilin. This was due to the composition of primary embryonic hippocampal cultures containing astrocytes and neurons and the preparation of total protein extracts targeting all cultured cell types. The cultured cells were harvested and the relative amount of protein was measured via Western Blot analysis.

The data of the Western Blot experiment indicated that all combinations of sgRNAs led to a significant reduction of profilin1 and 2a in the cells (Figure 14, A & B). The different combinations of sgRNAs did lead to a variation in the amount of profilins left in the cell (Figure 14, C). The combinations all reached a reduction of 40% of the protein with high variance in the case of sgRNA combination 1A+2B and 1C+2A.

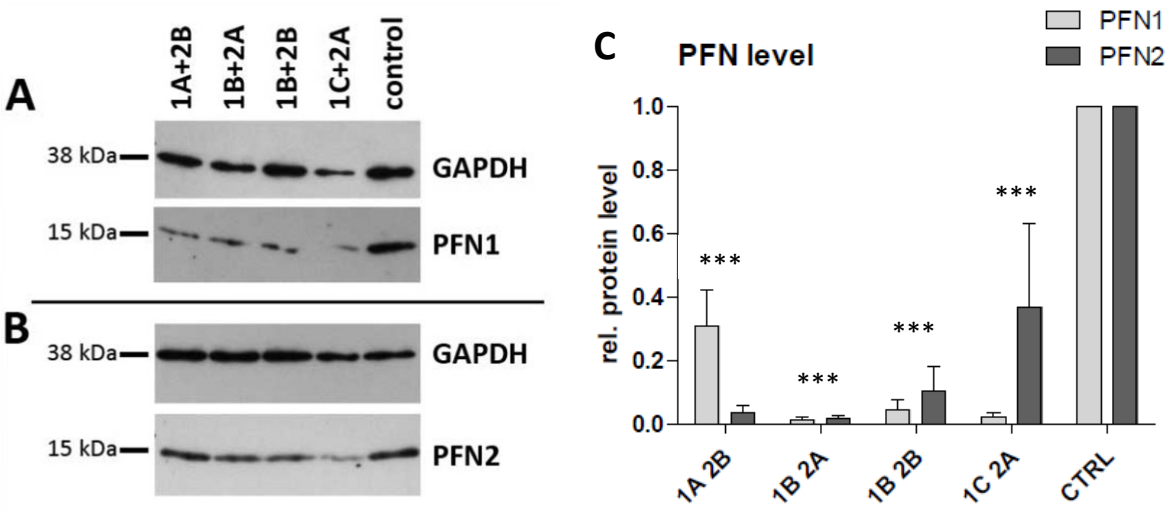

Figure 14: Analysis of Western Blot experiment (A) quantitative Western Blot of Pfn1 of different combinations of sgRNAs with GAPDH as reference **(B)** quantative Western Blot of Pfn2a of different combinations of sgRNAs with GAPDH as reference. C: relative protein level of Pfn1 and Pfn2a normalized to the level of GAPDH. All data is presented as mean ± SEM. Significances are indicated by *p value < 0.05, **p value < 0.01, ***p value < 0.001 and ****p value <0.0001 calculated by one-way ANOVA.

However, the combination of the 1B and 2A variant of sgRNAs resulted in a nearly 100% depletion of profilin1 and profilin2a. We therefore decided to use the combination of sgRNA 1B for the Knockout of pfn1 gene and the sgRNA of 2A to knockout the *pfn2* gene for both the simultaneous and single knockout respectively.

Simultaneous Profilin Knockout leads to a reduction in dendritic complexity

Previous publications could show that profilins are essential for neuronal morphology. Knocking down Pfn2a in hippocampal slice cultures was sufficient to reduce dendritic complexity and spine density in CA1 pyramidal neurons and decrease spine density. Strikingly, Pfn1 could compensate the loss of spines but not the reduction in dendritic complexity indicating redundant as well as specific functions of both isoforms (Michaelsen *et al.* 2010). Therefore, we introduced a double knockout (KO) of both profilin isoforms in primary embryonic neurons and analyzed dendritic complexity rule out the possibility of compensatory mechanisms.

Primary dissociated hippocampal cultures were transduced with the respective rAAVs of four different variants of sgRNAs (1A+2B, 1B+2B, 1B+2A and 1C+2A) for the KO of both profilin isoforms to compare the morphological changes. 24 h before fixation, cells were also transfected with plasmid DNA encoding mApple fluorescent protein for morphological analysis. Dendritic complexity as well as cell body morphology was traced and analyzed.

The cell body size was slightly but not significantly altered due to the transduction with the different variants (Figure 15, A) where as the number of dendritic nodes was strongly decreased compared to control level (Figure 15, B). This decrease of the number of nodes was most prominent in case of the Pfn sgRNA variant 1B+2B ($p < 0.0001$) but present in cells transduced with variants 1B+2A and 1A+2B, too. Transduction with the variant 1C+2A only resulted in a trend towards a decrease which was not significant. Analysis of the number of dendritic intersections showed a significantly reduced amount in cells expressing the 1B+2B sgRNA compared to 1A+2B and 1C+2A. The other constructs did not lead to a change in the number of intersections (Figure 15, C). Next the total dendritic length was measured. Cells transduced with the sgRNA variant 1B+2B exhibited a significant reduction of total dendritic length compared to the control cells. The variants 1A+2B and 1B+2A did not affect the total dendritic length whereas the 1B+2B variant lead to a significant difference compared to the 1A+2B and 1C+2A combinations (Figure 15, D).

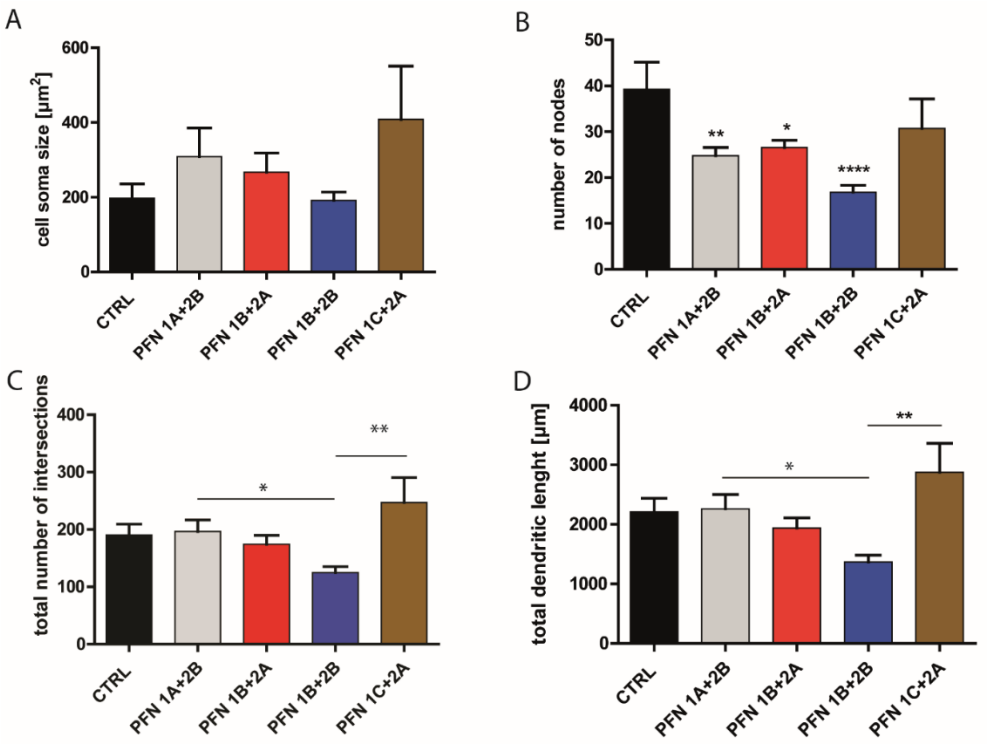

Figure 15: (A) Analysis of the Cas9 dissociated hippocampal neuron cell soma size mirrored no significant differences between different KO conditions. A trend of slightly enlarged cell bodies was notable. **(B)** The number of nodes was significantly reduced in cells of PFN 1+2 KO with the variants 1A+2B, 1B+2A with a $p<0.05$ and cell transduced with the sgRNA variant 1B+2B was reduced significantly to the extent of $p<0.0001$ compared to CTRL cells. The cells transduced with the 1C+2A sgRNA variants however showed no significant alteration. **(C)** The Analysis of the number of intersections exhibited no significant changes in the different sgRNA variants except for sgRNA variants 1B+ 2B, which was reduced significantly. **(D)** The analysis of the total dendritic length presented a similar picture. Only the sgRNA variants 1B+ 2B lead to a significant shrinkage in the total dendritic length. All data is presented as mean ± SEM. Significances are indicated by *p value < 0.05, **p value < 0.01, ***p value < 0.001 and ****p value <0.0001 calculated by one-way ANOVA.

Lastly, in course of the Sholl analysis the number of intersections was plotted against the proximity to the cell body as a parameter of dendritic complexity (). The cells revealed a significant decrease in structural complexity in close proximity to the cell soma for all variants of the PFN double KOs. Upon 100 µm far from the cell body the number of intersections were indifferent to those of the cells transduced with the control AAV.

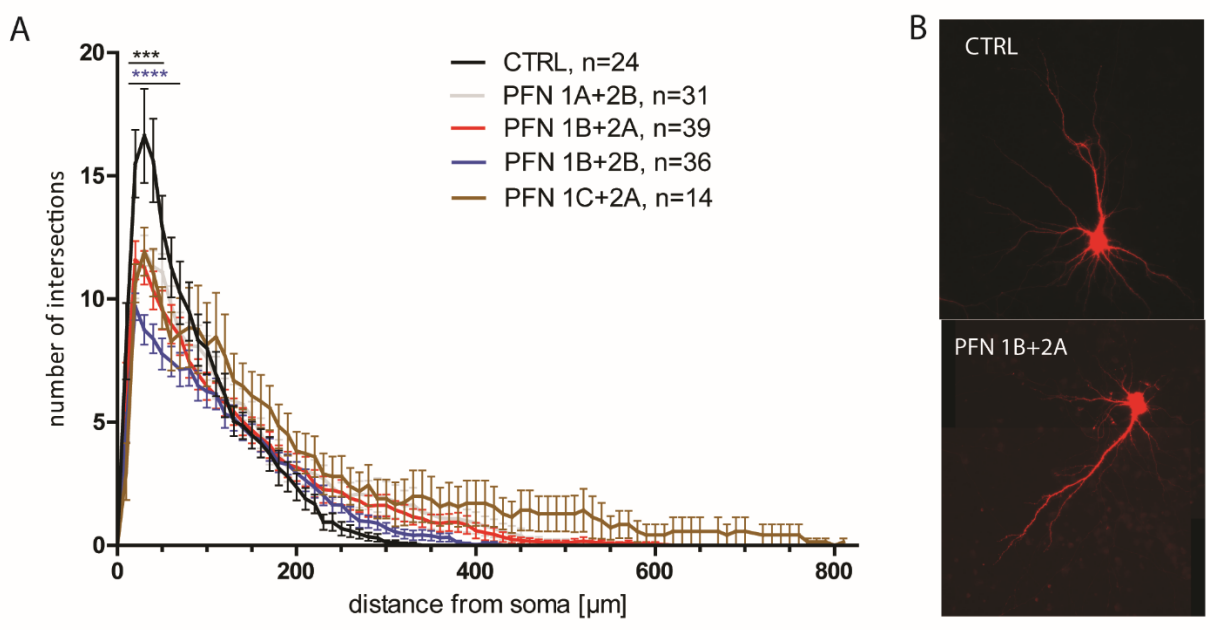

Figure 16 : (A) The Sholl analysis of the number of intersections according to the proximity to the cell body showed a clear reduction of complexity in all conditions in proximal distance to the soma. Upon a distance of ~100 µm no difference in the number of intersections could be detected. Notably the most drastic reduction of complexity was visible cells transduced with the 1B+2B variants with a p value <0.0001 from 0- 150 µm from the soma. The other sgRNA variants lead to a significance of p<0.001 from 0- 100 µm distance from the cell body. (B) Fluorescent image of primary hippocampal neurons transfected with plasmid DNA coding for mApple and transduced with CTRL AAV particles (upper image) and with AAV particles carrying the sgRNAs for profilin double KO (lower picture). The reduction of dendritic complexity from double profilin KO condition to CTRL was obvious. All data is presented as mean ± SEM. Significances are indicated by *p value < 0.05, **p value < 0.01, ***p value < 0.001 and ****p value <0.0001 calculated by one-way ANOVA.

In summary, the different sgRNA combinations had different effects on hippocampal neuronal morphology. Cells mostly reacted with a decrease in the different parameters measured as number of nodes and total dendritic length. Most prominently, phenotypes were visible in cells transduced with the variant 1B+2B. Interestingly, the transduction with the sgRNA variant 1C+2A led in some cases not to a decrease but rather a trend towards an increase, for example in cell soma size and total dendritic length.

Transduction of primary organotypic hippocampal slice cultures successfully induces Cas9 expression

It has been reported before that neuronal physiology is highly dependent on their morphology. The re-modulation of the actin cytoskeleton thereby plays a crucial role (Zagrebelsky and Korte, 2014, Michaelsen et al., 2010, Ackermann and Matus, 2003). The presynaptic vesicle release has been shown to be regulated via Pfn2a (Pilo Boyl et al., 2007)

and the postsynapse in its shape relies on dynamic, activity dependent regulation of the actin cytoskeleton. Therefore, in order to investigate synapse function in the absence of different profilin isoforms, primary organotypic hippocampal slice cultures (OHCs) were used to examine the electrophysiological properties of CA3 neurons. In comparison to primary embryonic hippocampal cultures, the OHCs had the advantage of intact and naive cell composition and architecture. To transduce OHCs, recombinant adeno associated virus particles were applied and thus the sgRNA and the Cre-recombinase were delivered to initiate the expression of the CRISPR Cas9 PFN KO system. For this purpose, postnatal day 5 old (P5) Cas9 mice were sacrificed and OHCs were cultured until DIV21. At DIV 5, the OHCs were transduced with 5 µL of the respective rAAV with a concentration of 1 *10^9 GC/µL . The efficiency of transduction was examined by fluorescence microscopy. Finally, the slice cultures were fixed at DIV21 and imaged with a fluorescence microscope. Almost all cells were showed expression of eGFP and thus also of the Cas9 cassette (Figure 17). In combination with the corresponding sgRNA, the successful induction of the genome editing system for the profilin KO was achieved.

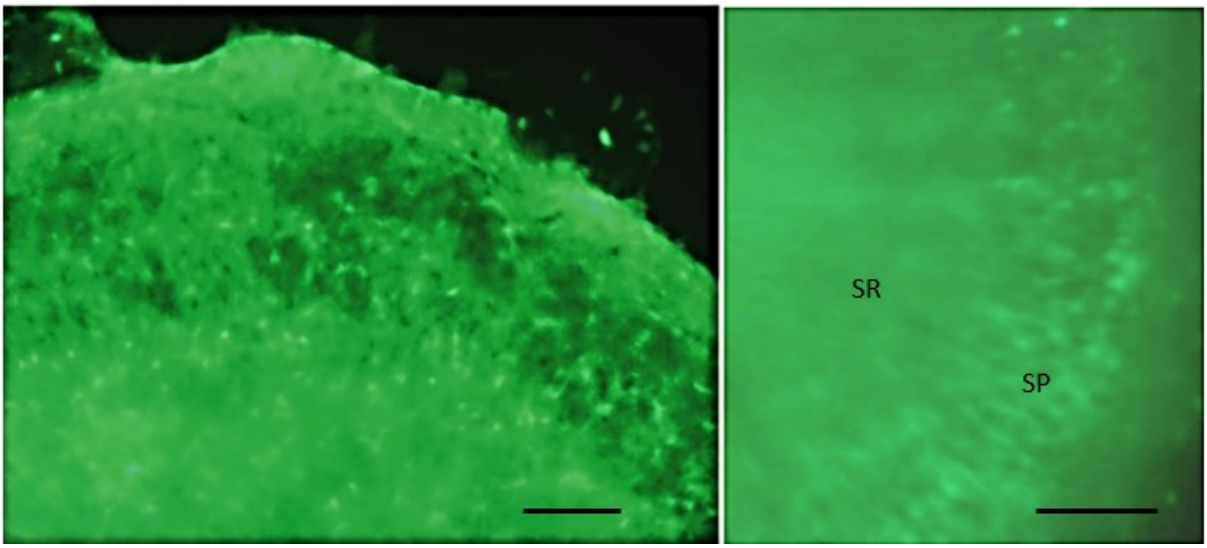

Figure 17: Fluorescent image of primary organotypic hippocampal slice culture CA1 region **(A)** with rAAVs inducing GFP expression and CA3 region **(B)** showed broad virus spread and infection of the mass of cells in different areas of the hippocampus. Green fluorescence of cells bodies in the stratum pyramidalis (SP) and the neuronal network the stratum radiatum (SR) indicate a successful transduction and expression of the Cas9- eGFP-cassette (scale bar 200 µm).

The generated rAAVs can be seen in the table below (Table 25):

Table 25 List of generated rAAVs for transduction of organotypic cultures

NAME	INSERT	TARGET PROTEIN
AAV-U6SGP1B-HSYN-CRE	sgP1B-hSyn-Cre	neuronal PFN1
AAV-U6SGP2A-HSYN-CRE	sgP2A-hSyn-Cre	neuronal PFN2a
AAV-U6SGP1B+2A-HSYN-CRE.	sgP1B+2A-hSynCre	neuronal PFN1 & PFN2a
AAV-U6SGP1B+2A-TGFAP	sgP1B+2A-tGFAP	astrocytic PFN1 & PFN2a
AAV-U6-SGLACZ-TGFAP-CRE	sgLacZ-tGFAP-Cre	astrocytical LacZ (CTRL)
AAV-U6-SGLACZ-HSYN-CRE	sgLacZ-hSyn-Cre	neuronal LacZ (CTRL)
AAV-2.13-DELTA-APPLE-MPFN2A_MOD	ShRNA PFN2a, WT Pfn2a	neuronal PFN2a, KI of WT Pfn2a
AAV-2.13-DELTA-MAPPLE-MPFN2A_S138AMOD	ShRNA PFN2a, S138A Pfn2a	neuronal PFN2a, KI of MT Pfn2a
AAV-2.13-DELTA-MAPPLE-MPFN2A_S138DMOD	ShRNA PFN2a, S138D Pfn2a	neuronal PFN2a, KI of MT Pfn2a
AAV-SGPFN2A-HSYN-CRE-T2A-APPLE-F	sgPFN2A-hSyn-Cre-T2A-Apple-F	neuronal PFN2a

Loss of profilins did not affect spine density and spine head morphology in CA3 neurons

After the investigation of morphological characteristics in primary dissociated hippocampal neurons, the question arose whether cells in a more physiological environment would reveal the same phenotype. Due to the protocol of preparation, the cell to cell connections of neurons and glia cells of primary hippocampus organotypic slice cultures remain intact. Following this approach, primary hippocampal slice cultures form Cas9 mice were prepared and transduced at DIV4 with the respective recombinant AAV particles to deplete one or both profilin isoforms. Since eGFP was expressed in almost all cells due to efficient transduction, an additional fluorescent reporter was used to allow for detailed morphological analysis.

Via single cell electroporation with plasmid DNA coding for the fluorescent protein mApple, CA3 pyramidal neurons were analyzed. The expression of eGFP indicated the successful transduction with the respective rAAV constructs and the mApple fluorescent signal allowed a morphological analysis of single neurons.

Thus, pyramidal neurons from the CA3 area of the hippocampus were examined at DIV21 after the transduction with the according AAV particles with virus load of 5 x 10^9 vg. Analysis of spine density revealed that no significant change was induced by transduction with rAAVs induction Pfn KO. Data of Pfn1 and 2a deficient cells as well as cell carrying the Pfn2a knockout indicated a small increase. However, none of the differences were significant.

Analysis of spine head diameter showed a similar result. Cells lacking both profilin isoforms and Pfn2a deficient cells showed a trend towards increased spine head diameter. The difference between data of Pfn2a KO cells were close to significance compared to the control (Figure 18, B).

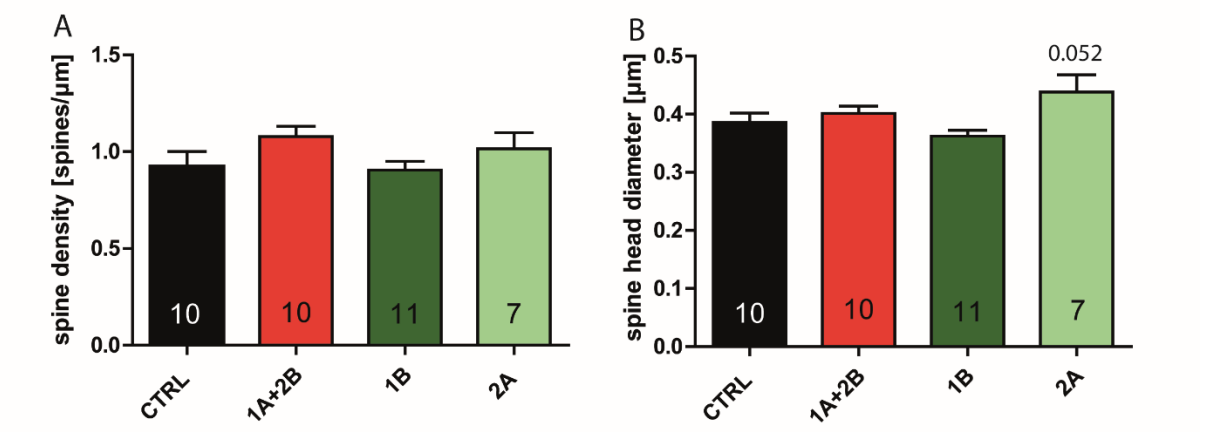

Figure 18: Results of morphological analysis of **(A**) spine density of CA3 pyramidal neurons prepared from primary organotypic hippocampal slice cultures at DIV21 and 17 dpt with the respective rAAV particles for profilin knockout induction. Only trends of slight increase of spine density of cells carrying the double Pfn KO and Pfn2a KO. Similar picture in **(B)** spine head diameter. Pfn2a deficient neurons reflected an increase compared to control which was close to significance.

Taken together the results demonstrate that the introduction of the genome editing system for profilin knockout did not affect the spine density or the spine head diameter of CA3 pyramidal neurons in organotypic hippocampal cultures. This data set showed that neuronal morphology was altered differentially in organotypic hippocampal slice cultures and primary embryonic hippocampal cultures.

Next, dendrite morphology of transduced neurons and cell body size were analyzed as well. The analysis of the number of dendritic nodes did not reveal significant changes between the different genotypes of cells. Only cells lacking the Pfn2a protein showed a trend of a mild decrease (Figure 19).

In the analysis of the cell soma size, the number of nodes and total dendritic length also no changes in the different conditions were visible. In the Pfn1 and 2a deficient cells, a minor decrease in cell soma size was found, but these differences were not significant.

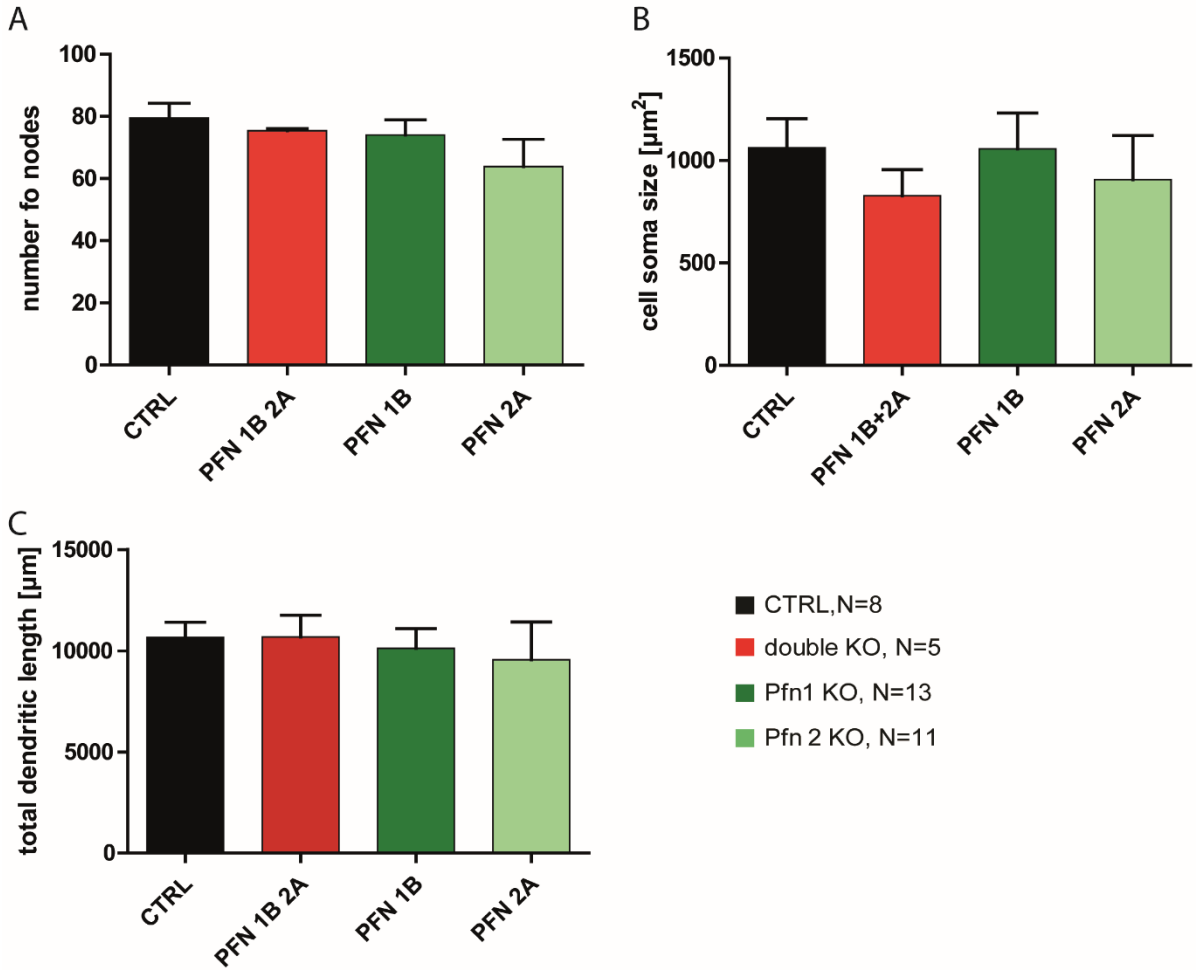

Figure 19: Results of the analysis of CA3 pyramidal neurons after transduction with rAAV particles which induced the respective Pfn KO or CTRL and single cell electroporation with plasmid DNA coding for expression of fluorescent protein mApple of primary organotypic hippocampal slice cultures. **(A)** Number of nodes did not show changes in different condition, only a trend of a reduction in Pfn2a deficient neurons. **(B)** Analysis of cell soma size also revealed no differences but a trend of shrinkage of soma size in cells lacking both profilin isoforms. **(C)** Total dendritic length of the four different genotypes displayed no variations at all. All data is presented as

mean ± SEM. Significances are indicated by *p value < 0.05, **p value < 0.01, ***p value < 0.001 and ****p value <0.0001 calculated by one-way ANOVA.

The data of total dendritic length did not indicate any variations upon the loss of profilins compared to the control group (CTRL). No changes or trends could be found here. Next, the overall dendritic complexity was analyzed.

In order to investigate the dendritic complexity, Sholl analysis was performed. Pyramidal neurons of the CA3 region in cultured slices were identified after single cell electroporation with plasmid DNA coding for the fluorescent protein mApple. The results of the Sholl analysis of the overall dendritic complexity exhibited no differences when the Pfn deficient groups were compared with the control. Basal and apical dendritic complexity was then analyzed separately, as it has previously reported that the different parts of the cells can vary (Michaelsen et al., 2010). The basal dendritic length of cells displayed a trend of reduction compared to the cells transduced with the CTRL rAAVs (Figure 20, B).

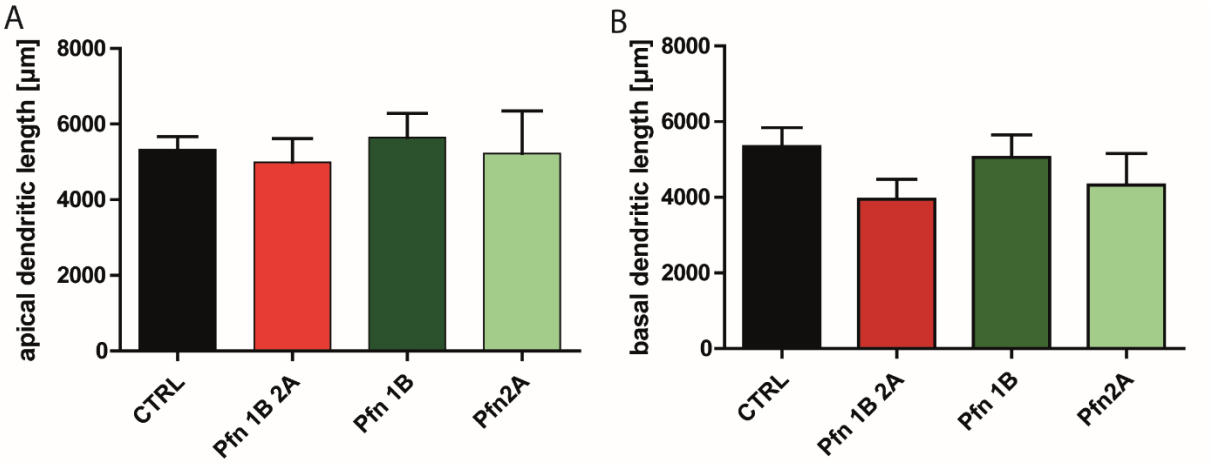

Figure 20: Analysis of dendritic length of CA3 hippocampal neurons after transduction at DIV5 with respective profilin knockout coding sgRNA carrying rAAV particles and single cell electroporation. **(A)** Results of the analysis of the apical dendritic length displayed no significant changes. No trends of any kind were visible. **(B)** Results of the analysis of the apical dendritic length displayed no significant changes. No trends of any kind were visible. All data is presented as mean ± SEM. Significances are indicated by *p value < 0.05, **p value < 0.01, ***p value < 0.001 and ****p value <0.0001 calculated by one-way ANOVA.

The analysis of the basal dendritic length exhibited a slightly decrease of cells which were transduced with the rAAV particles inducting the *profilin 1* and *2a* knockout. Neurons carrying the knockout of the profilin 1 isoform did not reveal any differences, whereas the basal dendritic length of cells lacking Pfn2a showed a trend in a reduction similar the double KO situation. However, this changes did not reach significance.

Interestingly, the Sholl analysis reflected a significant decrease in complexity of Pfn2a deficient cells compared to the control in basal dendritic tree. Likewise, to this finding but not significant was a reduction of dendritic complexity of the apical dendritic tree of cell of the Pfn2a KO.

Data of cells of the double KO of both profilins illustrated a similar picture in case of the basal dendritic tree and even a trend of an increase of dendritic complexity of the apical dendrites. Cells carrying a depletion of the *pfn1* gene showed a reduction of basal dendritic complexity like cells of the Pfn2a KO situation. This difference was not significant however (Figure 21).

Worth mentioning was the observation that the dendritic complexity of mutant cells of the single KOs was similar or reduced in case of basal and apical complexity compared to the control condition whereas the cell carrying the PFN1 and 2a KO displayed a similar complexity of the basal dendritic complexity and a trend of enlargement in the case of the apical dendritic complexity.

Taken together the morphological analysis of pyramidal neurons of the CA3 area of primary organotypic hippocampal slice cultures exhibited minor trends in cell properties like cell soma size, overall dendritic length and the number of nodes. The distinction between the apical and basal dendritic tree revealed no differences in the dendritic length of the 4 different conditions.

However, dendritic complexity analysis revealed significantly reduced complexity of pyramidal neurons after Pfn2a knockout compared with cells transduced with control rAAVs. This difference was only visible in the data dendritic complexity, not in the number of nodes.

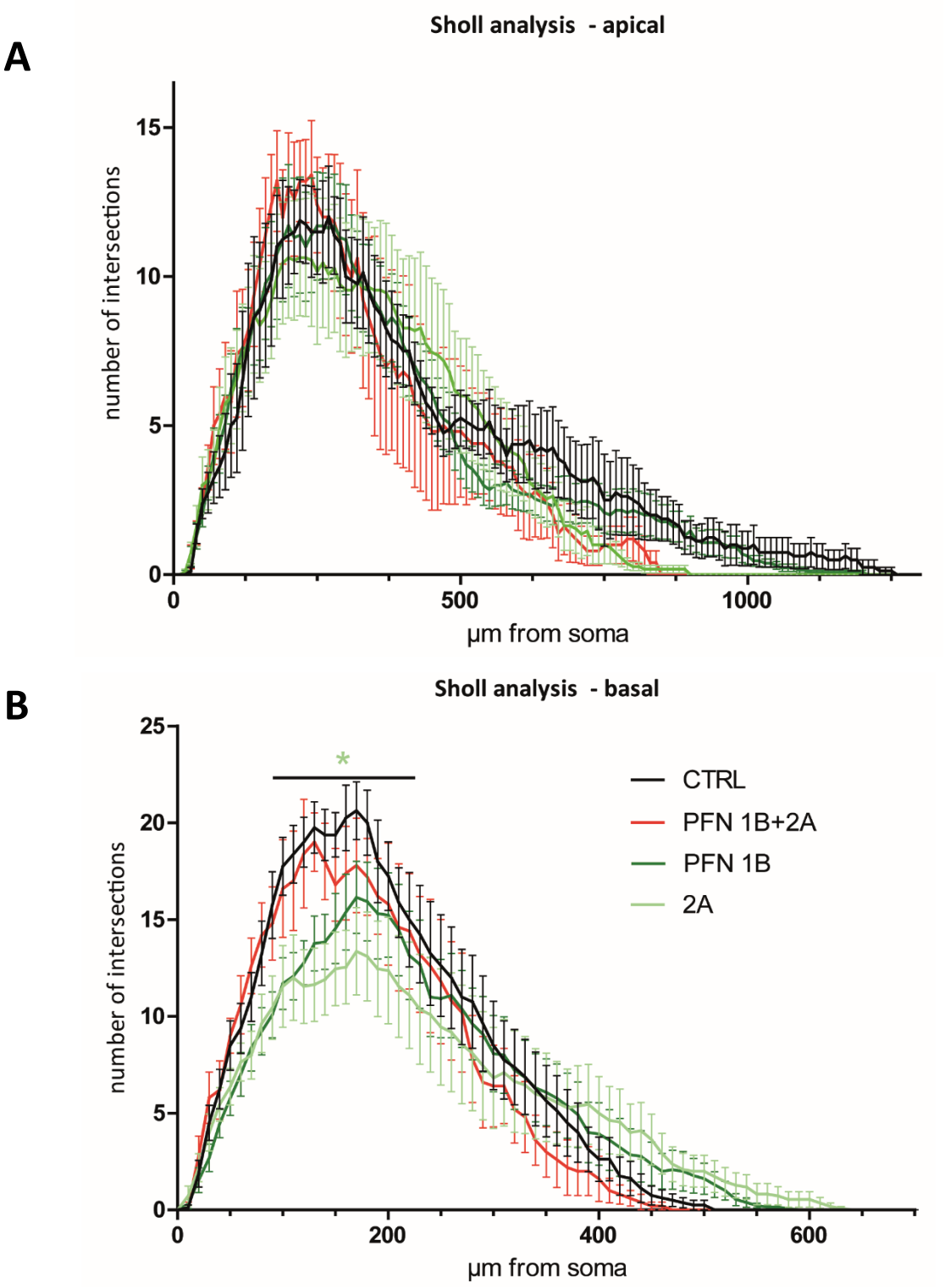

Figure 21: Results of the Sholl analysis of dendritic complexity divided into basal **(A, above)** and apical **(B, below).** Pyramidal neurons of the CA3 area of organotypic hippocampal slice cultures were analyzed at DIV 21 after transduction at DIV5 with the respective Pfn KO or CTRL rAAV particles and single cell electroporation at DIV20 with plasmid DNA encoding the fluorescent protein mApple for cell identification. **(A)** In the analysis of the Sholl experiment of the apical dendritic complexity no variations of the different KO conditions compared to the control were found. **(B)** Analysis of the Sholl experiment of the basal dendritic complexity displayed significant decrease of Pfn2a deficient neurons compared to CTRL and no changes of the double KO or Pfn1 KO condition.

All data is presented as mean ± SEM. Significances are indicated by *p value < 0.05, **p value < 0.01, ***p value < 0.001 and ****p value <0.0001 calculated by one-way ANOVA.

The role of profilin isoforms for processes of learning and memory formation

The previous analysis of morphological parameters revealed impairments upon the double knockout of Pfn1 and 2a in primary dissociated hippocampal neurons and the loss of Pfn2a led to a significant reduction of basal dendritic complexity in line with studies of Michaelsen and coworkers (2010).

The most exciting question now was whether alterations in neuronal morphology might indeed affect hippocampal function thereby leading to altered learning and memory formation. It has been shown that episodic memory formation is dependent to the hippocampus in rodents (Morris et al., 1982, Morris et al., 1986). Moreover, of the impact of a single or double profilin knockout on learning behavior was not investigated before.

Using stereotactic infection to achieve a region specific and isoform specific KO. For intracranial injection, the recombinant adeno associated virus particles were generated and purified by members of the virus core facility of the Charité, Berlin.

Males of Bl6Cas9 mouse line were used for these experiments. The purified recombinant adeno associated virus particles for the Pfn knockout induction were injected into both hemispheres of the hippocampus (HC) (approx. 5x 10^{13} vg/HC). After recovery, *in situ* studies of behavior of learning and memory were possible. For this purpose, anesthetized mice were injected and recovered under observation one month after surgery.

To reveal efficient transduction and rAAV spread in the injected area of the hippocampus, immuno-histochemistry was performed. Therefore, mice brains were prepared and cut into 40 µm thick slices with a cryotome. Hippocampal slices were then stained with 4',6-diamidino-2-phenylindole (DAPI, blue) for cell nuclei, anti GFP antibody (green) and anti Cre recombinase antibody (red). The cell nuclei were clearly visible in the dentate gyrus (DG) and stratum pyramidale of all areas in the hippocampus. The green fluorescent signal was visible throughout all strata in the hippocampus as well as the DG indicated eGFP expression and thus induction of the Cas9 genome editing system for profilin knockout. Moreover, fluorescence labeling of the Cre recombinase indicated expression in cell nuclei of the stratum pyramidalis

of the cornum ammonis (CA) CA1, CA2 and CA3. The fluorescent pattern of eGFP and Cre recombinase expression overlapped and implying that cells of the different areas were transduced with rAAV particles. Thus, virus particle spread due to stereotactic injection transfected nearly all cells in hippocampus with respective sgRNAs of the genome editing system for induction of the profilin knockout (Figure 22).

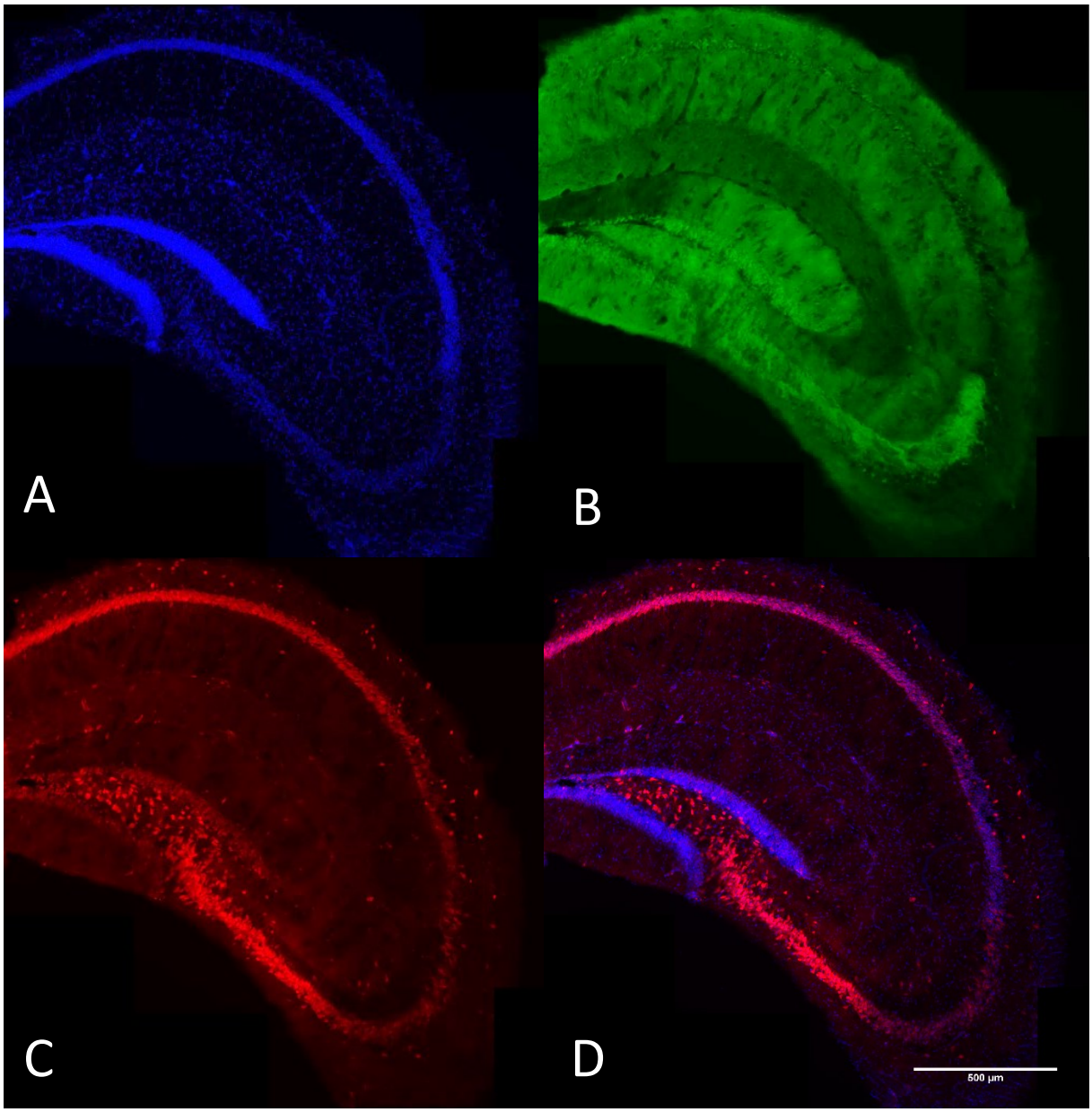

Figure 22: Immunohistochemistry of fixated hippocampal slices (40µm tick) prepared from B6 Cas9 mice after stereotactic injection. **(A)** Blue: 4',6-diamidino-2-phenylindole (DAPI) staining of nuclei, **(B**) Green: anti green fluorescent protein (GFP) staining indicating GFP expression. **(C)** Red: anti Cre recombinase staining overlapping

with blue indicating protein expression of Cre recombinase in the cells of the CA1, CA2 and C3 of the hippocampus. **(D)** Merge of the images A and C indicating the overlapp of DAPI and Cre staining.

To address the question, whether learning and memory formation were affected by the loss of profilins the injected mice were subjected to a spatial learning tasks in the Morris water maze (MWM). Spatial learning in the MWM has been shown to be hippocampus dependent (Morris et al., 1982). In MWM experiment set up, memory formation as well as consolidation and additionally the searching strategy could be studied. The memory formation was observed during eight consecutive days of training in which mice had to escape a circular water maze by climbing a submerged platform. The platform was located in a relative position to visual cues in the environment of the maze. The time mice needed to find and escape the maze served as a parameter of the learning process of the mice. At day three, six and nine, memory recall was assessed in the reference memory test (probe trial) prior to the training or 24 hours after the last training day, respectively. During this test, the platform was removed and the time mice spent in the quadrant of the former platform position was measured. During the eight days of training trajectories of the animals could be categorized into different searching strategies. Former studies split the different strategies into hippocampus dependent and independent strategies (Lisman et al., 2018). Due to the introduction of the profilin genome editing system in the hippocampus, the distinction between hippocampus dependent and independent searching strategies was of high interest.

2 months old, male Bl6Cas9 mice were injected with recombinant adeno associative virus particles (rAAVs) into the hippocampus and behavioral analysis was performed one month after surgery. The injection of both hippocampi with purified rAAVs enabled us to study learning behavior and to correlate potential cognitive impairments with morphological and functional alterations observed in cultured cells. The profilin targeting single guide RNAs as well as a control were injected rAAVs containing a sgRNA targeting the bacterial *lacZ* gene, respectively. To investigate the role of Pfn1 and 2 in the process of memory formation, the escape latency of mice in MWM was measured under PFN KO and CTRL conditions. Over the time course, the animals reach the platform position faster indicating a successful learning.

After observation and full recovery of the surgery, the 3 month old male Bl6Cas9 mice were placed in opaque water and should learn with the help of visual cues to escape the maze on a platform which was hidden under the water surface.

Results showed that mice of the different conditions learned over 8 consecutive days the position of the platform and showed a significant decrease in the escape latency indicated learning behavior. During all 8 days of the spatial learning task the searching strategy was monitored. The mice swimming pattern was tracked by a camera and the traces were categorized into random, chaining, scanning and direct search. At least 3 Cas9 mice of the different groups: CTRL-, single PFN KO and double PFN KO group were subjected to 3 days of pre-training using a visible platform to adapt to testing conditions. The learning task was of 60 sec duration and every mouse performed 4 tests a day (Figure 23, A).

Animals of the different groups reduced their escape latency over the duration of the training and reach the platform significantly faster after eight of training compared to the first day.

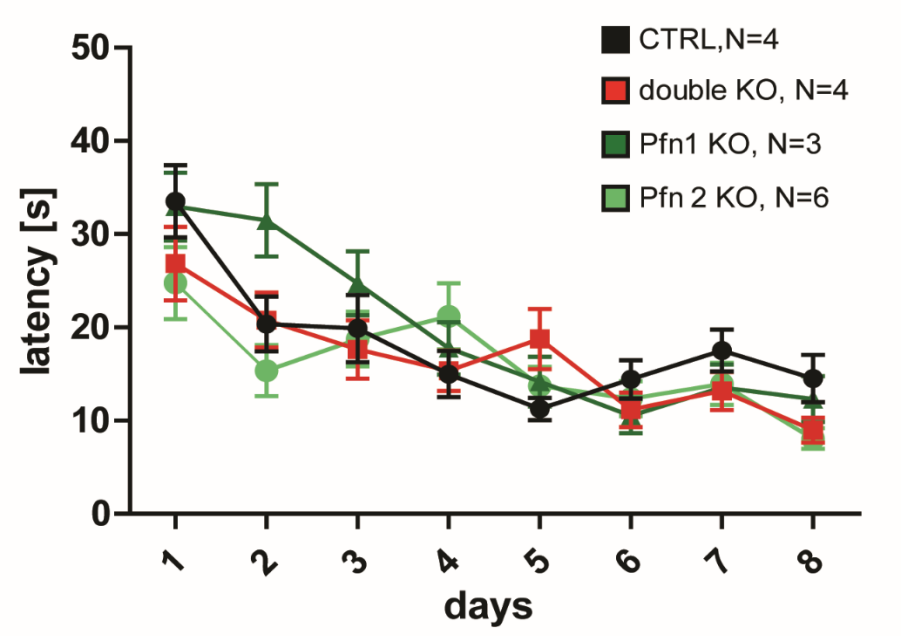

Figure 23: Cas9 mice injected with respective rAAV (PFN single KO of PFN1 and PFN 2, the double KO of PFN 1&2 and the CTRL littermates) showing no alteration in escape latency during eight days training in the hidden platform version of the Morris Water Maze (MWM). Differences between PFN1 and 2 single KO conditions at day 2 equalized during the days of the test. Statistics calculated with two-way ANOVA, mixed effects analysis F (3, 131) = 1.361. The CTRL group learned the platform position over time as differences of escape latency of 8 days were highly significant different F (7, 248) = 6.256, P<0.0001. All data is presented as mean ± SEM. Significances

are indicated by *p value < 0.05, **p value < 0.01, ***p value < 0.001 and ****p value <0.0001 calculated by one-way ANOVA and two-way ANOVA (mixed effects analysis) in case of the escape latency.

During the training at day 2, animals lacking PFN2 were quickest whereas animals lacking PFN1 were slowest though these differences vanished over the period of training. After 8 days of training, the animals of the different groups achieved similar escape latencies and only minor differences were detectable. During the training the swimming tracks analyzed and evaluated. The analysis of the searching strategies did not show changes between the different cohorts. All animals started with a high percentage of hippocampus independent searching strategies like random and scanning search. Mice of the double PFN KO and the PFN 1 single KO reached nearly 50% of hippocampus dependent searching strategies (Figure 24). As the CTRL group decreased in the percentage of direct search after day 4, it was merely possible to draw a conclusion as the CTRL group did not reach significance increase in usage of hippocampus dependent searching over the eight days of training.

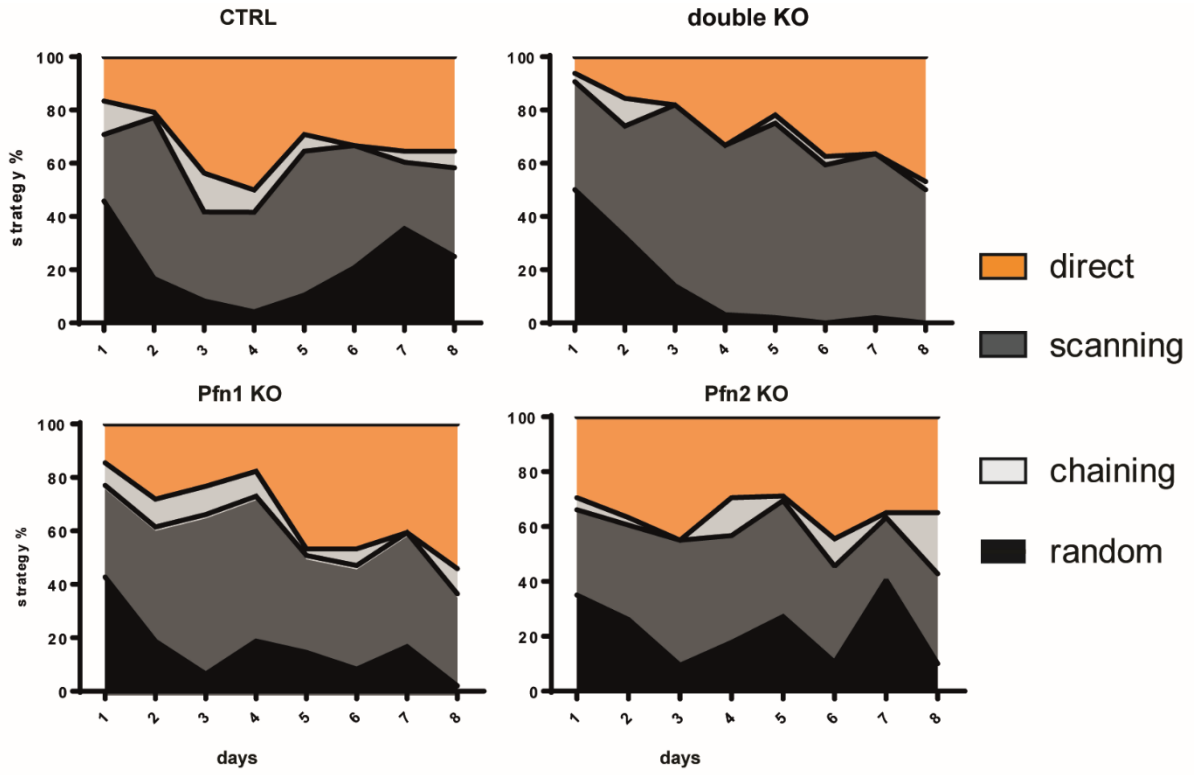

Figure 24: Analysis of the different searching strategies in different conditions used during the eight days of training; hippocampus-dependent (Direct, orange) and hippocampus-independent strategies like random search (black), Scanning (dark grey), Chaining (light grey). Mice used higher percentage of hippocampus- independent search strategies like random and scanning search within the first days and switched to hippocampus-dependent searching strategies over the 8 days of training. (N= 4 CTRL mice, 4 Pfn double KO mice, 3 Pfn1 KO and 6 Pfn2a KO). No significant changed in searching strategy of the different CTRL group could be observed during the 8 days of MWM learning task (Two way ANOVA repeated measure, Bonferroni's post hoc).

Taken together, analysis of the escape latency as well as the strategies used revealed no effect upon the loss of profilin isoforms in hippocampal neurons in learning behavior.

Profilins were essential for memory recall but not formation

Subsequently, we wanted to gain insight in the role of profilins for memory consolidation and recall. Therefore, efficiency of memory recall was assessed during the memory reference test (probe trial) performed at day three, six and nine. In the probe trial, the platform was removed and the time mice spent in the target quadrant (TQ) of the former platform position was measured. Also the number of platform crossings was monitored. Animals of different cohorts showed no significant differences in the number of platform crossings independent of the day the test was done.

Interestingly, animals behaved significantly different in preferring the TQ compared to non-target quadrants (NTQs). At day three no preference could be identified in none of the different mouse groups (Figure 25 , A). A similar result could be observed after six days of training

Interestingly, at day nine after eight days of consecutive learning in the MWM, mice lacking both Profilin isoforms stayed for 36.6% of the test duration in the TQ whereas the mice of the control group spent 51.1% of the time in the TQ. These findings reflect impairment in the memory consolidation and recall of the PFN double KO animals. The comparision of the TQ preferences of day nine between the different genotypes illustrate the difference of the preference of double knockout mice compared to the control littermates. It was close to significance.

The analysis of the memory reference test exposed a significant relevance of profilins in the hippocampus during memory consolidation and recall. The lack of one PFN isoform seemed to be compensated in the quadrant preferences after eight days in the MWM training whereas mice missing both PFN isoforms were not able to prefer the TQ with this former platform position. In summary, the abundance of profilin1 and profilin2a leads to a no significant preference for the target quadrant

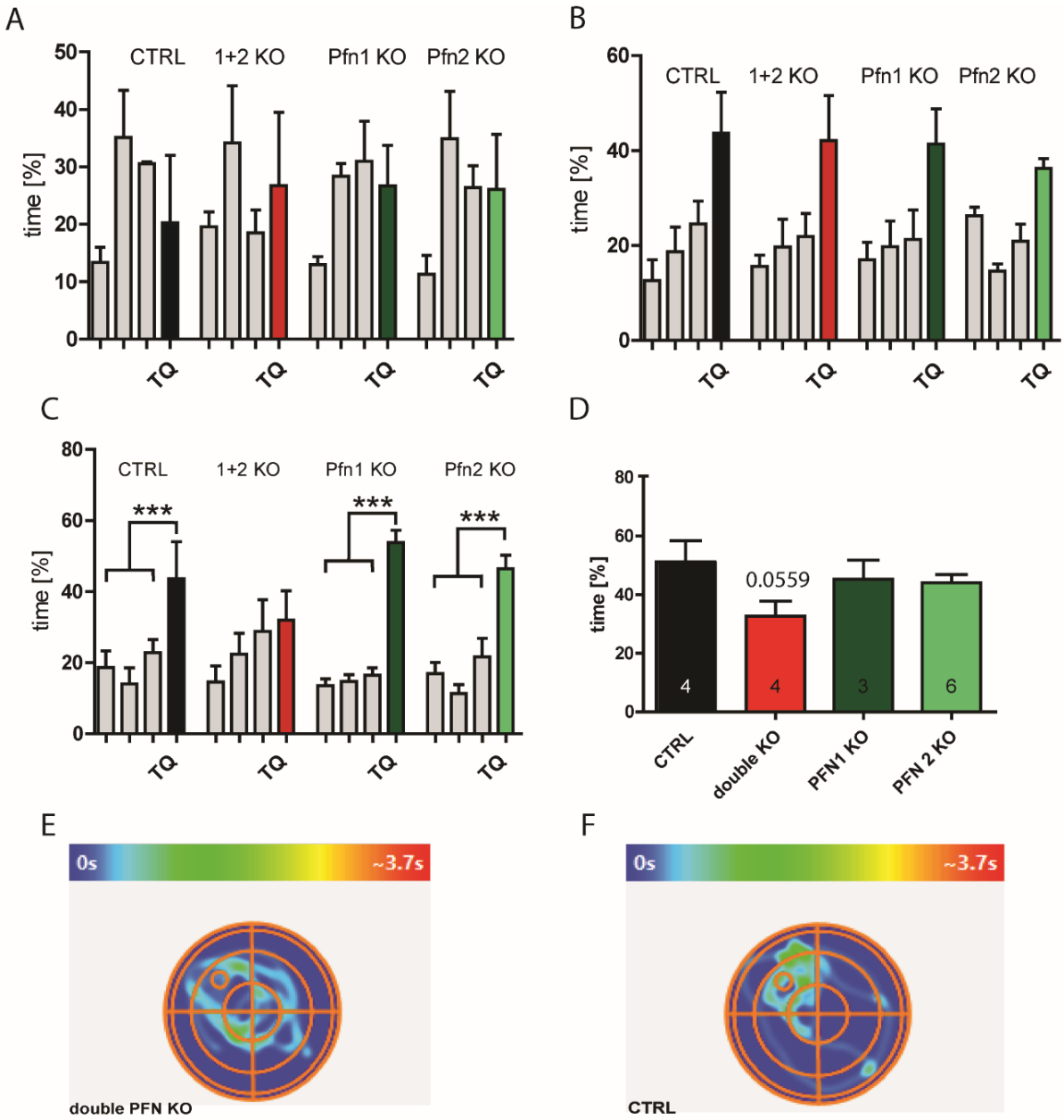

Figure 25: (A) Results of probe trail day 3: No differences could be observed in percentage of time mice spent in the target quadrant (TQ) compared to the three non- target quadrants (NTQs) at day three probe trail. **(B)** Results of probe trail day 6: A clear trend of preference in spending time in the TQ compared to NTQ in all groups of mice. **(C)** Results of probe trail day 9: Significant differences in preference of the TQ compared to NTQs in all groups but not of mice carrying the double PFN KO. Results of the probe trail at day 9: Percentage of time spent in the target quadrant (TQ) after 9 days of spatial learning task. **(D**) Animals of the CTRL group learned the platform position and spent approx. 50% in the TQ. Animals of the double Pfn KO group performed worse and spent less time in the TQ close to significance. Animals carrying the knockout of a single Pfn isoform behaved slightly worse compared to the CTRL but spent similar percentage of time in the TQ. **(E)** Heat map of singke traces of a Pfn double KO mouse performing probe trial test. Blue indicated areas where the mouse spent the least time and areas in red indicated where mice spent the most time. **(F)** CTRL spent more time in the TQ (NW, upper left)

compared to the mice carrying Pfn1 and 2a KO. All data is presented as mean ± SEM. Significances are indicated by *p value < 0.05, **p value < 0.01, ***p value < 0.001 and ****p value <0.0001 calculated by one-way ANOVA.

The CTRL littermates of Cas9 mice preferred the TQ to approximately 50% whereas the NTQs only to a ~20%. Animals lacking only one PFN isoform behaved similar to the CTRL littermates in the contrary to double PFN KO animals. These did not prefer the TQ and could not achieve the significance between time spent in the TQ compared to the NTQs.

Profilin Knockout did not alter spine density after learning task

The morphological effect in hippocampal neuronsdue to learning task Morris Water Maze (MWM) were analysed next. The three month old Cas9 male mice, which performed the spatial learning task of the water maze were sacrificed immediately after the last performance. Both hippocampi were extracted and incubated with solution for Golgi Staining ™. After performing the protocol, hippocampi were cut with a vibratome into 200 µm thin, sagittal slices from the dorsal to ventral side. Pyramidal neurons from the CA3 region of dorsal hippocampus were analyzed. Control littermates were transduced with the respective virus particles but did not undergo spatial training and were analyzed similarly (cohort was named Sitting CTRL).

The analysis of the spine density of pyramidal neurons in the CA3 region of hippocampi exhibited minor differences. The spine density in control animals after the learning pattern in the MWM task was higher compared to the double profilin knockout and profilin 1 knockout situation. The spine density analyzed in tissue from animals injected either with the Pfn1 or 2a knockout or double KO constructs were not significant different compared to control (Figure 26, A).

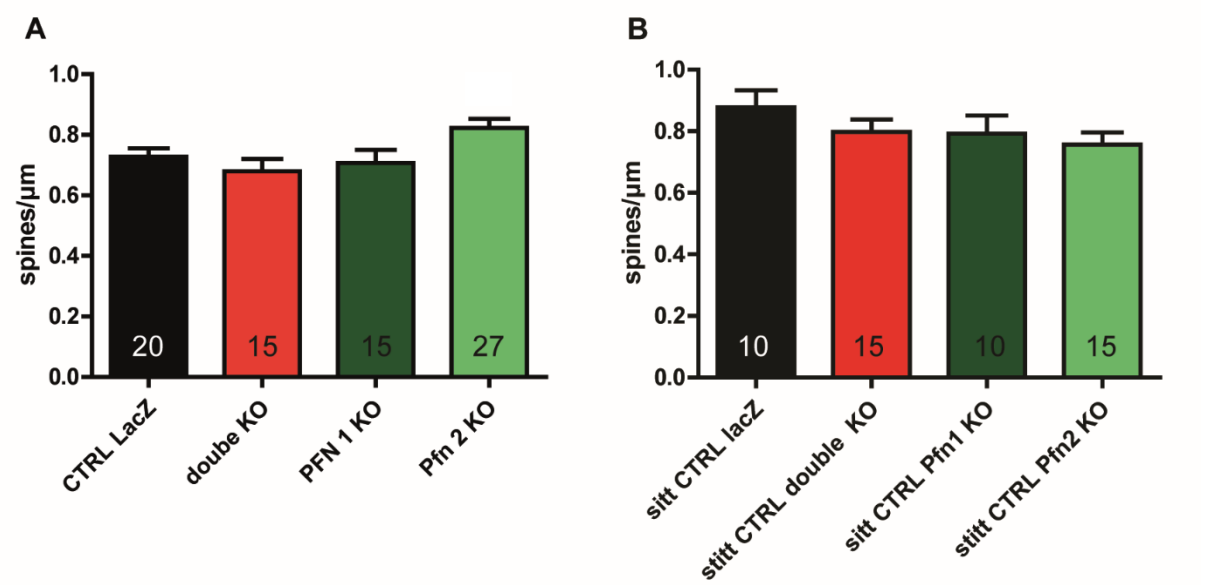

Figure 26: Results of the analysis of spine density in the CA3 region of hippocampi removed from mice which underwent stereotactic injection and performed in MWM spatial learning task. **(A)** Spine density of CA3 pyramidal neurons from mice carrying the double KO and mice carrying the Pfn1 KO showed no differences. **(B**) Results of the analysis of spine density of mice which did not perform the MWM spatial learning task but underwent stereotactic injection of the respective rAAV particles displayed no significant changes. All data is presented as mean ± SEM. Significances are indicated by *p value < 0.05, **p value < 0.01, ***p value < 0.001 and ****p value <0.0001 calculated by one-way ANOVA.

A similar picture could be found analyzing the spine density in the tissue of sitting control littermates. Here, the spine density of the animals injected with the control virus particles was the highest. Spine density of animals injected with the double or single knockouts showed slightly but not significant lower spine densities.

Loss of profilins results in impairments in synapse function

The results of the Morris Water Maze studies indicate a defect in the consolidation of memory in the Pfn-deficient mice. However, analysis of the spine density of the CA3 neurons of the mice after the learning task showed no significant changes in spine density compared with the control cohort. These findings suggested potential alterations in synapse physiology. Therefore, the influence of profilins on neuronal transmission was analyzed by electrophysiological studies. Primary organotypic hippocampal slice cultures of Bl6Cas9 mice were prepared on postnatal day 5 from both sexes. These slice cultures were transduced *in vitro* (DIV4) on day 4 with the appropriate recombinant adeno-associated virus particles

(rAAVs). To achieve a profilin knockout, rAAVs contained single guide RNAs (sgRNAs) targeting a profilin isoform (1 or 2a) or the combination of both sgRNAs for a profilin double knockout. As a control, rAAVs containing a sgRNA targeting the non-endogenous LacZ were applied.

Transduction of the slice cultures aimed to infect nearly all neurons to exclude side effects of a partially profilin-deficient neuronal network. After maturation of hippocampal slice cultures at DIV21, neuronal physiology and transmission of excitatory hippocampal neurons of the CA3 area were examined at the single-cell level by the whole-cell patch-clamp method using three different protocols. Of interest were the frequency of spontaneous excitatory postsynaptic currents (sEPSCs), the amplitude of sEPSCs, and the number of action potentials in response to current stimuli. Hippocampal CA3 pyramidal neurons were visually identified by cytoplasmic expression of enhanced green fluorescent protein, and interneurons were excluded from analysis based on their characteristic transmission pattern. Penetration of CA3 neurons with the glass pipette containing the internal solution and electrode was performed visually, and the viability of the penetrated cells was verified both visually and by the electrophysiological parameters. Sections were adapted to the set-up conditions for 20 min and kept in the fluid chamber for a maximum of 2 h before replacement. Subsequently, eGFP-positive and thus profilin-deficient pyramidal CA3 hippocampal neurons were examined, and sEPSC frequency and amplitude were monitored and recorded for 2 min. After this period, the examined cells were reevaluated visually as well as via the electrophysiological parameters, confirming viability and physiological integrity during measurement.

CA3 excitatory neurons of 21 DIV old organotypic hippocampal slice cultures which lacked both profilin isoforms showed no difference to neurons transduced with the control virus particles in sEPSCs frequency indicating that the presynaptic as well as the postsynaptic compartments maintain functions without the involvement of profilins (Figure 27, A). Most striking was the result that pyramidal neurons which either one of the isoform, independent of the respective isoform, showed a significant decrease in their sEPSC frequency.

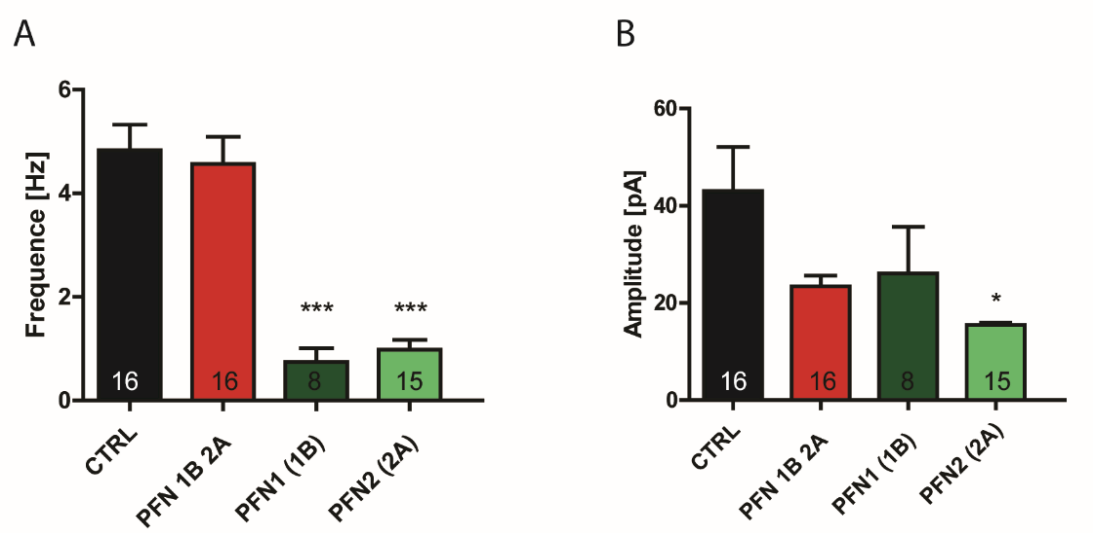

Figure 27: Results of whole cell patch clamp analysis **(A)** spontaneous excitatory postsynaptic currents (sEPSCs) frequency after 2 min of recording. Single profilin KO led to drastic decrease in sEPSCs frequency similar to the double profilin knockout in astrocytes adjacent to the examined neurons. Profilin double KO led to similar levels of sEPSCs frequency comparted to control conditions. Number of cells in bars (black, CTRL, 16; red, double KO, 16; dark green, 8; Pfn1 KO; light green,15, Pfn2a KO; white double Pfn KO in astrocytes. **(B)** Analysis of sEPSC amplitude (same color code and n). Pfn2a deficient neurons exhibited significant smaller sEPSCs amplitude compared to CTRL levels. All data is presented as mean ± SEM. Significances are indicated by *p value < 0.05, **p value < 0.01, ***p value < 0.001 and ****p value <0.0001 calculated by one-way ANOVA.

Next the sEPSC amplitude was examined during the 2 min recording. Here, the double KO of PFN in CA3 neurons led to significantly lower amplitude compared to the control. Interestingly, cells lacking PFN2 revealed significant reduction of amplitude in comparison to the conrtol indicating a critical role of PFN2 in the sEPSC amplitude.

Blocking action potentials rescues the reduction in sEPSC amplitude

The significant alterations in sEPSCs amplitude upon the loss of profilins led to the question if the underlying profilin functions are pre- or postsynaptic. It has been shown that Profilin 2a is required for proper presynaptic vesicle formation and release (Pilo Boyle 2012). Therefore, miniature excitatory post synaptic currents (mEPSCs) were measured under the application of tetrodoxin (TTX). TTX efficiently blocking action potential was used to distinguish between pre- and postsynaptic effects of the respective Pfn KO conditions (Figure 28). Again 2 min of recording was performed measuring the frequency and amplitude. Neither in mEPSC amplitude nor mEPSC frequency, a significant difference in cells carrying the double KO was detectable.

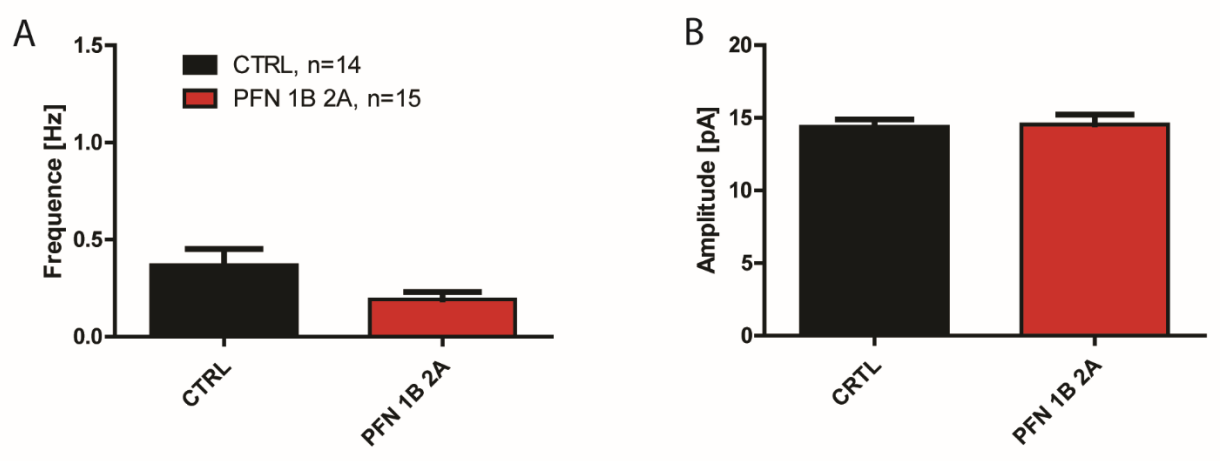

Figure 28: (A) mEPSCs frequency after 2 min of recording and TTX application. Significant differences from Figure 27 were not detectable upon TTX application. **(B)** mEPSCs amplitude after 2 min of recording and TTX application. Also in mEPSCs amplitude no variation of the double Pfn KO condition (red) was recognizable compared to CTRL. All data is presented as mean ± SEM. Significances are indicated by *p value < 0.05, **p value < 0.01, ***p value < 0.001 and ****p value <0.0001 calculated by two tailed t-test.

Notably both parameters decreased due to the influence of TTX. These results suggest that phenotype of a decreased sEPSC frequency and amplitude in a PFN deficient situation originates from the presynaptic compartment of the synapse and thereby supports the hypothesis of PFN2a being involved in receptor trafficking at the postsynaptic compartment.

Profilins are critical for neuronal firing and resting potential

To gain further insight of the role of PFNs in the transmission of excitatory neurons in the hippocampus, we were interested action potential properties under Pfn deficient conditions. Therefore, we tested the number of action potentials released by a CA3 pyramidal neuron after electrical stimuli in pfn1 and/or pfn2 knockout situations. Therefore, cells transduced with the respective rAAVs were identified again visually due to the eGFP expression. These profilin-lacking cells were hold in voltage clamp mode and triggered stepwise via an injection of 100 pA currents up to 1000 pA. The injected currents lasted for 400 ms and the number of responding action potentials were monitored. The analysis revealed a significant reduction of the number of action potentials evoked in all PFfn KO conditions. The trend was already visible upon 600 pA and reached significance at a level of 800 pA. The cells lacking one Pfn isoform released similar less action potentials whereas in neurons of double Pfn KO condition showed a stronger reduction. In summary, these data highlighted that both PFN isoforms were

essential in excitatory neurons for formation and/or release of action potentials (Figure 29) although the effect of reduction did not seem to be additive.

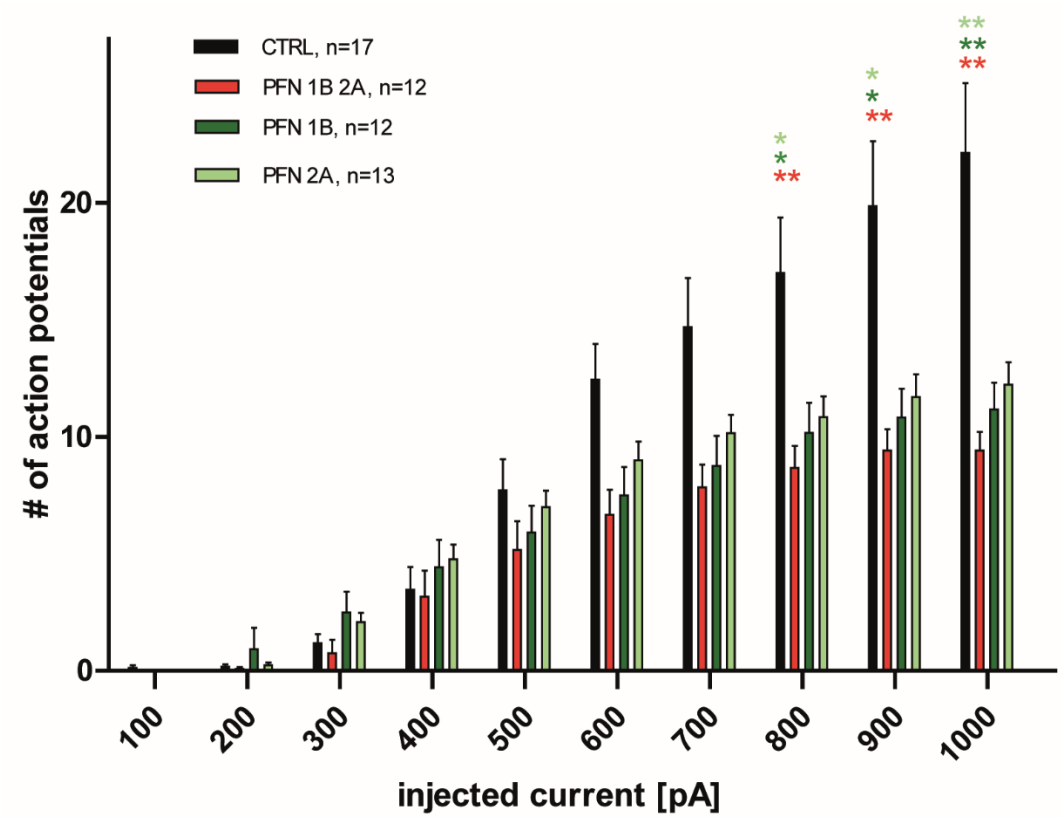

Figure 29: Analysis of numbers of action potential after stimulation protocol in absence of profilin. CA3 pyramidal hippocampal neurons were stimulated for 400 ms with a step wise scaling current of 100 pA up to a limit of 1000 pA. All data is presented as mean ± SEM. Significances are indicated by *p value < 0.05, **p value < 0.01, ***p value < 0.001 and ****p value <0.0001 calculated by two-way ANOVA.

To further characterize profilin deficient excitatory CA3 hippocampal neurons, we examined the resting membrane potential and identified the necessary electrical input to trigger an action potential. The cellular current threshold was determined by the needed stimuli to overcome it. Upon breaking point, an action potential was released and the underlying membrane potential could be calculated. Therefore, PFN lacking CA3 excitatory neurons were injected with 0.5 ms sweep wise currents of 40 pA (episodic stimulation) in current clamp mode.

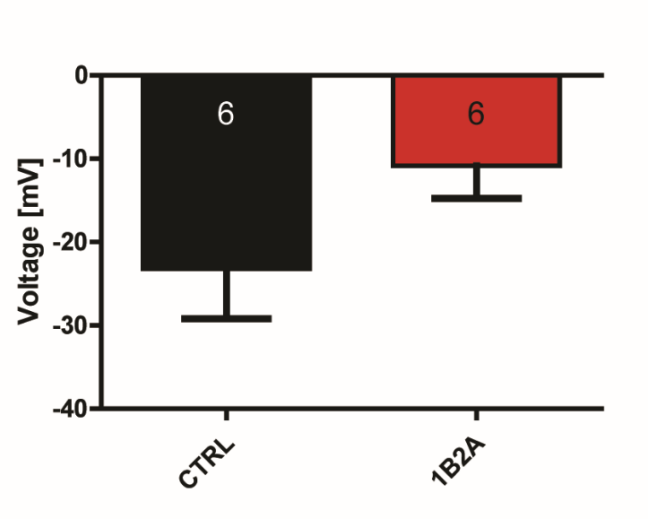

Figure 30 : Analysis of neuronal threshold after stimulation protocol in Ca3 double profilin KO neurons and control neurons. Trend of less negative resting potential in Pfn deficient cells was visible. All data is presented as mean ± SEM. Significances are indicated by *p value < 0.05, **p value < 0.01, ***p value < 0.001 and ****p value <0.0001 calculated by two-way ANOVA.

Cells which lacked both PFN1 and 2 were triggered earlier compared to the cell in control condition. Less current was necessary to provoke an action potential release and cells had a less negative membrane potential (Figure 30).

Profilin phosphorylation status influences neuronal transmission

Due the striking results of the electrophysiological experiments in which the single knockout of *pfn2* led to a significant reduction in sEPSC frequency and amplitude, the investigation of the molecular regulation of Pfn2a was of great interest. One way of the regulation of profilins is facilitated via phosphorylation. Profilin has multiple phosphorylation sites and is target of different kinases and phosphatases. A well-studied phosphorylation site is the serine residue 137, therefore, we wanted to test the impact of phosphorylation at a site specific amino acid (position 137) on neuronal transmission as its been reported to be a critical as well as well studied site of phosphorylation (Walter et al., 2020). Newly generated recombinant adeno associated viruses containing a short hairpin RNA (shRNA) that induced knockdown of endogenous profilin 2a RNA and encoded a shRNA-resistant mutant of this isoform. To mimic a phosphorylated form of profilin 2a, serine residue 137 was exchanged for an aspartate residue (PFN2a S137D), while substitution with an alanine residue represents a phospho-

deficient mutant (PFN2a S137A). By this approach, we were able to investigate the role of the phosphorylation of the serine residue 137 and the impact on synaptic transmission. A vector that expresses the wild-type form of the protein in addition to the profilin 2a-specific shRNA served as a control.

In two minutes of recording, the cells of both conditions, phosphor-mimicking form (137D) or the phospho-deficient form (S137A), did not show a significant difference but a trend of a reduction of sEPSCs frequency. This trend was pronounced more clearly in the phosphor-mimicking PFN2a S137D mutant. The number of recorded cells was too low to draw reliable conclusions here. However, in the sEPSC amplitude, the recorded cells reflected a significant change (Figure 31).

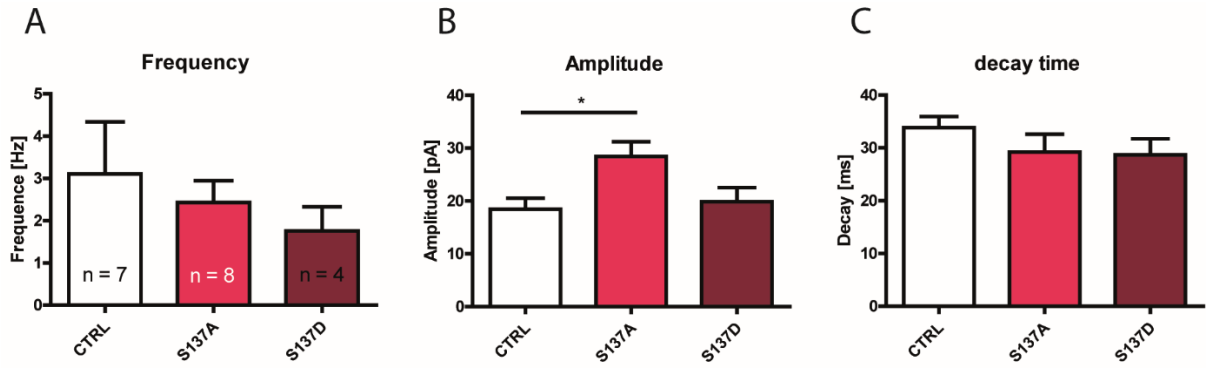

Figure 31: Patch Clamp data of CA3 pyramidal neurons expressing phosphorylation mutants **(A)** Analysis of sEPSC frequency within 2 min of recording **(B**) sEPSC amplitude showed significant increase in Pfn2 S137A mutant condition. **(C)** Data of decay time revealed no differences between both mutant and control group. All data is presented as mean ± SEM. Significances are indicated by *p value < 0.05, **p value < 0.01, ***p value < 0.001 and ****p value <0.0001 calculated by one-way ANOVA.

The cells which expressed the PFN2a S137A mutant revealed an increase compared to the control cells whereas cells expressing the mutant which mimicked the constitutive phosphorylated form was comparable to control level.

Finally, data of the decay time, indicating the receptors reset time, remained equal in all conditions. Subsequently, the action potentials of cells were analyzed (Figure 32). The protocol for evoking the action potentials was the same protocol as used for Pfn1 and 2a KO system. In the pyramidal neurons of the CA3 region of the primary organotypic hippocampal slice cultures a rising number of action potentials could be seen.

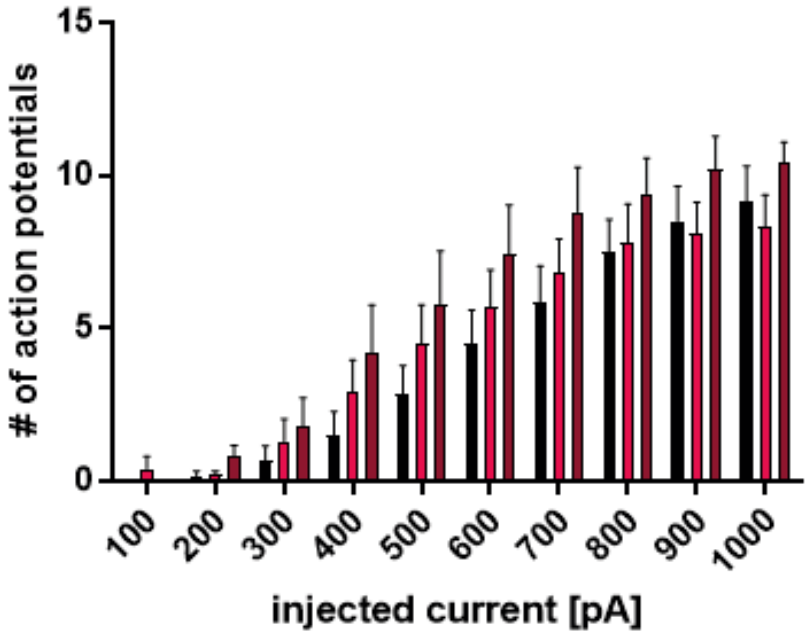

Figure 32: Analysis of the number of action potentials of CA3 pyramidal neurons after transduction with respective rAAV particles inducing the shRNA mediated knockdown of endogenous Pfn2 and knockin of phospho-mutant Pfn2a. Number of action potentials of cells of all 3 conditions (CTRL black, S137A light red, S137D dark red) rose according to the rising currents. No significant differences could be observed. All data is presented as mean ± SEM. Significances are indicated by *p value < 0.05, **p value < 0.01, ***p value < 0.001 and ****p value <0.0001 calculated by one-way ANOVA.

The knockin of the different Pfn2a mutants did not change the outcome significantly in number of action potential. Interestingly, a trend of an increase in the number of action potentials was visible in cells expressing the Pfn2a S137D mutant (dark red) whereas the number of action potentials of cells expressing Pfn2a S137A mutant (light red) displayed a more similar number compared to CTRL cell levels.

In summary, this work provides evidence of the less dendritic complexity in Pfn1 and 2a deficient neurons from embryonic cultures and in organotypic cultures upon the loss of Pfn2a. Mice carrying the double knockout showed impaired memory recall but no alteration in learning. No changes in behavior was observed in either single knockout of profilin which highlights the relevance for profilin in behavior. Furthermore, analysis of synaptic transmission revealed impairment in sEPSC amplitude and frequency in Pfn2a deficient cells. The loss of profilin lead to a decrease of sEPSC frequency. Moreover, neuronal firing was impaired in all cells lacking both and only one profilin isoforms. Additionally, a loss of profilins resulted in a trend of less negative resting membrane potential emphasizing the role of profilin for synaptic transmission. The dephosphorylation mimicking mutant Pfn2a S137A showed a significant increase in sEPSC amplitude.

Discussion

The biochemical properties of profilin as well as the regulation and involvement of this protein have been studied for several decades now. However, still the overall picture in neuroscience, especially the correlation of structural and functional plasticity and the role of two profilin isoforms in this machinery remains elusive. In the past, different effects of profilin were studied (Ackermann and Matus, 2003, Da Silva et al., 2003, Lamprecht et al., 2006) whereas profilin1 studies remained difficult due to the lethality of constitutive knock out. Furthermore, studies targeting only Pfn2a appear in a different light as soon as the study of Michaelsen and colleagues (Michaelsen-Preusse, 2009, Michaelsen et al., 2010) brought the idea of compensatory mechanisms between the two profilin isoforms into play. Moreover, studies related to profilin 1, which overcame the severity of a conventional *pfn1* depletion, could not unambiguously assign phenotypes to specific isoforms. In this thesis, a simultaneous and single knockout of profilins via the Ca9 genome editing system enabled isoform distinction. Thus, this work can provide reliable insight into the role of profilin functions, specific and overlapping, in structural and functional plasticity as well as behavior studies.

Cas9 genome editing system enables endogenous profilin isoform depletion

The CRISPR Cas9 system is today a common tool in genome editing. The easy and quick construction and application to the target gene are only some of the advantages of this technique as it might be of increased translational use in disease treatment (Bhaya et al., 2011). Nevertheless, a characterization of the genome editing system was elementary. As different combinations of sgRNA sequences were used, efficiency could be compared by quantitative Western blot analysis. Worth mentioning is that the efficiency of neuronal and astrocytic knock out constructs reached nearly complete eradication. Endogenous profilin in microglia or oligodendrocytes can be neglected as astrocytes are the most abundant form of glia cells in the brain (Herculano-Houzel, 2014).

Interestingly, we could see that the same sgRNA varied in its effectiveness depending on the combination with other sgRNAs. The 2A sgRNA for profilin 2a was much more effective in combination with the 1B variant compared to the combination with the 1C regarding the profilin 2a amount. This rises question about site effects of the CRSIPR Cas9 genome editing system as it is unclear how one sgRNA sequence might show differences in efficiency depending on a sequence. This results may be due to the tertiary structure it forms according

to the GC content leading to steric restriction during transcription but unfortunately there is no research done on this issue yet. However, it has been reported that efficiency of single sgRNAs which target multiple genes have similar impact in plants (Hunter, 2021). These findings support the importance if the characteristics of the sgRNA are crucial for its efficiency. Interestingly, there are online tools available which can calculate the most promising sgRNA in efficiency (on-target effects) as well as an algorithm for site effects and their occurrences (off target effects) (Cui et al., 2018).

Profilin2a loss reduces neuronal dendritic complexity

Profilin serves as an actin regulating protein and was reported as an important factor for neuronal morphology (Ackermann and Matus, 2003, Michaelsen et al., 2010, Da Silva et al., 2003, Michaelsen-Preusse et al., 2016). A knockdown of PFN2a via shRNA approach resulted in a reduction in dendritic complexity over time. This phenotype was observable in apical as well as basal dendrites. Moreover spine density of CA1 hippocampal neurons was reduced on basal and proximal apical dendrites (Michaelsen et al., 2010). The reduction of the overall dendritic complexity in primary embryonic hippocampal cultures reported in this thesis indicated a similar phenotype. However, during the dissociation process, the naïve organization of cells in the tissue as well as the allocation of neurons to specific subregions in the hippocampus is lost. Therefore, the morphological analysis was repeated in slice cultures and showed a similar reduction of basal dendritic complexity in the CA3 subregion after induction of Pfn2a knockout. Here, we could find minor changes of dendritic complexity compared with Sholl analysis of primary dissociated hippocampal neurons. Nevertheless, the differentiation between basal and apical dendritic trees revealed a reduction in dendritic complexity in Pfn2a deficient cells whereas the Pfn1 single KO and the double Pfn knockout remained unaltered compared to control cell morphology. This supports the previous findings that the profilin2 isoform is crucially involved in the regulation of dendritic complexity of hippocampal neurons expanding this to the CA3 subregion (Michaelsen et al., 2010).

Furthermore our results are in line with the finding that spine density and spine head diameter were not altered in $Pfn1^{-/-,CaMKII\text{-}cre}$ mice (Gorlich et al., 2012) underlining the crucial role of Pfn2a but not Pfn1 for spine density. In contrast, shRNA mediated Pfn1 knockdown resulted in significant reduction in spine density at 17 DIV but not at 34 DIV. The efficiency of the shRNA

mediated knockdown however only achieved a loss of 75% of the endogenous protein. Spine density was effected in CA1 and CA3 region (Michaelsen-Preusse et al., 2016).

In our approach the loss of pfn1 was not as severe compared to the depletion of pfn2a. This also indicate that no compensatory mechanism is involved. In summary, further investigation is needed to distinguish subregion specific effects, as our analysis relies on CA3 area only.

Interestingly, Michaelsen and colleagues reported that the knock in of Pfn1 after the Pfn2a knockdown could not rescue the reduction in dendritic complexity but was able to restore Pfn2a knockdown-induced spine loss (Michaelsen et al., 2010). This already led to the conclusion that profilins have isoform specific as well as overlapping functions. In this thesis we could show, that the spine density of CA3 hippocampal neurons were unchanged upon the loss of either both or just one profilin isoform. Although in contrast to the shRNA mediated knockdown of Pfn2a induced spine loss, our results did not reveal an alteration spine density due to the abundance of profilin. For a better understanding the monitoring of expression level of other actin modifying proteins would be interesting, as it has been shown that the spine density is also effected by other proteins like cortactin, cofilin, N-WASP, WAVE and Abp (Hering and Sheng, 2003, Wegner et al., 2008, Soderling et al., 2007). Furthermore, it remains unknown if regulation of actin dependent morphology results on the basis of the local concentration of profilin. The shRNA mediated approach achieved levels of 73.3% reduction quantified via immunostaining. The results of this thesis are based on the quantative western blot analysis. Thus the effect of profilin isoforms on spine density is still unclear, especial concerning the interaction and competition of other actin regulating proteins and maybe also dependent on the local concentration.

Loss of profilins results in strong impairment of neuronal firing

Profilin 1 and 2a are involved in presynaptic vesicle release (Pilo Boyl et al., 2007) as well as endocytosis (Gareus et al., 2006). In this thesis we showed that hippocampal excitatory neurons are not capable to generate or release action potentials properly upon the loss of profilins. The phenotype appears to limit the number of action potentials in profilin-deficient cells, whereas in control cells the number of action potentials increases. We hypothesize that the machinery of vesicle release and also recycling of neurotransmitter dependent on endocytosis are heavily effected due to the loss of profilin 1 and 2a. The data show that the effect sizes of the single and double knockout are equally strong, suggesting that the isoforms

have specific functions that are similarly important for neuronal transmission. So far, only the relevance of Pfn1 for myelination in Schwann cells with respect to action potentials has been reported (Montani et al., 2014)

The loss of Pfn1 and Pfn2a in the presynaptic site inducing the reduction of the number of action potentials is likely to result in a decrease of postsynaptic sEPSCs frequency and therefore might mask an enhanced vesicle release due to the loss of Pfn2a. The knockdown of Pfn1 resulted in a similar decrease of sEPSC frequence (Michaelsen-Preusse et al., 2016).

This highlights the importance of profilins in the process of generation and/or release of action potentials of hippocampal neurons. Due to the trend of a less negative resting potential and therefore increased excitability in a profilin double KO situation, the question rises whether PFNs are required to accumulate input, drive the signal from the soma to axonal terminals or for the release of neurotransmitters. However, the less negative membrane potential indicates a disturbance of the ion homeostasis in the cell. Interestingly, profilin has been shown to regulate CA^{2+} homeostasis in yeast (Yoshida et al., 2013). However, these findings have to be proven in mammalian cells of course.

Profilin single but not double knock out dramatically reduces sEPSC frequency

It's been known that profilin is not only essential for neuronal morphology but also to be involved in mechanisms which are important for neuronal transmission (Birbach, 2008). The postsynaptic density is a highly dynamic region with local protein synthesis in an activity dependent manner, receptor trafficking and vesicle transport (Ackermann and Matus, 2003, Hotulainen and Hoogenraad, 2010, Feuge, 2020). The analysis of sEPSC frequency displayed a drastic decrease in cells of both profilin single knockouts but not in cells lacking both profilins. For interpretation of this data set, it should be mentioned that the spontaneous postsynaptic current frequency is correlated to the number of synapses a neuron has formed. The more functional post synapses (Ackermann and Matus, 2003) there are, the more electric input can be recorded from a receiving cell. Thus, the dendritic complexity contributes to the number of functional synapses and is therefore an important factor.

However, the reduction of dendritic complexity after the loss of Pfn2a alone cannot be reason for the impairment of sEPSC frequency. The hypothesis of a reduced number of synapses decreasing sEPSC frequency contradicts the observation of no change in dendritic morphology

after the Pfn1 KO but a significant decrease of sEPSC frequency. In addition, it remains unclear if the reduction of dendritic complexity results in such a critical decrease of sEPSC frequency. The phenotype of a reduction in sEPSC frequency and amplitude in Pfn2a deficient cells might results from an impaired vesicle release from the presynapse in amount and intervals as we assume the abundance of profilin in almost every neuronal cell in the network. The reduction of sEPSC frequency in the absence of Pfn2a is contrary to the results of Pilo Boyl and colleagues who observed an increase of miniature and spontaneous EPSCs and concluded a higher presynaptic excitability in pfn2$^{-/-}$ mice (Pilo Boyl et al., 2007). Interestingly, the both shRNA mediated single knockdowns of Pfn2a and Pfn1 led each to a significant decrease in sEPSC frequency (Michaelsen-Preusse et al., 2016). Moreover, the loss of Pfn2a showed a significant decrease in sEPSC amplitude similar to our results. This opposing effects might reside in the differences of the constitutive pfn$^{-/-}$ mouse model to the genome editing sytems inducing conditional loss of profilin.

The findings of Görlich and colleagues of an unchanged miniature EPSC frequency in the absence of profilin1 (Gorlich et al., 2012) seem in line with our hypothesis of a profilin 1 specific presynaptic function causing impairment of neuronal firing which results in a significant decrease in sEPSC frequency and amplitude. Again assuming that the neuronal network is effected by viral particle infection and thus a loss of the respective isoform of both pre- and postsynaptic cell. Although it is conceivable that the unchanged mEPSC frequency in the absence of profilin1 is covered by an overlapping function of Pfn2a.

Beyond that, the unchanged level of postsynaptic sEPSCs frequency in cells carrying the double knock out seemed counter intuitive at first. The idea of a compensatory mechanism that is activated due to the severity of the loss of both isoforms seemed reasonable. We however postulate, that the loss of both profilins leads to a drastic impairment in the Ca^{2+} homeostasis in the postsynapse which is able to cover sEPSC frequency deficits and recover the sEPSC frequency to control level. In this theory, the elevation of the Ca^{2+} concentration then induces the depolarization of the membrane potential mimicking proper extra cellular ion influx. Supporting this, experiments revealed a higher sensitivity to Ca^{2+} entry and elevated vesicle release probability in profilin mutants (Pilo Boyl et al., 2007). In neuronal transmission, the Calcium signaling via the spine apparatus is of essential relevance.

Thus the sEPSC frequency appears to reach control level due to postsynaptic, intracellular Ca^{2+} levels whereas it might lack presynaptic input. This hypothesis is based on the interaction of profilins with membrane-bound PIP_2. The binding does not affect the profilin:actin interaction (Skare and Karlsson, 2002). Moreover, the $PI(4,5)P_2$:profilin binding prevents the hydrolysis by phospholipase Cγ (Goldschmidt-Clermont et al., 1990a)in absence of neuronal transmission (Goldschmidt-Clermont et al., 1991). Thus profilin regulate the intracellular concentration of the enzymatic cleavage product inositol trisphosphate (IP_3) (Berridge and Irvine, 1984, Nishizuka, 1988). IP_3 itself serves as a secondary messenger and is involved in the regulation of Ca^{2+} release of the endoplasmic reticulum (Irvine et al., 1986, Hirose et al., 1998, Taylor and Laude, 2002). In addition, the theory of an increased level of calcium ions is supported by data of the heightened membrane potential.

Taken together, the loss of profilin leads to an increase postsynaptic IP_3 level due to PLCγ activity. Thus, postsynaptic Ca^{2+} is release and induced membrane depolarization which mimics neuronal transmission and restores sEPSC frequency to control level. In a single knockout situation, the PLCγ is not able to hydrolyze of PIP_2 because the remaining isoform can bind to PIP_2.

This theory is further supported by the data from neuronal stimulation and action potential number. A clear and significant reducing in all groups was visible there. While under basal conditions the profilin isoforms could compensate the PIP_2 binding and thus stabilize Ca^{2+} homeostasis, during stimulation however the PLCγ gets phosphorylated and is able to hydrolyze PIP_2 independent from the binding to profilins(Goldschmidt-Clermont et al., 1991).

Taken together the electrophysiological data show a drastic decrease in neuronal firing which indicates a presynaptic impairment. This correlates with sEPSCs frequency and amplitude shrinking in case of the single KOs. The sEPSCs frequency in the profilin double KO situation is comparable to control level, which could be due to both a lack of presynaptic input and an elevated postsynaptic Ca^{2+} concentration due to a dysregulation of PIP_2 - IP_3 pathway.

Phosphorylation status of profilin influences postsynaptic currents

The phosphorylation and therefore a regulation of profilin 2a aroused our interest after the results of significant decrease in sEPSC amplitude and frequency after PFN2a knockout

induction. Recent studies investigated the phosphorylation *in vitro* and the resulting effects regarding ligand binding and actin dynamics (Diamond et al., 2015, Walter et al., 2020).

Shao and colleagues could show that profilin is phosphorylated at the position 137 via ROCK1, under the control of Rho-GTPases. The phosphorylation leads to only modest interference with the actin binding of profilin but reduces binding affinity to ligands containing polyproline stretches (Shao et al., 2008). This poly-L-proline stretches (PLP) relates to a hugh variety of ligands, so far over 50 candidates are listed in mammalian cells (for rev. see (Witke, 2004)).

Our results are based on the shRNA mediated knockdown– knockin approach described in Michaelsen *et. al* 2010 and analysis revealed a significant increase of sEPSC amplitude of cells transduced with the rAAV particles coding for the Pfn2a S137A mutant protein. The level of sEPSC amplitude of the cells expressing Pfn2a S137D mutant protein remained similar to the control. This indicates an important role of the phosphorylation at the position 137 for pre and postsynaptic function. The sEPSCs amplitude is correlating with the amount of presented receptors at the PSD as well as the number of presynaptic vesicle and their release.

However, the effects both S137 mutants do not seem to be relevant for the generation or release of action potentials, since the number of action potentials is not changed after the expression of Pfn2a mutants.

Neuronal profilins are important for memory recall

The question if and how learning and memory would be effected in a spatial learning task after the induction of neuron-specific profilin double knockout was thrilling as it had not been examined before. In this thesis, we can rule out the possibility of dysfunction of neurons, which have been accommodated with abnormal performance of learning and memory (Yin et al., 2011, Topuz et al., 2020). In this course of the behavior experiments, the immunohistochemistry did not reveal increased staining of microglia abundance or morphology in the injected areas (data not shown). Previous studies using fear conditioning reported that profilin is recruited into spines significantly in the lateral amygdala of rats following fear conditioning. Unfortunately, Lamprecht and colleagues did not differentiate isoform specificity (Lamprecht et al., 2006). Moreover, studies in $Pfn1^{flx/flx,\ CaMKII\text{-}cre}$ mice revealed unaltered spine density and spine morphology (Gorlich et al., 2012). In addition, Görlich and colleagues could discover that Pfn1 loss does not interfere with synaptic plasticity

at the Schaffer-collateral pathway as the LTP measurement was unaffected in Pfn1 deficient neurons.

One month after stereotactic injection of rAAV particles, 3 month old male mice were trained in the Morris water maze spatial learning task and sacrificed immediately after the last session, the spine density in the CA3 area of the hippocampus was analyzed. No alterations in escape latency due to the loss of profilins was detectable during the MWM training. The mice improved in a similar manner by finding the platform quicker which indicates that learning was not affected by the loss of profilins. These results are in line with unaltered LTP in profilin1 deficient mice (Gorlich et al., 2012). This determination indicates that memory acquisition does not necessary rely on profilins. This however could be due to compensatory mechanisms taking over in actin regulation or other cellular functions in structural or synaptic plasticity.

Recent studies could report that the CA3 area of the hippocampus is not directly involved in memory acquisition due to MWM experiments following injection of CA3 specific inhibitor (Florian and Roullet, 2004). In this regard, the unchanged spine density in the CA3 area in this work matches. Additionally, learning and memory processes do not necessary imply morphological changes (Jonas Feuge, *personal communication*).

In contrast of the unaffected escape latency, the preference of the target quadrant of the former platform position was impaired in Pfn double knockout mice. The littermates lacking only one profilin isoform behaved similar to control animals. The lack of target quadrant preference in double knockout mice strongly indicates a deficit in memory recall.

The behavioral impairment was not associated with a change in spine density in the CA3 area. This might reside from different functions in the areas in the hippocampus. Recent findings link most phenotypes or defects in learning and memory experiments to the CA1 hippocampus subregion. Hippocampal CA1 neurons and prefrontal cortex have been shown to pave successful retrieval as well as indexing the precision of the retrieved spatial memories in humans (Stevenson et al., 2018). Therefore, an alteration in neuronal morphology would be more likely to be found in the CA1 but not CA3 region. In our studies we focused on the CA3 area in order to achieve comparability to data from electrophysiological experiments. However, this is not easily possible due to the complexity and the small number of animals used in the MWM. Additionally, differences between patch clamp and behavior experiments

maybe due to sex differences which wouldn't be seen in patch clamp. In patch clamp experiments cultures of either sex were used.

However, memory retrieval might be impaired by presynaptic deficits, as the retrieval of experience relies on a more efficient activation of the neural network. In summary, these results indicate that profilin1 and 2a are not essential for learning. However, the data strongly indicate an important role of both profilin isoforms in spatial memory retrieval. Pfn1 and Pfn2a seem to possess overlapping functions as the phenotype was only revealed in the double profilin knockout situation. This indicates a compensatory effect in memory recall for profilin isoforms. The question arises if the cellular functions of profilins which were shown before in EPSCs and neuronal transmission could correlate with the deficits in memory recall.

Conclusion and Outlook

The work presented here aimed for a deeper understanding of the role of the two neural profilin isoforms on a cellular, physiological and behavior level. The use of the CRISPR Cas9 genome editing system allowed us to study both profilin isoforms and the effects of the conditional knockout. Additionally, the system enabled us to differentiate between isoform specific and overlapping functions as the existence of two profilin isoforms in one tissue is uncommon and their relevance was in question for a long time.

As it is known that profilins can bind actin and thereby regulating actin dynamics, the cellular morphology was analyzed revealing reduction of dendritic complexity in different culture systems in line with previous studies (Michaelsen et al., 2010). The reported effects on spine density in the CA1 area could not be observed in the CA3 area. Therefore, it would be of great interest to further reveal morphological differences in hippocampal subregions and to link these to the physiological roles of CA1 and CA3 pyramidal cells. Therefore, an interesting experimental design would be the overexpression of Pfn1 or Pfn2 and analyze viability, morphology and neuronal transmission to unravel further information to support past findings and incorporate studies which seem currently opposing.

In this work, functions of both profilin isoforms in learning behavior were examined simultaneously for the first time. On the base of our data, we claim that the profilins are involved in memory consolidation and retrieval but not in acquisition. A further investigation of the behavior relevance in learning and memory processes of profilin is therefore highly interesting. The distinction between consolidation and recall as well as the cellular tracing of the engram coding cells by further behavior experiments would be promising approaches. This could be done by cFos staining after recall tasks to trace engram cells in the hippocampal areas. The morphological analysis of engram cells could support the close correlation of structural and functional plasticity.

The shown deficits in neuronal transmission also need further investigation. Here, Ca^{2+} imaging in neuronal cultures could be performed. The combination of Ca^{2+} imaging during whole cell patch clamp experiments could proof a miss regulation of Ca^{2+}homeostasis due to the lack of profilin. In case of our hypothesis of a defect in calcium homeostasis should be detected in cells lacking both profilin isoforms but not in single knockout cells. Moreover, the blocking of AMPA and NMDA receptors and extracellular sources of calcium ions should make

no difference in sEPSC frequency in the absence of both profilins similar to the miniature EPSC frequency under the influence of TTX.

The impairment of neuronal firing in cells lacking either one or both profilins is worth studying, too. The distinction between a limitation in generation or the release of action potentials would be crucial here. The role of profilin and actin regulation might affect the voltage gated ion channels along the axon and could be a key factor in this process.

The involvement of astrocytes in neuronal transmission could be of interest as it was shown that astrocytes express both profilin isoforms (Schweinhuber et al., 2015) and are actively participating in neuronal transmission (Navarrete and Araque, 2011). The induction of an astrocyte specific profilin knockout might lead to peripheral astrocytic process retrieval from tripartite synapses and therefore impair memory formation as the PAPs have been shown to be regulated via profilins (Schweinhuber et al., 2015). In addition, the interaction of astrocytic profilins with the PLCδ expressed in astrocytes is highly interesting. This might bring insight into the regulation of Ca^{2+}homeostasis. The Ca^{2+} signaling of astrocytes have been shown to affect neuronal transmission and network but still the underlying mechanisms are poorly understood (Nedergaard et al., 2003, Navarrete and Araque, 2011, Bazargani and Attwell, 2016). Then of course the investigation of learning behavior in mice lacking astrocytic profilins would be the next step. These experiments would provide information about the neuron glia interaction in the hippocampus and of the tripartite synapse. In this course, morphological analysis of peripheral astrocytic protrusions, the number of synapses which are actively involved in engram coding and are engulfed by astrocytes could be measured. The application of the astrocyte specific profilin genome editing system of CRISPR Cas9 in the hippocampus could be achieved via stereotactic injection of recombinant adeno associated virus particles similar to the neuron specific knockout induction. Cell type-specific expression of Cre recombinase would be achieved here by using a tGFAP promoter. The application was already done for knockout efficiency in neuronal cultures in this thesis. The experimental design enables the distinction of isoform specific as well as overlapping functions of profilin in astrocytes and their relevance for neuronal physiology. This would help to further elucidate the functional role of profilins in neuronal networks.

Acknowledgements

First of all, I would like to thank Prof. Dr. Martin Korte for the supervision and the opportunity to do my doctoral thesis in this laboratory. Thanks especially for the professional as well as mental support during the final phase. I would like to thank Prof. Dr. Köster and Prof. Dr. Hiller for taking over the supervision and chairing the examination and supporting ambitious time schedules. My further thanks go to Dr. Martin Rothkegel for his many years of support, which was always available to me on the path of my personal and professional development. Thank you Martin! Very similar thanks go to Tania Meßerschmidt. Thank you for your help, professional assistance, practical teachings in so many areas and especially the many laughs. Thank you. Furthermore, my thanks go to Diane, who stood by me in all situations and made cultures of the highest quality a matter of course. Thanks also to Carmen and Heike, you are together with Mrs Demesvary-Steller and Sybille the backbone of this awesome working group. Thanks to Marta, Andreas and the Kristin Michaelsen-Preusse, for critical questions and advice as well as friendly chats besides work. Thanks for teaching methods (Gene gun and MWM) and "being a role model".I also thank Doro, Mark, Hendrik, Sarah, Stefan and Luisa who laid the foundation of this project. I am grateful and proud to have been able to start and continue this work through your dedication. Unforgettable for me and thus connected with deep gratitude is the time with my companions Shirin, Susi, Charlotte, Kristin, Abi, Akila, Melanie, Jenny, Caroline, Xizi, Steffen, Jonas, Hendrik and Niki (Herr Niklas). You have become friends like so many colleagues. You have created an extremely pleasant and at the same time productive working atmosphere. I am already looking forward to seeing you again and reviewing the time we have spent together here. Of course Reinhard 'Killer' Huwe should not be missing here. Thank you for the many lunches, in which you lighted up our everyday business and of course lifesaving several repairs of various devices. I would also like to thank my friends from Braunschweig and Münster. Whether it was jogging laps in the Prinzenpark or Zoom- Gin tastings, gaming evenings or walks - thanks to you I did not feel socially distant in times of Corona. I am deeply grateful to my girlfriend Sonja and my parents and brothers. You have supported me, endured me, built me up, driven me, valued me, respected me and celebrated me. I could not ask for more.

Thank you,

Max

Bibliography

ACKERMANN, M. & MATUS, A. 2003. Activity-induced targeting of profilin and stabilization of dendritic spine morphology. *Nat Neurosci,* 6**,** 1194-200.

ANDERSEN, P. 1975. Organization of Hippocampal Neurons and Their Interconnections. *In:* ISAACSON, R. L. & PRIBRAM, K. H. (eds.) *The Hippocampus: Volume 1: Structure and Development.* Boston, MA: Springer US.

BAZARGANI, N. & ATTWELL, D. 2016. Astrocyte calcium signaling: the third wave. *Nature neuroscience,* 19**,** 182-189.

BERRIDGE, M. J. & IRVINE, R. F. 1984. Inositol trisphosphate, a novel second messenger in cellular signal transduction. *Nature,* 312**,** 315-321.

BHAYA, D., DAVISON, M. & BARRANGOU, R. 2011. CRISPR-Cas systems in bacteria and archaea: versatile small RNAs for adaptive defense and regulation. *Annu Rev Genet,* 45**,** 273-97.

BIRBACH, A. 2008. Profilin, a multi-modal regulator of neuronal plasticity. *Bioessays,* 30**,** 994-1002.

BLASCO, R., COLE, N. B. & MOSS, B. 1991. Sequence analysis, expression, and deletion of a vaccinia virus gene encoding a homolog of profilin, a eukaryotic actin-binding protein. *Journal of Virology,* 65**,** 4598-4608.

CARLSSON, L., NYSTROM, L. E., SUNDKVIST, I., MARKEY, F. & LINDBERG, U. 1977. Actin polymerizability is influenced by profilin, a low molecular weight protein in non-muscle cells. *J Mol Biol,* 115**,** 465-83.

CHANG, F., WOOLLARD, A. & NURSE, P. 1996. Isolation and characterization of fission yeast mutants defective in the assembly and placement of the contractile actin ring. *J Cell Sci,* 109 (Pt 1)**,** 131-42.

CUI, Y., XU, J., CHENG, M., LIAO, X. & PENG, S. 2018. Review of CRISPR/Cas9 sgRNA Design Tools. *Interdiscip Sci,* 10**,** 455-465.

DA SILVA, J. S., MEDINA, M., ZULIANI, C., DI NARDO, A., WITKE, W. & DOTTI, C. G. 2003. RhoA/ROCK regulation of neuritogenesis via profilin IIa-mediated control of actin stability. *J Cell Biol,* 162**,** 1267-79.

DI NARDO, A., GAREUS, R., KWIATKOWSKI, D. & WITKE, W. 2000. Alternative splicing of the mouse profilin II gene generates functionally different profilin isoforms. *J Cell Sci,* 113 Pt 21**,** 3795-803.

DIAMOND, M. I., CAI, S., BOUDREAU, A., CAREY JR, C. J., LYLE, N., PAPPU, R. V., SWAMIDASS, S. J., BISSELL, M., PIWNICA-WORMS, H. & SHAO, J. 2015. Subcellular localization and Ser-137 phosphorylation regulate tumor-suppressive activity of profilin-1. *Journal of Biological Chemistry,* 290**,** 9075-9086.

DUPRET, D., FABRE, A., DOBROSSY, M. D., PANATIER, A., RODRIGUEZ, J. J., LAMARQUE, S., LEMAIRE, V., OLIET, S. H., PIAZZA, P. V. & ABROUS, D. N. 2007. Spatial learning depends on both the addition and removal of new hippocampal neurons. *PLoS Biol,* 5**,** e214.

FEUGE, J. 2020. *Local translation of actin-binding proteins in the healthy and diseased central nervous system.* Dissertation, TU Braunschweig.

FLORIAN, C. & ROULLET, P. 2004. Hippocampal CA3-region is crucial for acquisition and memory consolidation in Morris water maze task in mice. *Behav Brain Res,* 154**,** 365-74.

GAREUS, R., DI NARDO, A., RYBIN, V. & WITKE, W. 2006. Mouse profilin 2 regulates endocytosis and competes with SH3 ligand binding to dynamin 1. *J Biol Chem,* 281**,** 2803-11.

GOLDSCHMIDT-CLERMONT, P., MACHESKY, L., BALDASSARE, J. & POLLARD, T. 1990a. The actin-binding protein profilin binds to PIP2 and inhibits its hydrolysis by phospholipase C. *Science,* 247**,** 1575-1578.

GOLDSCHMIDT-CLERMONT, P. J., MACHESKY, L. M., BALDASSARE, J. J. & POLLARD, T. D. 1990b. The actin-binding protein profilin binds to PIP2 and inhibits its hydrolysis by phospholipase C. *Science,* 247**,** 1575-1578.

GOLDSCHMIDT-CLERMONT, P. J., MACHESKY, L. M., DOBERSTEIN, S. K. & POLLARD, T. D. 1991. Mechanism of the interaction of human platelet profilin with actin. *The Journal of cell biology,* 113**,** 1081-1089.

GORLICH, A., ZIMMERMANN, A. M., SCHOBER, D., BOTTCHER, R. T., SASSOE-POGNETTO, M., FRIAUF, E., WITKE, W. & RUST, M. B. 2012. Preserved morphology and physiology of excitatory synapses in profilin1-deficient mice. *PLoS One,* 7**,** e30068.

HEBB, D. O. 1949. *Organization of behavior. A Neuropsychological Theory,* New York, John Wiley & Sons.

HENNIG, S. 2017. *Quantitative und qualitative Analyse des Cas9-induzierten simultanen „knock out" des pfn1- und des pfn2-Gens in der Neuroblastoma-Zelllinie NSC19.* Tu Braunschweig.

HERCULANO-HOUZEL, S. 2014. The glia/neuron ratio: how it varies uniformly across brain structures and species and what that means for brain physiology and evolution. *Glia,* 62**,** 1377-91.

HERING, H. & SHENG, M. 2003. Activity-dependent redistribution and essential role of cortactin in dendritic spine morphogenesis. *Journal of Neuroscience,* 23**,** 11759-11769.

HIROSE, K., KADOWAKI, S. & IINO, M. 1998. Allosteric regulation by cytoplasmic Ca2+ and IP3 of the gating of IP3 receptors in permeabilized guinea-pig vascular smooth muscle cells. *The Journal of physiology,* 506**,** 407.

HONKURA, N., MATSUZAKI, M., NOGUCHI, J., ELLIS-DAVIES, G. C. & KASAI, H. 2008. The subspine organization of actin fibers regulates the structure and plasticity of dendritic spines. *Neuron,* 57**,** 719-29.

HOTULAINEN, P. & HOOGENRAAD, C. C. 2010. Actin in dendritic spines: connecting dynamics to function. *J Cell Biol,* 189**,** 619-29.

HUNTER, C. T. 2021. CRISPR/Cas9 Targeted Mutagenesis for Functional Genetics in Maize. *Plants (Basel),* 10.

IRVINE, R. F., LETCHER, A. J., HESLOP, J. P. & BERRIDGE, M. J. 1986. The inositol tris/tetrakisphosphate pathway—demonstration of Ins(l,4,5)P3 3-kinase activity in animal tissues. *Nature,* 320**,** 631-634.

JOCKUSCH, B. M., MURK, K. & ROTHKEGEL, M. 2007. The profile of profilins. *Rev Physiol Biochem Pharmacol,* 159**,** 131-49.

LAMPRECHT, R., FARB, C. R., RODRIGUES, S. M. & LEDOUX, J. E. 2006. Fear conditioning drives profilin into amygdala dendritic spines. *Nat Neurosci,* 9**,** 481-3.

LASSING, I. & LINDBERG, U. 1985. Specific interaction between phosphatidylinositol 4,5-bisphosphate and profilactin. *Nature,* 314**,** 472-474.

LISMAN, J., BUZSAKI, G., EICHENBAUM, H., NADEL, L., RANGANATH, C. & REDISH, A. D. 2018. Publisher Correction: Viewpoints: how the hippocampus contributes to memory, navigation and cognition. *Nat Neurosci,* 21**,** 1018.

MACHESKY, L. M., ATKINSON, S. J., AMPE, C., VANDEKERCKHOVE, J. & POLLARD, T. D. 1994. Purification of a cortical complex containing two unconventional actins from Acanthamoeba by affinity chromatography on profilin-agarose. *J Cell Biol,* 127**,** 107-15.

MAGEE, J. C. & JOHNSTON, D. 1997. A Synaptically Controlled, Associative Signal for Hebbian Plasticity in Hippocampal Neurons. *Science,* 275**,** 209-213.

MICHAELSEN-PREUSSE, K. 2009. *Molecular mechanisms regulating dendrite architecture of mature pyramidal neurons in the mouse hippocampus.* Dr. rer. nat., Tu Braunschweig.

MICHAELSEN-PREUSSE, K., ZESSIN, S., GRIGORYAN, G., SCHARKOWSKI, F., FEUGE, J., REMUS, A. & KORTE, M. 2016. Neuronal profilins in health and disease: Relevance for spine plasticity and Fragile X syndrome. *Proceedings of the National Academy of Sciences,* 113**,** 3365-3370.

MICHAELSEN, K., MURK, K., ZAGREBELSKY, M., DREZNJAK, A., JOCKUSCH, B. M., ROTHKEGEL, M. & KORTE, M. 2010. Fine-tuning of neuronal architecture requires two profilin isoforms. *Proc Natl Acad Sci U S A,* 107**,** 15780-5.

MIKI, H., SUETSUGU, S. & TAKENAWA, T. 1998. WAVE, a novel WASP-family protein involved in actin reorganization induced by Rac. *The EMBO journal,* 17**,** 6932-6941.

MOLOTKOV, D., ZOBOVA, S., ARCAS, J. M. & KHIROUG, L. 2013. Calcium-induced outgrowth of astrocytic peripheral processes requires actin binding by Profilin-1. *Cell calcium,* 53**,** 338-348.

MONTANI, L., BUERKI-THURNHERR, T., DE FARIA, J. P., PEREIRA, J. A., DIAS, N. G., FERNANDES, R., GONÇALVES, A. F., BRAUN, A., BENNINGER, Y., BÖTTCHER, R. T., COSTELL, M., NAVE, K.-A.,

FRANKLIN, R. J. M., MEIJER, D., SUTER, U. & RELVAS, J. B. 2014. Profilin 1 is required for peripheral nervous system myelination. *Development,* 141**,** 1553-1561.

MORRIS, R. G. 1999. D.O. Hebb: The Organization of Behavior, Wiley: New York; 1949. *Brain Res Bull,* 50**,** 437.

MORRIS, R. G., ANDERSON, E., LYNCH, G. S. & BAUDRY, M. 1986. Selective impairment of learning and blockade of long-term potentiation by an N-methyl-D-aspartate receptor antagonist, AP5. *Nature,* 319**,** 774-6.

MORRIS, R. G., GARRUD, P., RAWLINS, J. N. & O'KEEFE, J. 1982. Place navigation impaired in rats with hippocampal lesions. *Nature,* 297**,** 681-3.

MOSER, E. I. 2011. The multi-laned hippocampus. *Nat Neurosci,* 14**,** 407-8.

MURK, K., WITTENMAYER, N., MICHAELSEN-PREUSSE, K., DRESBACH, T., SCHOENENBERGER, C. A., KORTE, M., JOCKUSCH, B. M. & ROTHKEGEL, M. 2012. Neuronal profilin isoforms are addressed by different signalling pathways. *PLoS One,* 7**,** e34167.

NAVARRETE, M. & ARAQUE, A. 2011. Basal synaptic transmission: astrocytes rule! *Cell,* 146**,** 675-677.

NEDERGAARD, M., RANSOM, B. & GOLDMAN, S. A. 2003. New roles for astrocytes: redefining the functional architecture of the brain. *Trends in neurosciences,* 26**,** 523-530.

NISHIZUKA, Y. 1988. The molecular heterogeneity of protein kinase C and its implications for cellular regulation. *Nature,* 334**,** 661-665.

PEREA, G., YANG, A., BOYDEN, E. S. & SUR, M. 2014. Optogenetic astrocyte activation modulates response selectivity of visual cortex neurons in vivo. *Nat Commun,* 5**,** 3262.

PILO BOYL, P., DI NARDO, A., MULLE, C., SASSOE-POGNETTO, M., PANZANELLI, P., MELE, A., KNEUSSEL, M., COSTANTINI, V., PERLAS, E., MASSIMI, M., VARA, H., GIUSTETTO, M. & WITKE, W. 2007. Profilin2 contributes to synaptic vesicle exocytosis, neuronal excitability, and novelty-seeking behavior. *EMBO J,* 26**,** 2991-3002.

PLATT, R. J., CHEN, S., ZHOU, Y., YIM, M. J., SWIECH, L., KEMPTON, H. R., DAHLMAN, J. E., PARNAS, O., EISENHAURE, T. M., JOVANOVIC, M., GRAHAM, D. B., JHUNJHUNWALA, S., HEIDENREICH, M., XAVIER, R. J., LANGER, R., ANDERSON, D. G., HACOHEN, N., REGEV, A., FENG, G., SHARP, P. A. & ZHANG, F. 2014. CRISPR-Cas9 knockin mice for genome editing and cancer modeling. *Cell,* 159**,** 440-55.

REINHARD, M., GIEHL, K., ABEL, K., HAFFNER, C., JARCHAU, T., HOPPE, V., JOCKUSCH, B. & WALTER, U. 1995. The proline-rich focal adhesion and microfilament protein VASP is a ligand for profilins. *The EMBO journal,* 14**,** 1583-1589.

ROTTY, J. D., WU, C., HAYNES, E. M., SUAREZ, C., WINKELMAN, J. D., JOHNSON, H. E., HAUGH, J. M., KOVAR, D. R. & BEAR, J. E. 2015. Profilin-1 serves as a gatekeeper for actin assembly by Arp2/3-dependent and -independent pathways. *Dev Cell,* 32**,** 54-67.

SCHLUTER, K., JOCKUSCH, B. M. & ROTHKEGEL, M. 1997. Profilins as regulators of actin dynamics. *Biochimica et Biophysica Acta-Molecular Cell Research,* 1359**,** 97-109.

SCHWEINHUBER, S. K., MESSERSCHMIDT, T., HANSCH, R., KORTE, M. & ROTHKEGEL, M. 2015. Profilin isoforms modulate astrocytic morphology and the motility of astrocytic processes. *PLoS One,* 10**,** e0117244.

SCOVILLE, W. B. & MILNER, B. 1957. Loss of recent memory after bilateral hippocampal lesions. *J Neurol Neurosurg Psychiatry,* 20**,** 11-21.

SHAO, J., WELCH, W. J., DIPROSPERO, N. A. & DIAMOND, M. I. 2008. Phosphorylation of profilin by ROCK1 regulates polyglutamine aggregation. *Molecular and cellular biology,* 28**,** 5196.

SKARE, P. & KARLSSON, R. 2002. Evidence for two interaction regions for phosphatidylinositol (4, 5)-bisphosphate on mammalian profilin I. *FEBS letters,* 522**,** 119-124.

SODERLING, S. H., GUIRE, E. S., KAECH, S., WHITE, J., ZHANG, F., SCHUTZ, K., LANGEBERG, L. K., BANKER, G., RABER, J. & SCOTT, J. D. 2007. A WAVE-1 and WRP signaling complex regulates spine density, synaptic plasticity, and memory. *Journal of Neuroscience,* 27**,** 355-365.

SOHN, R. H., CHEN, J., KOBLAN, K. S., BRAY, P. F. & GOLDSCHMIDT-CLERMONT, P. J. 1995. Localization of a binding site for phosphatidylinositol 4, 5-bisphosphate on human profilin. *Journal of Biological Chemistry,* 270**,** 21114-21120.

SPENCER, R. L. & BLAND, S. T. 2019. Chapter 5 - Hippocampus and Hippocampal Neurons∗. *In:* FINK, G. (ed.) *Stress: Physiology, Biochemistry, and Pathology.* Academic Press.

TANAKA, K. Z. & MCHUGH, T. J. 2018. The Hippocampal Engram as a Memory Index. *J Exp Neurosci,* 12**,** 1179069518815942.

TAYLOR, C. & LAUDE, A. 2002. IP3 receptors and their regulation by calmodulin and cytosolic Ca2+. *Cell calcium,* 32**,** 321-334.

TOPUZ, R. D., GUNDUZ, O., TASTEKIN, E. & KARADAG, C. H. 2020. Effects of hippocampal histone acetylation and HDAC inhibition on spatial learning and memory in the Morris water maze in rats. *Fundam Clin Pharmacol,* 34**,** 222-228.

WALTER, L. M., FRANZ, P., LINDNER, R., TSIAVALIARIS, G., HENSEL, N. & CLAUS, P. 2020. Profilin2a-phosphorylation as a regulatory mechanism for actin dynamics. *FASEB J,* 34**,** 2147-2160.

WEGNER, A. 1976. Head to tail polymerization of actin. *J Mol Biol,* 108**,** 139-50.

WEGNER, A. M., NEBHAN, C. A., HU, L., MAJUMDAR, D., MEIER, K. M., WEAVER, A. M. & WEBB, D. J. 2008. N-wasp and the arp2/3 complex are critical regulators of actin in the development of dendritic spines and synapses. *Journal of Biological Chemistry,* 283**,** 15912-15920.

WITKE, W. 2004. The role of profilin complexes in cell motility and other cellular processes. *Trends in cell biology,* 14**,** 461-469.

WITKE, W., PODTELEJNIKOV, A. V., DI NARDO, A., SUTHERLAND, J. D., GURNIAK, C. B., DOTTI, C. & MANN, M. 1998. In mouse brain profilin I and profilin II associate with regulators of the endocytic pathway and actin assembly. *EMBO J,* 17**,** 967-76.

WITKE, W., SUTHERLAND, J. D., SHARPE, A., ARAI, M. & KWIATKOWSKI, D. J. 2001. Profilin I is essential for cell survival and cell division in early mouse development. *Proceedings of the National Academy of Sciences,* 98**,** 3832-3836.

YIN, J. X., TURNER, G. H., LIN, H. J., COONS, S. W. & SHI, J. 2011. Deficits in spatial learning and memory is associated with hippocampal volume loss in aged apolipoprotein E4 mice. *J Alzheimers Dis,* 27**,** 89-98.

YOSHIDA, M., OHNUKI, S., YASHIRODA, Y. & OHYA, Y. 2013. Profilin is required for Ca2+ homeostasis and Ca2+-modulated bud formation in yeast. *Molecular Genetics and Genomics,* 288**,** 317-328.

ZAGREBELSKY, M. & KORTE, M. 2014. Form follows function: BDNF and its involvement in sculpting the function and structure of synapses. *Neuropharmacology,* 76 Pt C**,** 628-38.

Supplements

Table 26 Statistic parameter of quantative Western Blot analysis of Pfn1

Table Analyzed	Pfn1 stats
One-way analysis of variance	
P value	< 0.0001
P value summary	***
Are means signif. different? (P < 0.05)	Yes
Number of groups	5
F	188,7
R squared	0,9869

Bonferroni's Multiple Comparison Test	Mean Diff.	Significant? P < 0.05?	Summary	95% CI of diff
1A 2B vs 1B2a	0,2980	Yes	***	0.1425 to 0.4535
1A 2B vs 1B2B	0,2650	Yes	**	0.1095 to 0.4205
1A 2B vs 1C 2A	0,2873	Yes	***	0.1319 to 0.4428
1A 2B vs CTRL	-0,6890	Yes	***	-0.8445 to -0.5335
1B2a vs 1B2B	-0,0330	No	ns	-0.1885 to 0.1225
1B2a vs 1C 2A	-0,01067	No	ns	-0.1661 to 0.1448
1B2a vs CTRL	-0,9870	Yes	***	-1.142 to -0.8315
1B2B vs 1C 2A	0,02233	No	ns	-0.1331 to 0.1778
1B2B vs CTRL	-0,9540	Yes	***	-1.109 to -0.7985
1C 2A vs CTRL	-0,9763	Yes	***	-1.132 to -0.8209

Table 27 Statistic parameter of quantative Western Blot analysis Pfn2a

Table Analyzed	Data 1
One-way analysis of variance	
P value	< 0.0001
P value summary	***
Are means signif. different? (P < 0.05)	Yes
Number of groups	5
F	55,54
R squared	0,9174

Bonferroni's Multiple Comparison Test	Mean Diff.	Significant? P < 0.05?	Summary	95% CI of diff
1A 2B P2 vs 1B 2A P2	0,0186	No	ns	-0.2279 to 0.2651
1A 2B P2 vs 1B 2B P2	-0,0702	No	ns	-0.3167 to 0.1763
1A 2B P2 vs 1C 2A P2	-0,3300	Yes	**	-0.5765 to -0.08353
1A 2B P2 vs CTRL P2	-0,9620	Yes	***	-1.208 to -0.7155
1B 2A P2 vs 1B 2B P2	-0,0888	No	ns	-0.3353 to 0.1577
1B 2A P2 vs 1C 2A P2	-0,3486	Yes	**	-0.5951 to -0.1021
1B 2A P2 vs CTRL P2	-0,9806	Yes	***	-1.227 to -0.7341
1B 2B P2 vs 1C 2A P2	-0,2598	Yes	*	-0.5063 to -0.01333

1B 2B P2 vs CTRL P2	-0,8918	Yes	***	-1.138 to -0.6453
1C 2A P2 vs CTRL P2	-0,6320	Yes	***	-0.8785 to -0.3855

Table 28 Statistical analysis of Sholl analysis of dissociated hippocampal cultures "total number of intersections"

Number of families	1
Number of comparisons per family	10
Alpha	0,05

Bonferroni's multiple comparisons test	Mean Diff.	95.00% CI of diff.	Summary	Adjusted P Value
PFN 1A+2B vs. PFN 1B+2A	22,12	-43.45 to 87.7	ns	>0.9999
PFN 1A+2B vs. PFN 1B+2B	71,55	4.325 to 138.8	*	0,0289
PFN 1A+2B vs. PFN 1C+2A	-50,57	-151.9 to 50.81	ns	>0.9999
PFN 1A+2B vs. CTRL	6,435	-70.02 to 82.89	ns	>0.9999
PFN 1B+2A vs. PFN 1B+2B	49,43	-14 to 112.9	ns	0,2746
PFN 1B+2A vs. PFN 1C+2A	-72,69	-171.6 to 26.21	ns	0,3729
PFN 1B+2A vs. CTRL	-15,69	-88.83 to 57.45	ns	>0.9999
PFN 1B+2B vs. PFN 1C+2A	-122,1	-222.1 to -22.11	**	0,0069
PFN 1B+2B vs. CTRL	-65,12	-139.7 to 9.506	ns	0,1384
PFN 1C+2A vs. CTRL	57	-49.42 to 163.4	ns	>0.9999

Table 29 Statistical analysis of Sholl analysis of dissociated hippocampal cultures "total number of nodes"

Number of families	1
Number of comparisons per family	10
Alpha	0,05

Bonferroni's multiple comparisons test	Mean Diff.	95.00% CI of diff.	Summary	Adjusted P Value
PFN 1A+2B vs. PFN 1B+2A	-1,769	-11.87 to 8.335	ns	>0.9999
PFN 1A+2B vs. PFN 1B+2B	7,975	-2.383 to 18.33	ns	0,2932
PFN 1A+2B vs. PFN 1C+2A	-5,932	-21.55 to 9.689	ns	>0.9999
PFN 1A+2B vs. CTRL	-14,47	-26.25 to -2.687	**	0,0064
PFN 1B+2A vs. PFN 1B+2B	9,744	-0.02916 to 19.52	ns	0,0513
PFN 1B+2A vs. PFN 1C+2A	-4,163	-19.4 to 11.08	ns	>0.9999
PFN 1B+2A vs. CTRL	-12,7	-23.97 to -1.429	*	0,0165
PFN 1B+2B vs. PFN 1C+2A	-13,91	-29.32 to 1.502	ns	0,1099
PFN 1B+2B vs. CTRL	-22,44	-33.94 to -10.94	****	<0.0001
PFN 1C+2A vs. CTRL	-8,536	-24.93 to 7.862	ns	>0.9999

Table 30 Statistical analysis of Sholl analysis of dissociated hippocampal cultures "cell soma size"

Number of families	1
Number of comparisons per family	10
Alpha	0,05

Bonferroni's multiple comparisons test	Mean Diff.	95.00% CI of diff.	Summary	Adjusted P Value
PFN 1A+2B vs. PFN 1B+2A	41,55	-169.9 to 253	ns	>0.9999
PFN 1A+2B vs. PFN 1B+2B	117,1	-99.61 to 333.9	ns	>0.9999
PFN 1A+2B vs. PFN 1C+2A	-99,19	-426 to 227.6	ns	>0.9999
PFN 1A+2B vs. CTRL	111,6	-145.1 to 368.2	ns	>0.9999
PFN 1B+2A vs. PFN 1B+2B	75,57	-128.9 to 280.1	ns	>0.9999

PFN 1B+2A vs. PFN 1C+2A	-140,7	-459.6 to 178.1	ns	>0.9999
PFN 1B+2A vs. CTRL	70,01	-176.4 to 316.4	ns	>0.9999
PFN 1B+2B vs. PFN 1C+2A	-216,3	-538.7 to 106.1	ns	0,5677
PFN 1B+2B vs. CTRL	-5,563	-256.6 to 245.4	ns	>0.9999
PFN 1C+2A vs. CTRL	210,7	-139.7 to 561.2	ns	0,8716

Table 31 Statistical analysis of Sholl analysis of dissociated hippocampal cultures "total number of Sholl analysis"

Table Analyzed	sholl analysis
Two-way RM ANOVA	Matching: Stacked
Alpha	0,05

Source of Variation	% of total variation	P value	P value summary	Significant?
Interaction	2,343	<0.0001	****	Yes
intersection	56,2	<0.0001	****	Yes
profilin	0,2718	0,2484	ns	No
Subjects (matching)	6,958	<0.0001	****	Yes

ANOVA table	SS	DF	MS	F (DFn, DFd)	P value
Interaction	4151	316	13,14	F (316, 11060) = 2.915	P<0.0001
intersection	99583	79	1261	F (79, 11060) = 279.7	P<0.0001
profilin	481,6	4	120,4	F (4, 140) = 1.367	P=0.2484
Subjects (matching)	12328	140	88,06	F (140, 11060) = 19.54	P<0.0001
Residual	49844	11060	4,507		

Table 32 Statistical analysis of spine density of primary hippocampal dissociated slice cultures

Table Analyzed	spine density
One-way analysis of variance	
P value	0,1920
P value summary	ns
Are means signif. different? (P < 0.05)	No
Number of groups	4
F	1,669
R squared	0,1284

Bonferroni's Multiple Comparison Test	Mean Diff.	Significant? P < 0.05?	95% CI of diff
CTRL vs 1A+2B	-0,1557	No	-0.4047 to 0.09339
CTRL vs 1B	0,01684	No	-0.2265 to 0.2602
CTRL vs 2A	-0,09214	No	-0.3666 to 0.1823
1A+2B vs 1B	0,1725	No	-0.07083 to 0.4159
1A+2B vs 2A	0,06354	No	-0.2109 to 0.3380
1B vs 2A	-0,1090	No	-0.3782 to 0.1603

Table 33 Statistical analysis of spine head diameter of primary hippocampal dissociated slice cultures

Table Analyzed	spine head
One-way analysis of variance	
P value	0,0258
P value summary	*
Are means signif. different? (P < 0.05)	Yes
Number of groups	4
F	3,500
R squared	0,2359

Bonferroni's Multiple Comparison Test	Mean Diff.	Significant? P < 0.05?	95% CI of diff
1B vs CTRL	-0,02330	No	-0.07799 to 0.03140
CTRL vs 1A+2B	-0,01593	No	-0.07191 to 0.04006
CTRL vs 2A	-0,05261	No	-0.1143 to 0.009082

Table 34 Statistics of primary hippocampal dissociated slice cultures of cell soma size

Table Analyzed	cell soma size
One-way analysis of variance	
P value	0,8289
P value summary	ns
Are means signif. different? (P < 0.05)	No
Number of groups	4
F	0,2947
R squared	0,02610

Bonferroni's Multiple Comparison Test	Mean Diff.	Significant? P < 0.05?	95% CI of diff
CTRL vs PFN 1B 2A	234,1	No	-703.6 to 1172
CTRL vs PFN 1B	5,371	No	-733.7 to 744.5
CTRL vs PFN 2A	154,7	No	-609.6 to 918.9
PFN 1B 2A vs PFN 1B	-228,7	No	-1094 to 636.8
PFN 1B 2A vs PFN 2A	-79,39	No	-966.5 to 807.7
PFN 1B vs PFN 2A	149,3	No	-524.5 to 823.1

Table 35 Statistics of primary hippocampal dissociated slice cultures of number of nodes

Table Analyzed	total dendritic length
One-way analysis of variance	
P value	0,9312
P value summary	ns
Are means signif. different? (P < 0.05)	No
Number of groups	4
F	0,1465
R squared	0,01276

Bonferroni's Multiple Comparison Test	Mean Diff.	Significant? P < 0.05?	95% CI of diff
CTRL vs PFN 1B 2A	-21,31	No	-6375 to 6332
CTRL vs PFN 1B	546,6	No	-4740 to 5833
CTRL vs PFN 2A	1110	No	-4357 to 6576
PFN 1B 2A vs PFN 1B	568,0	No	-5238 to 6374
PFN 1B 2A vs PFN 2A	1131	No	-4840 to 7102
PFN 1B vs PFN 2A	563,2	No	-4256 to 5383

Table 36 Statistics of primary hippocampal dissociated slice cultures of total dendritic length

Table Analyzed	# nodes
One-way analysis of variance	
P value	0,4007
P value summary	ns
Are means signif. different? (P < 0.05)	No
Number of groups	4
F	1,011
R squared	0,08657

Bonferroni's Multiple Comparison Test	Mean Diff.	Significant? P < 0.05?	95% CI of diff
CTRL vs PFN 1B 2A	4,029	No	-28.98 to 37.04
CTRL vs PFN 1B	5,352	No	-21.08 to 31.78
CTRL vs PFN 2A	15,52	No	-11.74 to 42.78
PFN 1B 2A vs PFN 1B	1,323	No	-28.35 to 30.99
PFN 1B 2A vs PFN 2A	11,49	No	-18.92 to 41.90
PFN 1B vs PFN 2A	10,17	No	-12.93 to 33.27

Table 37 Statistics of apical Sholl analysis primary hippocampal dissociated slice cultures

Table Analyzed	sholl analysis apical
Two-way RM ANOVA	Matching by cols

Source of Variation	% of total variation	P value
Interaction	1,29	1,0000
distance	46,43	< 0.0001
Column Factor	0,12	0,9401
Subjects (matching)	10,1714	< 0.0001

Source of Variation	P value summary	Significant?
Interaction	ns	No
distance	***	Yes
Column Factor	ns	No
Subjects (matching)	***	Yes

Source of Variation	Df	Sum-of-squares	Mean square	F
Interaction	375	1693	4,514	0,3903
distance	125	60720	485,8	42,01
Column Factor	3	160,0	53,33	0,1323
Subjects (matching)	33	13300	403,1	34,85
Residual	4125	47700	11,56	

Table 38 Statistics of basal Sholl analysis primary hippocampal dissociated slice cultures

Table Analyzed	sholl analysis basal	
Two-way RM ANOVA	Matching by cols	
Source of Variation	% of total variation	P value
Interaction	3,03	0,0073
distance	57,27	< 0.0001
Column Factor	0,28	0,8184
Subjects (matching)	9,9033	< 0.0001
Source of Variation	P value summary	Significant?
Interaction	**	Yes
distance	***	Yes
Column Factor	ns	No
Subjects (matching)	***	Yes

Source of Variation	Df	Sum-of-squares	Mean square	F
Interaction	237	4599	19,41	1,252
distance	79	86840	1099	70,91
Column Factor	3	422,4	140,8	0,3094
Subjects (matching)	33	15020	455,0	29,35
Residual	2607	40420	15,50	

Table 39 Tabel of statistic values of escape latency analysis

Table Analyzed	Data 1		
Mixed-effects model (REML)	Matching: Stacked		
Assume sphericity?	No		Geisser-Greenhouse's epsilon
Alpha	0,05		0,7913
Fixed effects (type III)	P value	P value summary	F (DFn, DFd)
days	<0.0001	****	F (5.539, 718.5) = 23.16
Genotype	0,2576	ns	F (3, 131) = 1.361
days x Genotype	0,0080	**	F (21, 908) = 1.914
Random effects	SD	Variance	
Subject	6,406	41,04	
Residual	14,73	217,0	
Was the matching effective?			
Chi-square, df	59.92, 1		
P value	<0.0001		
P value summary	****		
Is there significant matching (P < 0.05)?	Yes		
Data summary			
Number of columns (Genotype)	4		
Number of rows (days)	8		
Number of subjects (Subject)	135		
Number of missing values	9		

Table 40 Statistic values of searching strategy analysis of CTRL

Table Analyzed	CTRL 1-4 Kohorte ohne%

Two-way ANOVA	Ordinary
Alpha	0,05

Source of Variation	% of total variation	P value	P value summary	Significant?
Row Factor	16	0,9486	ns	No
Column Factor	24,12	0,1370	ns	No

ANOVA table	SS	DF	MS	F (DFn, DFd)	P value
Row Factor	0,05054	7	0,00722	F (7, 7) = 0.2671	P=0.9486
Column Factor	0,0762	1	0,0762	F (1, 7) = 2.819	P=0.1370
Residual	0,1892	7	0,02703		

Number of missing values	0

Table 41 Statistic values from probe trial d9 all quadrants

Number of families	1
Number of comparisons per family	15
Alpha	0,05

Dunnett's multiple comparisons test	Mean Diff.	95.00% CI of diff.	Significant?	Summary	Adjusted P Value	D-?	
TQ vs. Column A	35,72	18.4 to 53.05	Yes	****	0,0001	A	Column A
TQ vs. Column B	38,53	21.21 to 55.85	Yes	****	0,0001	B	Column B
TQ vs. Column C	33,2	15.87 to 50.52	Yes	****	0,0001	C	Column C
TQ vs. Column E	36,14	18.81 to 53.46	Yes	****	0,0001	E	Column E
TQ vs. Column F	28,06	10.73 to 45.38	Yes	***	0,0001	F	Column F
TQ vs. Column G	23,92	6.594 to 41.24	Yes	**	0,0016	G	Column G
TQ vs. TQ	18,53	1.204 to 35.85	Yes	*	0,0290	H	TQ
TQ vs. Column I	37,21	20.38 to 54.05	Yes	****	0,0001	I	Column I
TQ vs. Column J	33,41	16.57 to 50.25	Yes	****	0,0001	J	Column J
TQ vs. Column K	30,47	13.64 to 47.31	Yes	****	0,0001	K	Column K
TQ vs. TQ	5,857	-10.98 to 22.69	No	ns	0,9716	L	TQ
TQ vs. Column M	36,08	19.24 to 52.91	Yes	****	0,0001	M	Column M

TQ vs. Column N	37,26	20.43 to 54.1	Yes	****	0,0001	N	Column N
TQ vs. Column O	28,89	12.06 to 45.73	Yes	****	0,0001	O	Column O
TQ vs. TQ	6,029	-10.81 to 22.87	No	ns	0,9645	P	TQ

Test details	Mean 1	Mean 2	Mean Diff.	SE of diff.	n1	n2	q
TQ vs. Column A	51,14	15,42	35,72	6,027	8	8	5,927
TQ vs. Column B	51,14	12,61	38,53	6,027	8	8	6,393
TQ vs. Column C	51,14	17,95	33,2	6,027	8	8	5,508
TQ vs. Column E	51,14	15	36,14	6,027	8	8	5,997
TQ vs. Column F	51,14	23,08	28,06	6,027	8	8	4,656
TQ vs. Column G	51,14	27,22	23,92	6,027	8	8	3,969
TQ vs. TQ	51,14	32,61	18,53	6,027	8	8	3,074
TQ vs. Column I	51,14	13,93	37,21	5,857	8	9	6,354
TQ vs. Column J	51,14	17,73	33,41	5,857	8	9	5,705
TQ vs. Column K	51,14	20,67	30,47	5,857	8	9	5,203
TQ vs. TQ	51,14	45,28	5,857	5,857	8	9	1
TQ vs. Column M	51,14	15,06	36,08	5,857	8	9	6,16
TQ vs. Column N	51,14	13,88	37,26	5,857	8	9	6,362
TQ vs. Column O	51,14	22,25	28,89	5,857	8	9	4,933
TQ vs. TQ	51,14	45,11	6,029	5,857	8	9	1,029

Table 42 Statistic values of TQ comparison

Column C vs. Column B	CTRL vs. double KO
Unpaired t test	
P value	0,0559
P value summary	ns
Significantly different? (P < 0.05)	No
One- or two-tailed P value?	Two-tailed
t, df	t=2.085 df=14
How big is the difference?	
Mean ± SEM of column B	32.61 ± 5.190, n=8
Mean ± SEM of column C	51.14 ± 7.215, n=8
Difference between means	18.53 ± 8.888
95% confidence interval	-0.5347 to 37.59
R squared	0,2369

F test to compare variances	
F,DFn, Dfd	1.932, 7, 7
P value	0,4044
P value summary	ns
Significantly different? (P < 0.05)	No

Table 43Statistic values of spine density after learning

Table Analyzed	Data 1				
One-way analysis of variance					
P value	0,0178				
P value summary	*				
Are means signif. different? (P < 0.05)	Yes				
Number of groups	4				
F	3,571				
R squared	0,1235				
Bartlett's test for equal variances					
Bartlett's statistic (corrected)	1,388				
P value	0,7084				
P value summary	ns				
Do the variances differ signif. (P < 0.05)	No				
ANOVA Table	SS	df	MS		
Treatment (between columns)	0,2565	3	0,08550		
Residual (within columns)	1,820	76	0,02394		
Total	2,076	79			
Tukey's Multiple Comparison Test	Mean Diff.	q	Significant? P < 0.05?	Summary	95% CI of diff
PFN 1 KO vs Pfn 2 KO	-0,1156	3,350	No	ns	-0.2442 to 0.01289
PFN 1 KO vs doube KO	0,02740	0,696 8	No	ns	-0.1190 to 0.1738
PFN 1 KO vs CTRL LacZ	-0,02056	0,571 9	No	ns	-0.1544 to 0.1133
Pfn 2 KO vs doube KO	0,1430	4,059	Yes	*	0.01185 to 0.2742
Pfn 2 KO vs CTRL LacZ	0,09508	3,025	No	ns	-0.02193 to 0.2121
doube KO vs CTRL LacZ	-0,04796	1,309	No	ns	-0.1844 to 0.08845

Table 44 Statistic values sEPSC amplitude

Number of families	1
Number of comparisons per family	10
Alpha	0,05

Bonferroni's multiple comparisons test	Mean Diff.	95.00% CI of diff.	Significant?	Summary
PFN 1B 2A vs. PFN1 (1B)	-2,682	-33.23 to 27.86	No	ns
PFN 1B 2A vs. PFN2 (2A)	7,933	-17.42 to 33.29	No	ns
PFN 1B 2A vs. tGFAP 1B2A	-3,094	-32.49 to 26.3	No	ns
PFN 1B 2A vs. CTRL	-19,59	-44.53 to 5.352	No	ns
PFN1 (1B) vs. PFN2 (2A)	10,62	-20.27 to 41.5	No	ns
PFN1 (1B) vs. tGFAP 1B2A	-0,4115	-34.69 to 33.87	No	ns
PFN1 (1B) vs. CTRL	-16,91	-47.45 to 13.64	No	ns
PFN2 (2A) vs. tGFAP 1B2A	-11,03	-40.77 to 18.72	No	ns
PFN2 (2A) vs. CTRL	-27,52	-52.88 to -2.17	Yes	*
tGFAP 1B2A vs. CTRL	-16,5	-45.89 to 12.9	No	ns

Table 45 Statistic values of sEPSCs frequency

Number of groups	5			
F	23,85			
R squared	0,6179			
Bartlett's test for equal variances				
Bartlett's statistic (corrected)	21,87			
P value	0,0002			
P value summary	***			
Do the variances differ signif. (P < 0.05)	Yes			
ANOVA Table	SS	df		
Treatment (between columns)	230,8	4		
Residual (within columns)	142,7	59		
Total	373,6	63		
Tukey's Multiple Comparison Test	Mean Diff.	q	Summary	95% CI of diff
PFN 1B 2A vs PFN1 (1B)	3,827	8,035	***	1.931 to 5.722
PFN 1B 2A vs PFN2 (2A)	3,584	9,066	***	2.010 to 5.157
PFN 1B 2A vs CTRL	-0,2664	0,6852	ns	-1.814 to 1.281
PFN1 (1B) vs PFN2 (2A)	-0,2433	0,5052	ns	-2.160 to 1.673
PFN1 (1B) vs CTRL	-4,093	8,595	***	-5.989 to -2.198
PFN2 (2A) vs CTRL	-3,850	9,740	***	-5.423 to -2.277

Table 46 Statistic values from mESPCs analysis

Table Analyzed	Frequency
Column A	CTRL
vs	vs
Column B	PFN 1B 2A
Unpaired t test	
P value	0,0597
P value summary	ns
Are means signif. different? (P < 0.05)	No
One- or two-tailed P value?	Two-tailed
t, df	t=1.965 df=27
How big is the difference?	

Mean ± SEM of column A	0.3686 ± 0.08318 N=14
Mean ± SEM of column B	0.1913 ± 0.03968 N=15
Difference between means	0.1772 ± 0.09018
95% confidence interval	-0.007814 to 0.3623
R squared	0,1252
F test to compare variances	
F,DFn, Dfd	4.101, 13, 14
P value	0,0133
P value summary	*
Are variances significantly different?	Yes

Table 47 statistic values of action potential threshold analysis

Table Analyzed	AP threshold
Column A	1B2A
vs.	vs.
Column B	CTRL
Unpaired t test	
P value	0,1163
P value summary	ns
Significantly different? (P < 0.05)	No
One- or two-tailed P value?	Two-tailed
t, df	t=1.719 df=10
How big is the difference?	
Mean ± SEM of column A	-10.84 ± 3.917, n=6
Mean ± SEM of column B	-23.17 ± 6.009, n=6
Difference between means	12.33 ± 7.173
95% confidence interval	-3.651 to 28.31
R squared	0,2281
F test to compare variances	
F,DFn, Dfd	2.353, 5, 5
P value	0,3693
P value summary	ns
Significantly different? (P < 0.05)	No

Table 48 Statistic values of sEPSCs frequency of phospho-mimicking mutants

Data sets analyzed	A : S137A	B : S137D	C : CTRL
ANOVA summary			
F	0,8552		
P value	0,4437		
P value summary	ns		
Significant diff. among means (P < 0.05)?	No		
R square	0,09658		
Brown-Forsythe test			
F (DFn, DFd)	0.6423 (2, 16)		

P value	0,5391
P value summary	ns
Are SDs significantly different (P < 0.05)?	No

Bartlett's test	
Bartlett's statistic (corrected)	1,459
P value	0,4821
P value summary	ns
Are SDs significantly different (P < 0.05)?	No

ANOVA table	SS	DF	MS	F (DFn, DFd)	P value
Treatment (between columns)	5,079	2	2,54	F (2, 16) = 0.8552	P=0.4437
Residual (within columns)	47,51	16	2,969		
Total	52,59	18			

Data summary	
Number of treatments (columns)	3
Number of values (total)	19

Table 49 Statistic values of sEPSC amplitude of phospho-mimickng mutants

Table Analyzed	Amplitude		
Data sets analyzed	A : S137A	B : S137D	C : CTRL

ANOVA summary	
F	3,781
P value	0,0452
P value summary	*
Significant diff. among means (P < 0.05)?	Yes
R square	0,3209

Brown-Forsythe test	
F (DFn, DFd)	0.4195 (2, 16)
P value	0,6644
P value summary	ns
Are SDs significantly different (P < 0.05)?	No

Bartlett's test	
Bartlett's statistic (corrected)	1,118
P value	0,5717
P value summary	ns
Are SDs significantly different (P < 0.05)?	No

ANOVA table	SS	DF	MS	F (DFn, DFd)	P value
Treatment (between columns)	364,2	2	182,1	F (2, 16) = 3.781	P=0.0452
Residual (within columns)	770,6	16	48,16		
Total	1135	18			

Data summary	
Number of treatments (columns)	3
Number of values (total)	19

Table 50 Statistic values of number of action potentials analysis

	# of AP step		
Table Analyzed	10		
Data sets analyzed	A : CTRL	B : 137D	C : 137A
ANOVA summary			
F	0,9003		
P value	0,4240		
P value summary	ns		
Significant diff. among means (P < 0.05)?	No		
R square	0,09094		
Brown-Forsythe test			
F (DFn, DFd)	0.5507 (2, 18)		
P value	0,5860		
P value summary	ns		
Are SDs significantly different (P < 0.05)?	No		
Bartlett's test			
Bartlett's statistic (corrected)	2,47		
P value	0,2909		
P value summary	ns		
Are SDs significantly different (P < 0.05)?	No		

ANOVA table	SS	DF	MS	F (DFn, DFd)	P value
Treatment (between columns)	14,82	2	7,41	F (2, 18) = 0.9003	P=0.4240
Residual (within columns)	148,1	18	8,23		
Total	163	20			

Data summary	
Number of treatments (columns)	3
Number of values (total)	21